

**FM SIGNALS-BASED ENERGY HARVESTER  
OPTIMISATION FOR LOW POWER WIRELESS  
SENSOR NETWORKS**

SULTAN MUKHLIS HAMID

MASTERS OF SCIENCE  
(Mechatronic Engineering)

JOMO KENYATTA UNIVERSITY OF AGRICULTURE AND  
TECHNOLOGY

2016

**FM Signals-Based Energy Harvester Optimisation for Low  
Power Wireless Sensor Networks**

By: SULTAN MUKHLIS HAMID

Reg. No. EN392-1842/2011

MASTERS OF SCIENCE

(Mechatronic Engineering)

A thesis submitted in partial fulfillment of the requirements for the  
award of Master of Science degree in Mechatronic Engineering in the  
Jomo Kenyatta University of Agriculture and Technology

2016

# DECLARATION

This research thesis is my original work and to the best of my knowledge it has not been presented for the award of a degree in this or any other university.

Mukhlis Hamid Sultan

Reg No: EN392-1842/2011

Sign..... Date.....

This research thesis has been submitted to the Department of Mechatronics Engineering, School of Mechanical, Manufacturing and Materials Engineering, College of Engineering and Technology, Jomo Kenyatta University of Agriculture and Technology, with our approval as the supervisors:

Prof. George N. Nyakoe

Sign..... Date.....

Dr. James N. Keraita

Sign..... Date.....

## DEDICATION

I wish to dedicate this work to my mother, Maimuna. My father, Hamid. My wife, Himdat and my daughter Riham for their continuous support and encouragement.

## ACKNOWLEDGEMENTS

I would wish to express my sincere thanks to the Almighty God for bestowing me with his mercy and support by giving me the opportunity to carry out this work. I would also wish to express my heartfelt gratitude to my supervisors Prof. George N. Nyakoe and Dr. James N. Keraita for their support, guidance and positive criticism which has seen me through this work.

I also wish to thank Dedan Kimathi University of Technology for giving me the necessary funds to purchase the components and software needed for this research. My sincere thanks also goes to all the technologists in the department of Electrical Engineering at Dedan Kimathi University of Technology for assisting me to carry out the experimental work in the Laboratory as well as teaching me how to use the equipment.

Finally, I wish to acknowledge the contributions of my colleagues and fellow post-graduate students in both the Mechanical and Mechatronic Engineering Departments at JKUAT for their selfless assistance and constructive comments during the course of this work.

## TABLE OF CONTENTS

DECLARATION	ii
DEDICATION	iii
ACKNOWLEDGEMENT	iv
TABLE OF CONTENTS	v
LIST OF TABLES	ix
LIST OF FIGURES	x
LIST OF APPENDICES	xii
LIST OF ABBREVIATIONS	xiv
NOMENCLATURE	xvi
ABSTRACT	xviii
<b>1 INTRODUCTION</b>	<b>1</b>
1.1 Background . . . . .	1
1.2 Problem statement . . . . .	3
1.3 Objectives . . . . .	3
1.3.1 Main objectives . . . . .	3

1.3.2	Specific objectives . . . . .	3
1.4	Justification of the study . . . . .	4
1.5	Outline of the thesis . . . . .	4
<b>2</b>	<b>LITERATURE REVIEW</b>	<b>5</b>
2.1	Introduction . . . . .	5
2.2	Wireless sensor networks . . . . .	5
2.3	RF Energy harvesting . . . . .	6
2.3.1	RF-to-DC converted power . . . . .	8
2.3.2	Power density of RF sources . . . . .	10
2.3.3	Mathematical analysis of FM signals . . . . .	14
2.4	Usage and storage of harvested RF energy . . . . .	20
2.4.1	Voltage multiplier . . . . .	20
2.4.1.1	Voltage multiplier configurations . . . . .	22
2.4.1.2	Input/Output relationship of a multiplier . . . . .	25
2.4.1.3	Power efficiency of the multiplier . . . . .	25
2.4.1.4	Ripple voltage of the multiplier output . . . . .	27
2.4.2	Common approaches used in powering WSNs . . . . .	28
2.4.3	Supercapacitors . . . . .	29
2.5	Previous work on RF energy harvesting and optimisation . . . . .	31
2.6	Research gaps . . . . .	39
<b>3</b>	<b>METHODOLOGY</b>	<b>40</b>
3.1	Introduction . . . . .	40
3.2	Design of the FM harvester . . . . .	41
3.2.1	Antenna design . . . . .	41
3.2.2	Band pass filter design . . . . .	43
3.2.3	Voltage multiplier design . . . . .	45
3.3	Computer simulation of the FM harvester sub-systems . . . . .	46

3.3.1	Simulation of the RLC band pass filter . . . . .	46
3.3.2	Simulation of voltage multiplier . . . . .	47
3.3.3	Simulation of WSN . . . . .	50
3.4	Development and analysis of the performance of the FM harvester .	52
3.4.1	Implementation of the FM harvester . . . . .	52
3.4.2	Analysis of the performance of the harvester . . . . .	53
3.4.3	Measurement of signal strength . . . . .	54
3.5	Integration of the harvester into WSN . . . . .	55
3.6	Summary . . . . .	57
<b>4</b>	<b>RESULTS AND DISCUSSIONS</b>	<b>59</b>
4.1	Verification and optimisation of harvester sub-systems through sim- ulations . . . . .	59
4.1.1	Effect of RF source on the received power . . . . .	59
4.1.2	Verification of the operation of the RLC filter . . . . .	62
4.1.3	Effect of stage capacitance on the multiplier output . . . . .	62
4.1.4	Effect of number of stages on the multiplier output . . . . .	66
4.2	Analysis of the performance of the FM harvester . . . . .	72
4.2.1	Effect of input frequency on the harvester output . . . . .	72
4.2.2	Effect of input power on harvester output . . . . .	76
4.2.3	Effect of load resistance on harvester output . . . . .	77
4.3	Integration of the harvester into the wireless sensor network . . . . .	80
4.4	Summary . . . . .	82
<b>5</b>	<b>CONCLUSIONS AND RECOMENDATIONS</b>	<b>84</b>
5.1	Conclusions . . . . .	84
5.2	Recommendations . . . . .	85
<b>6</b>	<b>REFERENCES</b>	<b>86</b>

<b>A APPENDICES</b>	<b>93</b>
A.1 APPENDIX A: C++ code for Transmitter . . . . .	93
A.2 APPENDIX B: C++ code for receiver . . . . .	95
A.3 APPENDIX C: C++ header file for sketch.h . . . . .	97
A.4 APPENDIX D: C++ header file for pin.h . . . . .	98
A.5 APPENDIX E: C++ header file for newserial.h . . . . .	106
A.6 APPENDIX F: Transfer function of RLC Band pass filter . . . . .	110

## LIST OF TABLES

2.1	Energy harvesting techniques [12] . . . . .	7
2.2	E-field intensities of some RF sources [9] . . . . .	8
2.3	Comparison between Li-Ion battery and Supercapacitor [26] . . . . .	30
3.1	Operating Parameters of XBee WSN Node [37] . . . . .	41
3.2	SPICE parameters of HSMS 285X [37,40] . . . . .	48

## LIST OF FIGURES

1.1	Principle of energy harvesting from RF signals [1] . . . . .	1
1.2	Typical WSN architecture [4] . . . . .	2
2.1	Working principle of a typical energy harvester [8] . . . . .	7
2.2	RF energy harvester [12] . . . . .	7
2.3	Effect of Range on Power Density . . . . .	10
2.4	Arbitrary transmit/receive antenna system . . . . .	11
2.5	Graph of Bessel functions of an FM signal . . . . .	17
2.6	Amplitude Spectrum of FM signal for $\beta = 0.4$ and $\beta = 5$ . . . . .	18
2.7	Band Separation in FM broadcasting [17] . . . . .	19
2.8	Single stage voltage doubler . . . . .	20
2.9	Multiple stage voltage multiplier. . . . .	21
2.10	Common configurations for voltage multipliers . . . . .	22
2.11	Transient and steady modes of a voltage multiplier. [19] . . . . .	23
2.12	Construction of a Schottky diode. . . . .	24
2.13	Equivalent circuit of a Schottky diode. . . . .	25
2.14	Construction of a supercapacitor [23] . . . . .	30
2.15	Crossover point for LPD and HPD [32] . . . . .	34
2.16	Charge pump [12] . . . . .	36
3.1	XBee Wireless Sensor Node [37] . . . . .	40
3.2	Selected antenna . . . . .	42

3.3	FM Antenna output . . . . .	43
3.4	Flow diagram of a Band Pass Filter . . . . .	43
3.5	Passive RLC Band Pass Filter . . . . .	44
3.6	LTSPICE IV model of the designed RLC filter . . . . .	47
3.7	Circuit Model of single stage multiplier in LTSPICE IV . . . . .	48
3.8	Circuit Model of 13-stage CW multiplier in LTSPICE IV . . . . .	50
3.9	Circuit designs for the XBee transceiver . . . . .	51
3.10	Layout of sensors . . . . .	52
3.11	Multiplier PCB . . . . .	53
3.12	FM mode of the signal generator . . . . .	53
3.13	Experimental analysis of the FM harvester . . . . .	54
3.14	Field strength meter . . . . .	55
3.15	Infrared sensor . . . . .	56
3.16	WSN implementation . . . . .	56
3.17	Receiver set-up . . . . .	57
4.1	Received power for different RF sources . . . . .	60
4.2	Power spectrum for frequency range of 0-2.5GHz . . . . .	61
4.3	Signal identity in power spectrum . . . . .	61
4.4	Output of RLC filter . . . . .	62
4.5	Effect of stage capacitance on output voltage . . . . .	63
4.6	Effect of stage capacitance on RMS voltage . . . . .	64
4.7	Effect of stage capacitance on ripple factor and voltage . . . . .	65
4.8	Effect of stage capacitance on efficiency . . . . .	66
4.9	Effect of number of stages on output voltage . . . . .	67
4.10	Variation of output voltage with number of stages . . . . .	68
4.11	Variation of efficiency with number of stages . . . . .	69
4.12	Variation of output current with number of stages . . . . .	70

4.13	Effect of number of stages on output power . . . . .	70
4.14	Variation of output power with number of stages . . . . .	71
4.15	Effect of frequency on output voltage . . . . .	72
4.16	Effect of frequency on rise time . . . . .	73
4.17	Effect of frequency on efficiency . . . . .	74
4.18	Effect of input frequency on output power . . . . .	75
4.19	Variation of ripple factor with frequency . . . . .	76
4.20	Variation of efficiency with input power . . . . .	77
4.21	Effect of load resistance on output power . . . . .	78
4.22	Effect of load resistance on average power . . . . .	79
4.23	Effect of load resistance on efficiency . . . . .	79
4.24	Snapshot of data received from WSN . . . . .	80
4.25	Variation of battery charge with time . . . . .	81
4.26	Linear relationship between charge and time . . . . .	82
A.1	Passive RLC Band Pass Filter . . . . .	110

## LIST OF APPENDICES

A1. APPENDIX A: C++ code for transmitter	93
A2. APPENDIX B: C++ code for receiver	95
A2. APPENDIX C: C++ header file for sketch.h	97
A2. APPENDIX D: C++ header file for pin.h	98
A2. APPENDIX E: C++ header file for new serial.h	106
A2. APPENDIX F: transfer function of RLC band pass filter	110

## LIST OF ABBREVIATIONS

<b>A.C</b>	Alternating Current
<b>ADS</b>	Advanced Design Simulation
<b>AM</b>	Amplitude Modulation
<b>BPF</b>	Band Pass Filter
<b>CDMA</b>	Code Division Multiple Access
<b>D.C</b>	Direct Current
<b>DTV</b>	Digital Television
<b>FM</b>	Frequency Modulation
<b>FSPA</b>	Folded Shorted Patch Antenna
<b>FSPL</b>	Free Space Path Loss
<b>GSM</b>	Global System for Mobile Communication
<b>GPS</b>	Global Positioning System
<b>GUI</b>	Graphical User Interface
<b>HPD</b>	High Power Density
<b>IC</b>	Integrated Circuit
<b>IEEABR</b>	Improved Energy Efficient Ant Based Routing
<b>IP</b>	Internet Protocol
<b>IR</b>	Infra Red
<b>Li-Ion</b>	Lithium Ion
<b>LPD</b>	Low Power Density
<b>LPF</b>	Low Pass Filter
<b>MEMS</b>	Micro-Electromechanical Systems
<b>PCB</b>	Printed Circuit Board
<b>PM</b>	Phase Modulation
<b>PSD</b>	Power Spectral Density
<b>RF</b>	Radio Frequency

<b>RFID</b>	Radio Frequency Identification
<b>RMS</b>	Root Mean Square
<b>SMSA</b>	Square Micro-Strip Antenna
<b>UHF</b>	Ultra-High Frequency
<b>VSWR</b>	Voltage Standing Wave Ratio
<b>WSN</b>	Wireless Sensor Network

## NOMENCLATURE

$A_c$	Carrier amplitude [V]
$A_m$	Modulation signal amplitude [V]
$B_T$	Bandwidth [Hz]
$C$	Capacitance [F]
$c$	Speed of light [m/s]
$C_j$	Junction capacitance [F]
$C_{out}$	Output capacitance [F]
$f$	Frequency [Hz]
$f_c$	Carrier frequency [Hz]
$f_i$	Single input frequency [Hz]
$f_m$	Modulation frequency [Hz]
$f_{\Delta}$	Frequency deviation [Hz]
$G_r$	Receiver gain [dBm]
$G_t$	Transmitter gain [dBm]
$C_{out}$	Output capacitance [F]
$I$	Amplitude [V]
$I_{in}$	Input current [A]
$I_{out}$	Output current [A]
$J_n$	Sideband amplitude [dBm]
$n$	Number of stages
$P_D$	Power density [mW/m <sup>3</sup> ]
$P_{in}$	Input power [W]
$P_{out}$	Output power [W]
$P_r$	Received power [W]
$P_{RF}$	Average RF power [W]
$P_t$	Transmitted power [W]

$Q_L$	Charge lost [C]
$R$	Distance between transmitter and receiver [m]
$R_{in}$	Antenna input resistance [ $\Omega$ ]
$R_j$	Junction resistance [ $\Omega$ ]
$R_L$	Load resistance [ $\Omega$ ]
$t$	Time [s]
$V_d$	Diode forward voltage [V]
$V_{in}$	Input voltage [V]
$V_L$	Load voltage [V]
$V_{out}$	Output voltage [V]
$w_r$	Power density at receiver [mW/m <sup>3</sup> ]
$Z_{DC}$	D.C Load impedance [ $\Omega$ ]
$\beta$	Modulation index
$\eta$	Efficiency
$\Gamma$	Reflection co-efficient [dBm]
$\theta_r$	Receiver polarisation angle [radians]
$\theta_t$	Transmitter polarisation angle [radians]
$\phi_r$	Receiver incidence angle [radians]
$\phi_t$	Transmitter incidence angle [radians]
$\lambda$	Wavelength [m]
$\rho$	Impedance match coefficient
$\tau$	Time constant [s]

## ABSTRACT

Energy harvesting from ambient sources has attracted a lot of research recently due to the high demand for cheaper and greener energy. Several researchers have investigated the possibility of harvesting energy from ambient Radio Frequency (RF) energy sources such as Wi-Fi, Global System for Mobile communications (GSM), microwaves, Code Division Multiple Access (CDMA), Ultra High Frequency (UHF) and even Amplitude Modulation (AM) signals. But in most of these researches, the harvested energy is too low, especially when the energy harvester is far from the transmitting station. Furthermore, very little effort has been directed towards harvesting energy from Frequency Modulation (FM) signals which are abundant in most parts of the world.

The energy harvested is mainly used in Wireless Sensor Networks (WSN). WSNs are becoming popular due to their low cost, long ranges of transmission as compared to wired sensor networks, long life due to low power requirements and ability to operate in hard-to reach areas. However, powering these wireless sensor networks has posed a challenge since battery replacement would require constant access to the location of the sensors. The aim of this research was to harvest energy from FM signals and use the energy to power a wireless sensor network. This approach will help reduce the frequency of battery replacement and consequently reduce the maintenance costs, improve safety and increase the overall efficiency of the system.

In this study, the signal strength of different signals within the vicinity was investigated. The sub-systems that make up an FM harvester were designed based on the given constraints of the WSN. Appropriate mathematical formulations were used to come up with the values of the components in a passive RLC filter as well as the voltage multiplier. Computer simulations using LTSPICE IV were carried out to verify the operation of the designed filter. The software was also used to assess the effect of stage capacitance and the number of stages on the performance

of the multiplier. .

An XBee WSN was designed and implemented using an ATMEGA328P micro-controller programmed in the C++ language. The receiver was connected to the computer to receive data sent by the transmitter which was powered by a 3200 mAh rechargeable battery. A graphical user interface (GUI) was also developed to display the data received from the transmitter.

The experimental analysis showed that the harvester could produce a maximum voltage of 2.95 V when the optimum system parameter obtained from simulations were used. The output of the harvester was used to recharge the battery in the transmitter. Data collected over a period of 48 hours showed that the harvester reduced the battery draining speed from -16.418 mAh per hour to -5.8315 mAh per hour which represented a 64% improvement in the speed. The battery life was extended from 196 hours to 555 hours, which represented a 180% increase in the life of the battery.

# 1. INTRODUCTION

## 1.1 Background

Radio waves are electromagnetic waves in the frequency range of 3 kHz to 300 GHz [1]. Radio Frequency (RF) signals are being used in wireless communications such as FM, AM, Wi-Fi, microwaves, GSM, and UHF. Harvesting energy from RF signals involves capturing the signal with an antenna and then conditioning the signal to produce a D.C signal that can be used to supply electrical energy to devices. Figure 1.1 shows a block diagram of a typical RF harvester.

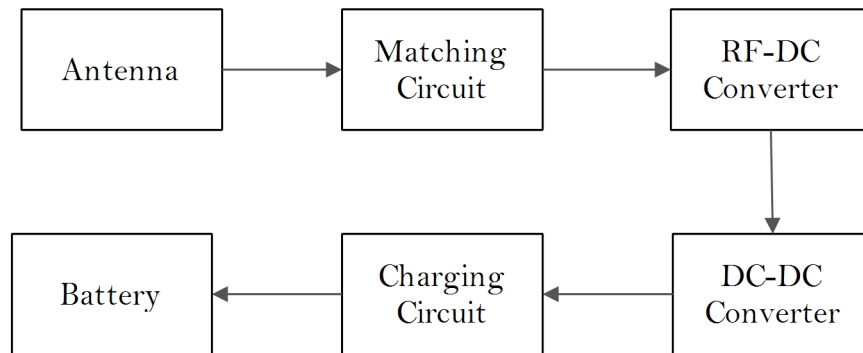


Figure 1.1: Principle of energy harvesting from RF signals [1]

Frequency Modulation (FM) signals are RF signals with frequency ranges of 85-105 MHz that are used to broadcast signals for radio stations [2]. In Kenya there are about 90 FM channels, each broadcasting at a given frequency. These signals have low power densities compared to other types of RF signals, but they are the most abundant signals due to the high number of transmitting stations [3].

A Wireless sensor network (WSN) is an array of sensors that remotely sends data to a central processing unit for analysis and evaluation through wireless or Global Positioning System (GPS) signals. The wireless signals may be Internet Protocol (IP) based Wi-Fi signals, GSM signals or RF signals. These networks have longer communication ranges compared to wired sensor networks, longer life due to their low power requirements and have the ability to operate in harsh and hard-to-reach

environment. They could number up to hundreds of them in a single setup. These sensors have found applications in many fields such as manufacturing, health, environment, agriculture, transport and communication. Figure 1.2 shows a typical WSN architecture.

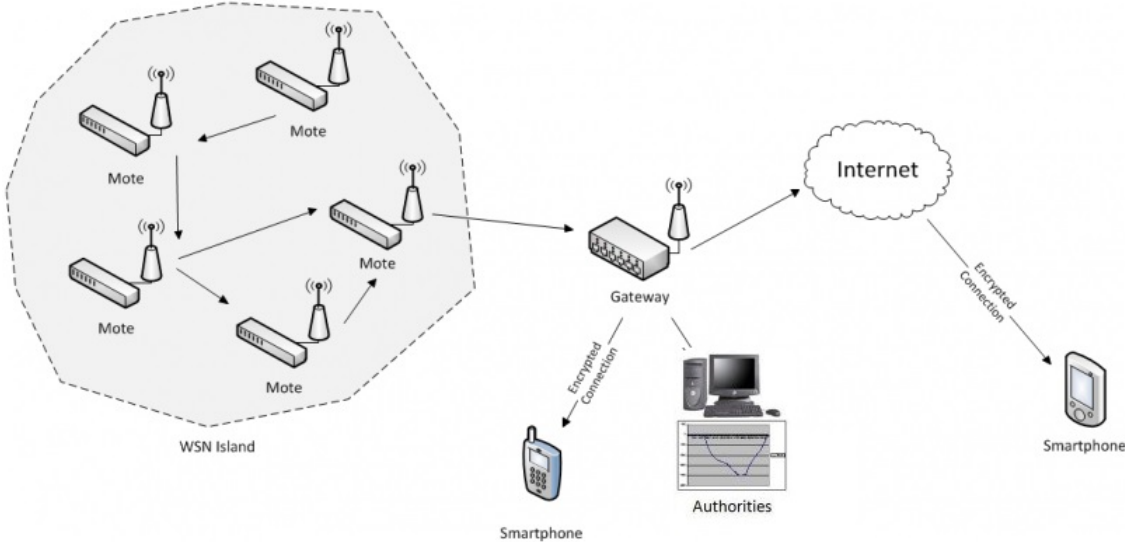


Figure 1.2: Typical WSN architecture [4]

Wireless sensor networks require a local power source that will power the sensor and other circuits within the sensor package. This is achieved by using a rechargeable battery on each sensor. The use of a rechargeable battery on each sensor in a network brings about the need to replace several batteries routinely on a large network, this is cumbersome, costly and in some cases impossible if the sensors are located in areas that are hard to access [5]. In order to tackle the problem of routinely replacing the batteries, most researchers have investigated the possibility of powering the WSN from energy harvested from the surrounding. The energy harvested from RF sources can either be used directly or stored in a battery. The most common and suitable option is to store it to prevent the fluctuations in signal strength from affecting the performance of the circuit.

## **1.2 Problem statement**

Wireless sensor network provide numerous advantages over wired sensors. They are very useful in system monitoring and diagnosis, and provide an early indication of any defects or abnormalities in the system performance. However, the use of batteries in a network containing several sensor nodes brings about the need to replace the batteries routinely. This is costly, cumbersome and may even cause loss of vital data if not done in good time.

## **1.3 Objectives**

### **1.3.1 Main objectives**

The main objective of this research was to design, optimise and investigate the performance of an FM energy harvester.

### **1.3.2 Specific objectives**

To achieve the main objective, the following were the specific objectives:

1. To design an optimised FM energy harvester based on the relevant mathematical formulations
2. To simulate the FM energy harvester sub-systems to verify their operation and optimise their performance.
3. To implement an FM energy harvester system based on the simulations and carry out experiments on the circuit to analyse its performance.
4. To integrate the FM energy harvester into a WSN to assess its effect on battery life.

## 1.4 Justification of the study

Successful large scale deployment of wireless sensor nodes require them to be energy self-sufficient for their entire useful lifetime. Otherwise, the operational cost of replenishing their energy source will be enormous, especially when deployed in areas that are not readily accessible. Therefore, there is a need to find a means of constantly replenishing the charge of the battery powering these sensor networks while they are still in operation. This research sought to develop an optimised energy harvester that harvests energy from FM signals broadcast by the local radio stations and use this energy to recharge the battery in a low power WSN. This approach was aimed at increasing the service time of the batteries and thus reducing the frequency of battery replacement in WSN.

## 1.5 Outline of the thesis

This thesis contains five chapters. The first chapter provides an introduction to the research by highlighting the existing problem, the objective and the justification of the research work. Chapter 2 provides a literature review on RF energy harvesting and the various approaches employed in the optimisation and simulation of RF energy harvester system. It also provides a literature review on FM signals. In Chapter 3, the methodology used to carry out the research is explained, and both the simulations and experimental procedures are discussed. Chapter 4 discusses the results obtained and finally, Chapter 5 presents the conclusions and recommendations.

## 2. LITERATURE REVIEW

### 2.1 Introduction

The emerging fields of Radio Frequency (RF) energy harvesting and wireless sensor networks (WSN) creates a new paradigm in the way we interact with our environment. Recent technological advances in Micro-Electromechanical systems (MEMS), energy scavenging, energy storage and Integrated Circuit (IC) packaging, coupled with the availability of low power, low cost digital and analogue electronics have made it possible to realize a dense network of inexpensive wireless sensor nodes, each having sensing, computational and communication capabilities [6].

In this research, the two fields are coupled to form a WSN that is energy self-sufficient by harvesting the energy from FM signals and feeding it to a WSN.

### 2.2 Wireless sensor networks

Wireless sensors are expected to transform the way humanity interacts with the physical world. They have been deployed in a wide variety of applications such as habitat monitoring, structure monitoring and emergency medical response [7]. While the application space seems limitless, it is actually limited by the lifetime of the battery. Commercial sensors use electronic ICs which are not designed to minimise the usage of power and thus drain the battery quickly. However some research has been done to design low power WSN that consume little power from the battery and hence increase the operational lifetime [6].

Some applications dictate a node lifetime to last up to ten years (e.g. seismic detection in buildings), and this can impose severe constraints on the node's power consumption [6]. For efficient and economical use of a WSN, the average power consumption of each node in the WSN should be less than or equal to  $100 \mu\text{W}$  [8]. This value has been achieved by a few manufacturers of commercial WSN [1]. The

power requirements are very low for manufacturers of WSN to achieve, but these requirements make it easier to design systems that will power the WSN nodes for a very long time [6].

Significant research has already been conducted on the field of energy harvesting from RF signals [6]. Some of these researches have investigated the possibility of harvesting energy from Wi-Fi signals, GSM signals, microwave signals and AM signals [8]. In most of these researches, the power produced by the harvester was too low, especially when the harvester is far from the transmitting station. The need to have a harvester that is capable of increasing the operational lifetime of a wireless sensor is a major challenge for wireless sensors manufacturers. As a result, there is increased interest in energy sources that can power WSN autonomously for a very long time without replacing the primary battery [9].

## 2.3 RF Energy harvesting

Energy harvesting refers to the process by which energy is derived, captured and stored from external sources [10]. Energy has been harvested from several external sources such as thermal, mechanical, optical, RF signals and salinity gradient [8]. Some of the energy harvesting techniques include RF energy, piezoelectric, pyroelectric, electrostatic, photovoltaic, Biomechanical, magnetostatic and thermoelectric [11].

The basic structure of an energy harvester includes a harvesting element, a conditioning circuit and a means of storing or using the harvested energy. Figure 2.1 shows the working principle of a typical energy harvester. The amount of energy harvested is greatly affected by the method of energy harvesting employed. The power density for the different energy harvesting technique is summarized in Table 2.1. Harvesting energy from RF signals has attracted a lot of attention because of the simplicity of the harvester. Figure 2.2 shows the block diagram of a simple

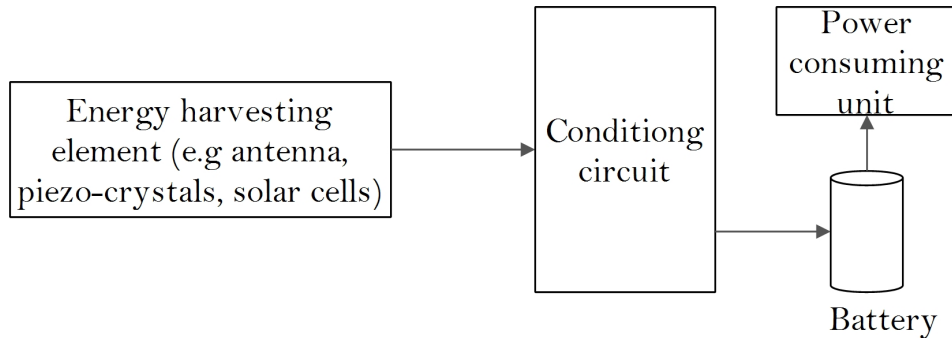


Figure 2.1: Working principle of a typical energy harvester [8]

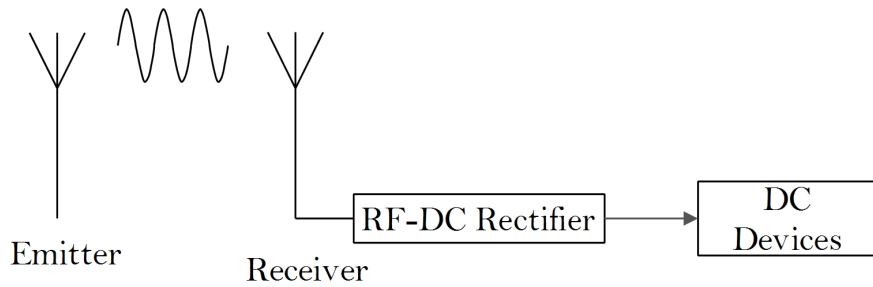


Figure 2.2: RF energy harvester [12]

RF energy harvester.

However, RF energy harvesters suffer from low power outputs and this is attributed to the unpredictable nature of the input power [13]. The received signal is also prone to attenuation by obstacles and bad weather and has very low power den-

Table 2.1: Energy harvesting techniques [12]

<b>ENERGY HARVESTING TECHNIQUE</b>	<b>CLASSIFICATION</b>	<b>POWER DENSITY</b>
Piezoelectric	Mechanical Energy	$200 \mu\text{W}/\text{cm}^3$
Air flow	Mechanical Energy	$177 \mu\text{W}/\text{cm}^3$
Blood Flow	Mechanical Energy	$0.93 \text{ W}/100\text{mmHg}$
Body Motion	Mechanical Energy	$800 \mu\text{W}/\text{cm}^3$
External Heat	Thermal Energy	$153 \mu\text{W}/\text{cm}^3$
RF Energy	Radiant Energy	$0.03 \mu\text{W}/\text{cm}^3$ at 500 m for FM
Solar Energy	Radiant Energy	$100\text{m W}/\text{cm}^3$

Table 2.2: E-field intensities of some RF sources [9]

<b>SOURCE</b>	<b>V/m</b>	<b>dBm</b>
FM Radio	0.15 to 3	
Analogue TV	0.3 to 2	
Digital TV	0.2 to 2.4	-40 to 0.0
Cellular		-65 to 0.0
Wi-Fi		-30

sity as compared to other sources. Nevertheless, many researchers have investigated the possibility of harvesting power from RF sources that will be enough to drive commercial components such as wireless chargers, WSN and wireless ear-phones [1, 6, 7, 9, 12]. RF sources can be classified into three categories:

1. **Dedicated sources:** These are sources that are dedicated to supply RF energy to an array of sensors within a limited distance at known frequency.
2. **Anticipated sources:** These are sources such as cell towers, radio or TV signal transmitter that are within a short distance and their behaviour can be easily predicted although the signal is prone to attenuational fading.
3. **Unknown sources:** This class of sources has the least power density with the highest levels of distortions and are highly unpredictable.

The E-field intensities of some of the RF signals are shown in Table 2.2. It can be seen from Table 2.2 that FM signals have the highest E-field intensities which means they have potential to produce the highest power when energy is harvested from them. However, due to the requirements for a large antenna size and the challenges for simulations and measurements at the FM frequency, very little energy harvesting research has been done on them [9].

### 2.3.1 RF-to-DC converted power

The input signal to the harvester comes from the antenna. The signal is usually a combination of several signals from different transmitters, and therefore, the

resultant signal received by the antenna is superposition of several waves received from different transmitters [14]. The received FM signal power is composed of individual power from each signal, this represents a high potential for increased energy harvesting unlike in other less dense signals. The total RF-to-DC converted power is roughly the integral over the FM band [10]. The total received power can be expressed as in Equation (2.1).

$$P_{DC(FM)} = \alpha \int_{80}^{108} \partial P_{DC}(f) df \quad (2.1)$$

where  $\alpha$  is the attenuation factor on the rectifying antenna's RF-to-DC conversion efficiency due to multiple incident signal excitation.  $\partial P_{DC}$  is the small converted DC power from each of the single FM signals in the 80 MHz to 108 MHz band. The incident power density on the rectifying antenna (rectenna),  $S(\theta, \phi, f, t)$ , is a function of incident angles, and can vary over the FM spectrum and in time. The effective area of the antenna,  $A_{eff}(\theta, \phi, f)$ , will be different at different frequencies, for different incident polarizations and incidence angles. The average RF power over a range of frequencies at any instant in time is given by Equation (2.2).

$$P_{RF}(t) = \frac{1}{f_{high} - f_{low}} \int_{f_{low}}^{f_{high}} \int_0^{4\pi} S(\theta, \phi, f, t) A_{eff}(\theta, \phi, f) d\Omega df \quad (2.2)$$

The DC power for a single frequency ( $f_i$ ) input RF power, is given by

$$P_{DC}(f_i) = P_{RF}(f_i, t) \cdot \eta(P_{RF}(f_i, t), \rho, Z_{DC}) \quad (2.3)$$

where  $\eta$  is the conversion efficiency, and depends on the impedance match between the antenna and the rectifier circuit, as well as the DC load impedance. The reflection coefficient,  $\rho$ , in turn is a nonlinear function of power and frequency. The estimated conversion efficiency is calculated by:

$$\eta = \frac{P_{RF}}{P_{DC}} \quad (2.4)$$

### 2.3.2 Power density of RF sources

Power Density is defined as the power received per unit area at a distance  $R$  from an omnidirectional transmitter. Radio Frequency (RF) propagation is defined as the travel of electromagnetic waves through or along a medium. For RF propagation between approximately 100 MHz and 10 GHz, radio waves travel very much as they do in free space and travel in a direct line of sight and a slight. For air, the dielectric is 1 [15]. In antennas theory, an isotropic radiator is a theoretical, lossless, omnidirectional (spherical) antenna [15]. That is, it radiates uniformly in all directions. The power of a transmitter that is radiated from an isotropic antenna will have a uniform power density in all directions. Power density at any distance  $R$  from an isotropic antenna is the ratio of the transmitted power by the surface area of a sphere ( $4\pi R^2$ ) at that distance. The surface area of the sphere increases by the square of the radius, therefore the power density,  $P_D$ , decreases by the square of the radius.

$$P_D = \frac{P_t}{4\pi R^2} \quad (2.5)$$

The effect of the distance  $R$  can be demonstrated using Figure 2.3.

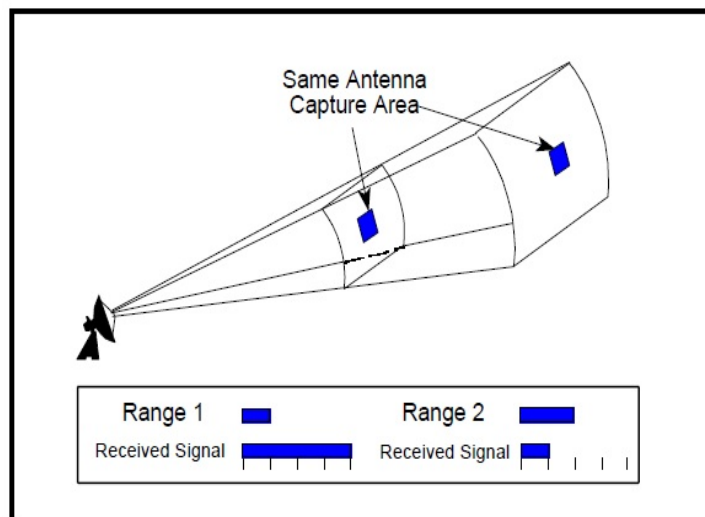


Figure 2.3: Effect of Range on Power Density

From Figure 2.3, it is obvious that in order to harvest maximum energy from RF

sources, it is important to be as close to the transmitting stations as possible. However, this may not be practical because the position of the harvester will be primarily dictated by the position of the WSN.

The received power can be estimated using the Friis transmission equation. The Friis transmission equation relates the RF power received and the RF power transmitted. It can be used to predict the received power given the transmitted power, the distance from the transmitter and the antenna gains. The Friis transmission equation defines the relationship between transmitted power and received power in an arbitrary transmit/receive antenna system. Given arbitrarily oriented transmitting and receiving antennas shown in Figure 2.4, the power density at the receiving antenna ( $W_r$ ) is [8];

$$W_r = \frac{P_t}{4\pi R^2} G_t(\theta_t, \phi_t) = e_{ot} \frac{P_t}{4\pi R^2} D_t(\theta_t, \phi_t) \quad (2.6)$$

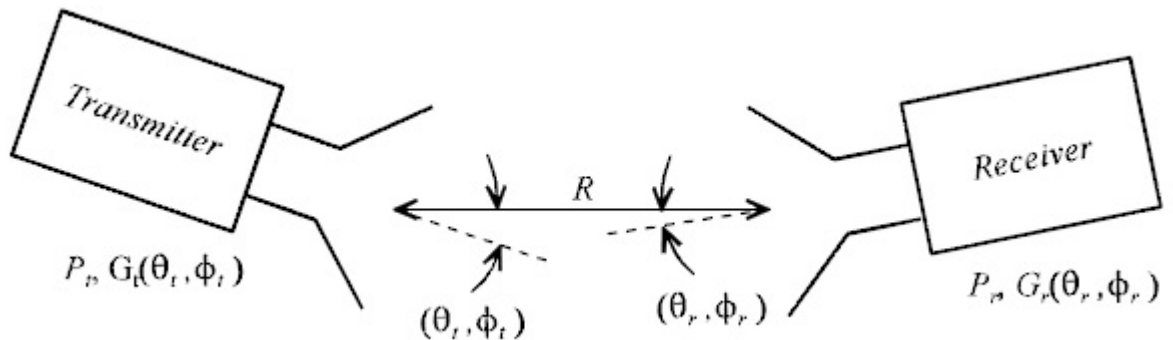


Figure 2.4: Arbitrary transmit/receive antenna system

Where  $P_t$  is the input power at the terminals of the transmit antenna and where the transmit antenna gain and directivity for the system performance are related by the overall efficiency

$$G_t(\theta_t, \phi_t) = e_{ot} D_t(\theta_t, \phi_t) = e_{cdt} (1 - |\Gamma|^2) D_t(\theta_t, \phi_t) \quad (2.7)$$

where  $e_{cdt}$  is the radiation efficiency of the transmit antenna and  $\Gamma$  is the reflection coefficient at the transmit antenna terminals. This definition of the transmit antenna gain includes the mismatch losses for the transmit system in addition to the conduction and dielectric losses. A manufacturer's specification for the antenna gain will not include the mismatch losses. The total received power delivered to the terminals of the receiving antenna ( $P_r$ ) is

$$P_r = W_r A_{er} \quad (2.8)$$

where the effective aperture of the receiving antenna ( $A_{er}$ ) must take into account the orientation of the antenna. For an antenna oriented for maximum response, the effective aperture is

$$A_{er} = e_{or} \left( \frac{\lambda^2}{4\pi} \right) D_{or} \quad (2.9)$$

For an arbitrarily oriented antenna, the effective aperture is

$$A_{er}(\theta_r, \phi_r) = e_{or} \left( \frac{\lambda^2}{4\pi} \right) D_r(\theta_r, \phi_r) \quad (2.10)$$

The total power received will then be

$$P_r = e_{or} e_{ot} \left( \frac{\lambda^2}{4\pi} \right) D_r(\theta_r, \phi_r) D_t(\theta_t, \phi_t) P_t \quad (2.11)$$

Such that the ratio of the received power to transmitted power becomes

$$\frac{P_r}{P_t} = e_{or} e_{ot} (1 - |\Gamma_t|^2) (1 - |\Gamma_r|^2) \left( \frac{\lambda^2}{4\pi} \right) D_r(\theta_r, \phi_r) D_t(\theta_t, \phi_t) \quad (2.12)$$

When polarisation losses at the transmitter and receiver ( $a_t$  and  $a_r$ ) are considered, Equation (2.12) becomes

$$\frac{P_r}{P_t} = e_{or} e_{ot} (1 - |\Gamma_t|^2) (1 - |\Gamma_r|^2) \left( \frac{\lambda^2}{4\pi} \right) D_r(\theta_r, \phi_r) D_t(\theta_t, \phi_t) (a_t \cdot a_r) \quad (2.13)$$

For antennas aligned for maximum response, reflection-matched and polarization

matched, the Friis transmission equation reduces to

$$P_r = P_t G_t G_r \left[ \frac{\lambda}{4\pi R} \right]^2 \quad (2.14)$$

where

$P_r$  is the received power

$P_t$  is the transmitted power

$G_t$  is the gain of the transmitter antenna

$G_r$  is the gain of the receiver antenna

$R$  is the distance between the transmitter and the receiver

$\lambda$  is the wavelength of the RF wave signal

But

$$\lambda = \frac{c}{f} \quad (2.15)$$

where

$c$  is the speed of light

$f$  is the frequency of the wave

The Friis equation can then be written as follows

$$P_r = P_t G_t G_r \left[ \frac{c}{4\pi R f} \right]^2 \quad (2.16)$$

Due to polarisation mismatch, a coefficient of Polarisation Loss Factor (PLF) is introduced into the equation

$$P_r = PLF \times P_t G_t G_r \left[ \frac{c}{4\pi R f} \right]^2 \quad (2.17)$$

When the received power is expressed in dB, a simplified form of the Friis equation can be obtained by evaluating the  $\log_{10}$  on both sides of Equation (2.17) to obtain:

$$P_{r_{dB}} = P_{t_{dB}} + G_{t_{dB}} + G_{r_{dB}} + FSPL_{dB} \quad (2.18)$$

where  $FSPL$  is the free space path loss, given by

$$\begin{aligned}
 FSPL &= \left[ \frac{4\pi R}{\lambda} \right]^2 \\
 &= \left[ \frac{4\pi Rf}{c} \right]^2
 \end{aligned} \tag{2.19}$$

A convenient way to express FSPL in terms of dB is given below;

$$\begin{aligned}
 FSPL(dB) &= 10 \log_{10} \left[ \frac{4\pi Rf}{c} \right]^2 \\
 FSPL(dB) &= 20 \log_{10}(R) + 20 \log_{10}(f) + 20 \log_{10} \left( \frac{4\pi}{c} \right)
 \end{aligned} \tag{2.20}$$

The value of  $c$  is known, and if the distance is expressed in km and the frequency in MHz, then FSPL is given by

$$FSPL_{dB} = 20 \log_{10}(R) + 20 \log_{10}(f) + 32.45 \tag{2.21}$$

When Equation (2.21) is substituted into Equation (2.18), the resultant Friis equation becomes.

$$P_r = P_t + G_t + G_r - (20 \log_{10}(R) + 20 \log_{10}(f) + 32.45) \tag{2.22}$$

### 2.3.3 Mathematical analysis of FM signals

Modulation is a special technique employed in signal communication. The information signal can rarely be transmitted as it is, it must go through modulation, this involves superimposing the information signal with a carrier wave. There are three forms of modulation namely:

1. **Frequency Modulation (FM):** the instantaneous frequency is varied while the amplitude remains constant

2. **Amplitude Modulation (AM):** this technique of modulation involves varying the amplitude of the signal while the frequency remains constant
3. **Phase Modulation (PM):** the phase angle of the signal is varied while other parameters remain constant

Frequency modulation (FM) is most often associated with communication systems. In communication systems the baseband signal has a bandwidth similar to that of speech or music (8 kHz to 20 kHz) [16], and the modulating frequency is several orders of magnitude higher. The FM radio band is 88 MHz to 108 MHz.

If the baseband data signal (the message) to be transmitted is  $x_m(t)$  and the sinusoidal carrier is  $x_c(t) = A_c \text{Sin}(2\pi f_c t)$  where  $f_c$  is the carrier's base frequency and  $A_c$  is the carrier's amplitude, the modulator combines the carrier with the baseband data signal to get the transmitted signal as given by Equation (2.23) [16].

$$y(t) = A_c \text{Sin} \left( 2\pi \int_0^t f(\tau) d\tau \right) \quad (2.23)$$

This can be rewritten as

$$y(t) = A_c \text{Sin} \left( 2\pi \int_0^t [f_c + f_\Delta x_m(\tau)] d\tau \right)$$

or

$$y(t) = A_c \text{Sin} 2\pi \left( f_c t + f_\Delta \int_0^t x_m(\tau) d\tau \right) \quad (2.24)$$

In Equations (2.23) and (2.24),  $f(\tau)$  is the instantaneous frequency of the oscillator and  $f_\Delta$  is the frequency deviation, which represents the maximum shift away from  $f_c$  in one direction, assuming  $x_m(t)$  is limited to the amplitudes  $\pm 1$ . Mathematically, a baseband modulated signal may be approximated by a sinusoidal continuous wave signal with a frequency  $f_m$ . The integral of such a signal is:

$$\int_0^t x_m(\tau) d\tau = \frac{A_m \text{Sin}(2\pi f_m t)}{2\pi f_m} \quad (2.25)$$

Substituting Equation (2.25) into (2.24) yields

$$y(t) = A_c \text{Sin} \left( 2\pi f_c t + \frac{f_\Delta}{f_m} \text{Sin}(2\pi f_m t) \right) \quad (2.26)$$

where  $f_m$  is the highest frequency component present in the modulating signal and the amplitude  $A_m$  of the modulating sinusoid is represented by the peak deviation  $f_\Delta$ .

The term  $\frac{f_\Delta}{f_m}$  is known as modulation index, expressed as  $\beta$ . The modulation index  $\beta$ , is expressed as the ratio of the peak frequency deviation to the modulating frequency, and is thus varied by varying the modulating frequency. As can be seen from Equation (2.26),  $\beta$  is equal to the peak deviation caused when the signal is modulated by the frequency of the modulating signal; therefore,  $\beta$  is a function of both the modulating signal amplitude and frequency. Furthermore,  $\beta$  can take on any value from 0 to infinity. Its range is not limited as it is for AM.

Equation (2.26) can be rewritten in the form

$$y(t) = A_c R e^{j(f_c t + \beta \text{sin} f_m t)} \quad (2.27)$$

Equation (2.27) can be recast into

$$y(t) = A_c R e^{j f_c t} e^{j \beta \text{sin} f_m t}$$

The second part of the exponential function can be expressed as

$$e^{j \beta \text{sin} f_m t} = \sum_{n=-\infty}^{\infty} J_n \beta e^{j n f_m t} \quad (2.28)$$

Substituting Equation (2.28) into (2.27) will yield

$$y(t) = A_c R e^{j f_c t} \times \sum_{n=-\infty}^{\infty} J_n \beta e^{j n f_m t}$$

Or

$$y(t) = A_c R \sum_{n=-\infty}^{\infty} J_n \beta e^{j(f_c t + n f_m t)} \quad (2.29)$$

When Equation (2.29) is plotted in MatLab, the graph produced is as shown in Figure 2.5. The curves of Figure 2.5 show the relation between the carrier and sideband amplitudes of the modulated wave as a function of the modulation index  $\beta$  in terms of Bessel Functions. The carrier component  $J_0$  and the various sidebands  $J_n$  go to zero amplitude at specific values of  $\beta$ . From these curves it is possible to determine the amplitudes of the carrier and the sideband components in relation to the unmodulated carrier. For example, for a modulation index of  $\beta = 3$  the following amplitudes are realised.

Carrier	$J_0 = -0.27$
First Order Sideband	$J_1 = 0.33$
Second Order Sideband	$J_2 = 0.48$
Third Order Sideband	$J_3 = 0.33$

From Figure 2.5, it can be deduced that:

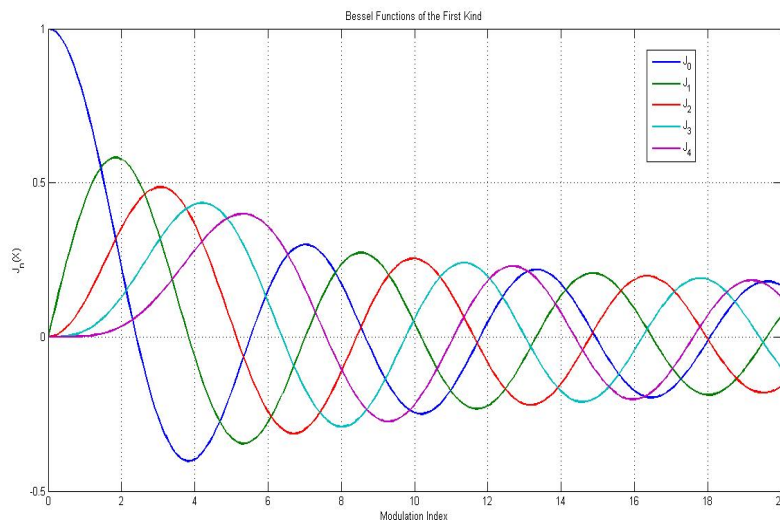


Figure 2.5: Graph of Bessel functions of an FM signal

1. The number of significant spectral components is a function of  $\beta$ . When  $\beta \ll 1$ , only  $J_0$ , and  $J_1$ , are significant so that the spectrum will consist of carrier plus two sideband components.
2. A large value of  $\beta$  implies a large bandwidth since there will be many significant sideband components.
3. Carrier and sidebands null many times at special values of  $\beta$ .

The above information can be represented by an amplitude spectrum of FM signal for particular values of  $\beta$  as shown in Figure 2.6. From the foregoing properties, it can be concluded that the number of significant sidebands  $n$  is affected by  $\beta$ , while the bandwidth  $B_T$  of an FM signal is determined by the number of significant sidebands. Therefore,  $\beta$  has a direct effect on the bandwidth of the signal and the two are related through Equation (2.30) [16].

$$B_T \approx 2(\beta + 1)f_m \quad (2.30)$$

In FM commercial radio stations the modulating signal is not just a simple sinusoid as discussed previously, but a more complex audio signal such as speech or music. Each radio station modulates its specific carrier by an audio signal producing a modulated signal that occupies a small band of frequencies centered about the station's carrier frequency. As shown in Figure 2.7, the signal received by an antenna consists of the signals sent from all stations, whose signals are spaced far

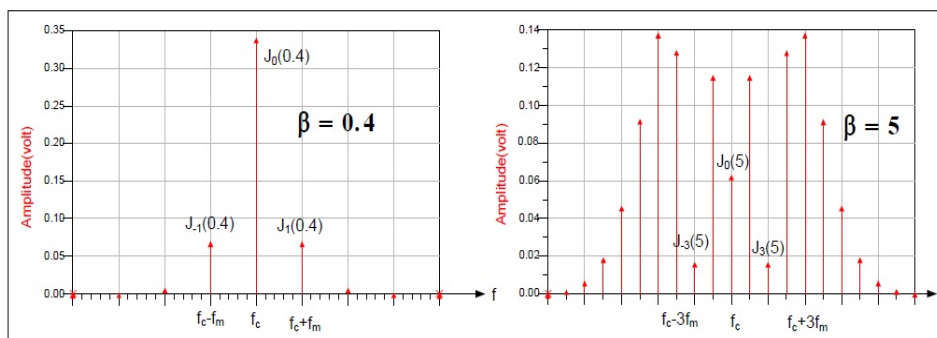


Figure 2.6: Amplitude Spectrum of FM signal for  $\beta = 0.4$  and  $\beta = 5$

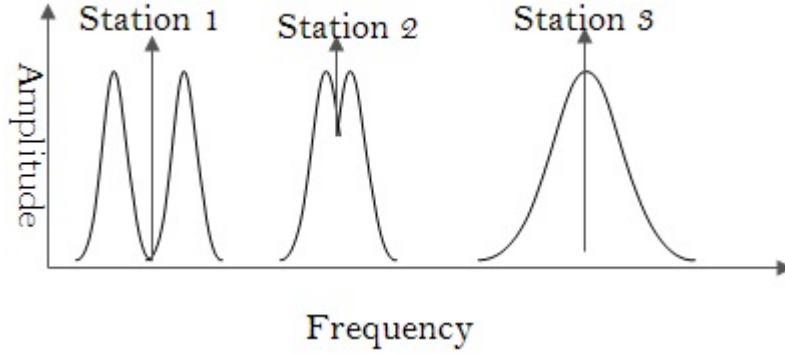


Figure 2.7: Band Separation in FM broadcasting [17]

enough to prevent overlap.

In most countries, AM radio stations are spaced 20 KHz apart and FM radio stations are spaced 200 KHz apart [17]. Tuning of the radio dial selects one of the small frequency bands of a given station. A demodulator in the radio extracts the modulating audio signal from the received signal. FM radio has a number of performance advantages over AM radio, including better power efficiency and noise rejection, but FM radio provides these advantages at the expense of using a larger channel bandwidth of 200 KHz. The energy contained in any continuous-time signal  $x(t)$  is defined as [17]

$$E_s = \langle y(t) \rangle = \int_{-\infty}^{\infty} |x(t)|^2 dt \quad (2.31)$$

In the case of FM signals, the energy present can be expressed as

$$E_s = \langle y(t) \rangle = \int_{-\infty}^{\infty} \left| A_c \cos \left( 2\pi f_c t + \frac{f_\Delta}{f_m} \cos(2\pi f_m t) \right) \right|^2 dt \quad (2.32)$$

Equation (2.32) demonstrates the fact that energy is available in FM signals and this research sought to harvest this energy and optimise it to power a WSN.

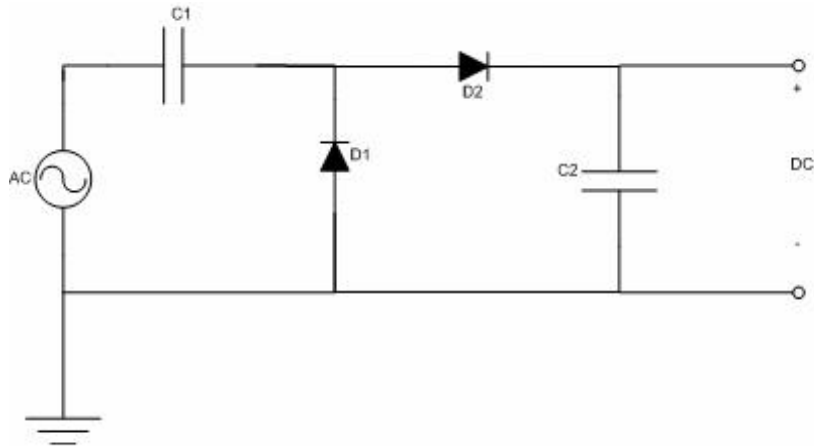


Figure 2.8: Single stage voltage doubler

## 2.4 Usage and storage of harvested RF energy

The voltage from the RF energy harvested is first boosted to suitable levels using a voltage multiplier. It is then stored for usage by the the load, the storage device could either be a rechargeable battery or a supercapacitor.

### 2.4.1 Voltage multiplier

The signal received from RF sources is usually very low to directly power devices, it is therefore, necessary to boost it to higher levels using circuit configurations that do not require any external powering. A voltage multiplier is a specialized rectifier circuit producing an output which is theoretically an integer times the AC peak input, for example, 2, 3, or 4 times the AC peak input [18]. A voltage doubler is the most widely used rectifier circuit which consists of two diodes or diode-connected transistors and two coupling capacitors, and provides an output voltage that is about twice the input signal amplitude. Figure 2.8 shows a single stage voltage multiplier

The voltage doubler circuit is essentially composed of two sections in cascade. The first section is a clamped capacitor circuit composed of  $C_1$  and  $D_1$ . Assuming ideal

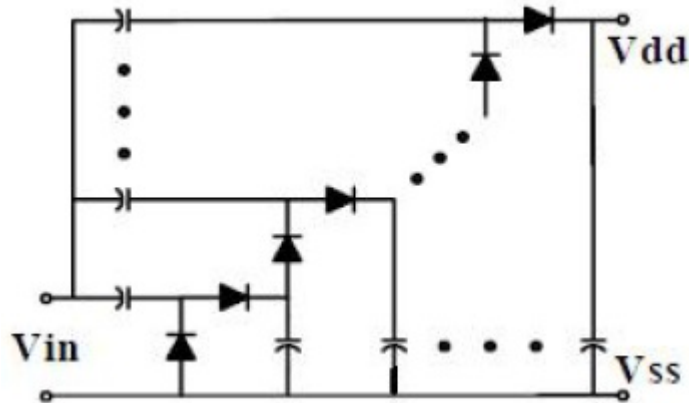


Figure 2.9: Multiple stage voltage multiplier.

diodes, when this circuit is excited by a sinusoid of amplitude  $V_p$ , it provides a voltage waveform similar to the input but shifted up by  $V_p$  across diode  $C_1$ . While the negative peaks are clamped to 0 V, the positive peaks reach  $2V_p$ . The second section is a peak rectifier circuit that is formed by  $D_2$  and  $C_2$ . In response to the voltage across the first diode, this circuit provides a DC voltage of magnitude  $2V_p$  across capacitor  $C_2$ . Since in the ideal case the output voltage is double the input voltage amplitude, the circuit is called voltage doubler [13].

In the ideal operation, during the negative half cycle of the AC input source, diode  $D_1$  conducts while diode  $D_2$  is off. Thus all the voltage drops across capacitor  $C_1$  and charges it up to the peak amplitude of the input signal. During the positive half cycles  $D_2$  is forward biased while  $D_1$  is reverse biased. Hence both the source voltage and the voltage stored on  $C_1$  drop across  $C_2$  charging it up to a DC value equal to two times the input signal amplitude

Multiple stages of the basic doubler circuit can be cascaded to provide higher output voltages. As depicted in Figure 2.9. The output of each stage provides the DC input of the next stage, while the direct coupling from the source provides the AC input for each stage. Despite achieving higher output voltage, the increase in number of stages degrades conversion efficiency due to increase in power dissipation.

The trade-offs involved in cascading voltage doubler stages have to be investigated to determine the optimum number of stages that will provide sufficient voltage levels without compromising the efficiency of the system.

### 2.4.1.1 Voltage multiplier configurations

The way a voltage doubler is cascaded to form a multistage multiplier can produce a variety of configurations, but all have the same building block of a single voltage doubler. The most common multiplier configurations are shown in Figure 2.10. Each configuration provides a unique set of merits that would justify its choice over the other configurations, the performance of a voltage multiplier is mainly judged by the output voltage and RF to DC conversion efficiency.

The multiplier operates in two modes: transient mode and steady-state mode, both of which are shown in Figure 2.11. Transient mode occurs when the charge pump is first turned on. Before being turned on, the stage capacitors and the

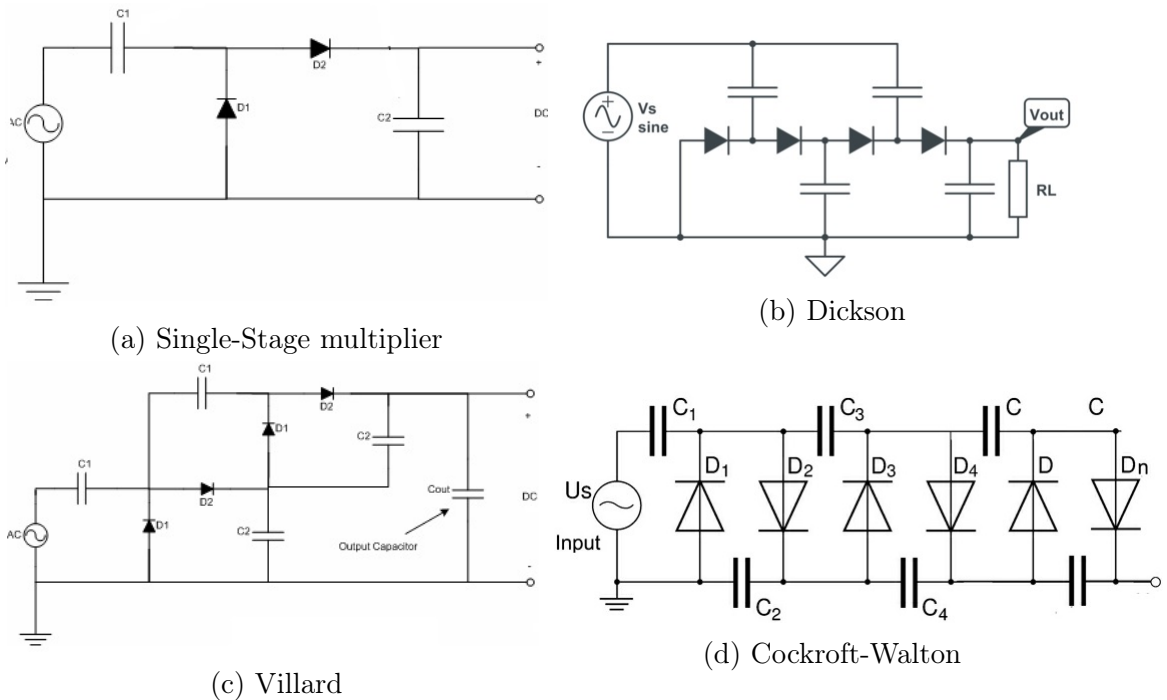


Figure 2.10: Common configurations for voltage multipliers

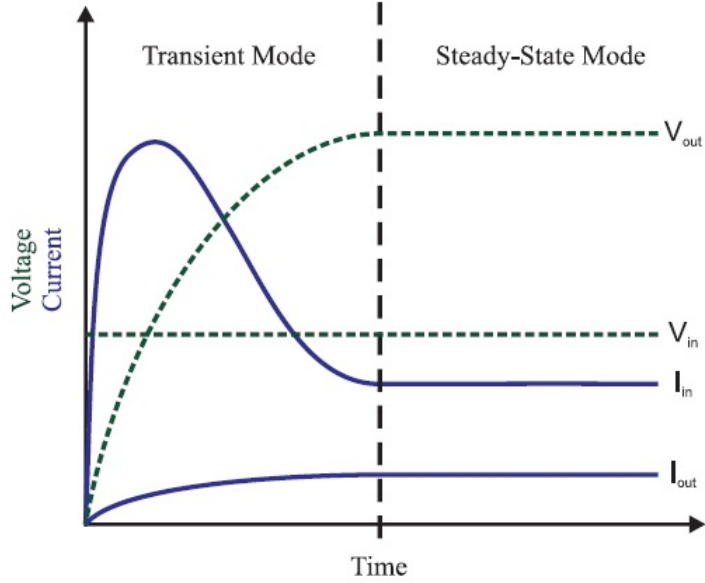


Figure 2.11: Transient and steady modes of a voltage multiplier. [19]

output capacitor hold no charge. They must be charged up to reach steady state mode. During transient mode, the source provides much more current than during steady-state mode. This extra current is used to charge up the capacitors. Steady-state mode occurs when the capacitors operate under charge balance.

A straightforward DC steady-state analysis of the doubler circuit with non-ideal identical diodes yields the following expression for the output voltage.

$$V_{out} = 2n(V_{in} - V_d) \quad (2.33)$$

where  $n$  is the number of stages,  $V_{in}$  is the amplitude of the input RF signal, and  $V_d$  is the voltage drop across each rectifying element, i.e. a p-n junction diode or a diode-connected transistor [13]. For the case of ideal diodes with no threshold voltage, Equation (2.33) simplifies to  $V_{out} = 2nV_{in}$  as expected. In order to optimise  $V_{out}$ ,  $V_d$  has to be as low as possible. This can be achieved by selecting diodes with very low Forward voltage. Schottky diodes are specially designed to have very low  $V_d$  for small signal applications. Schottky diodes are suitable

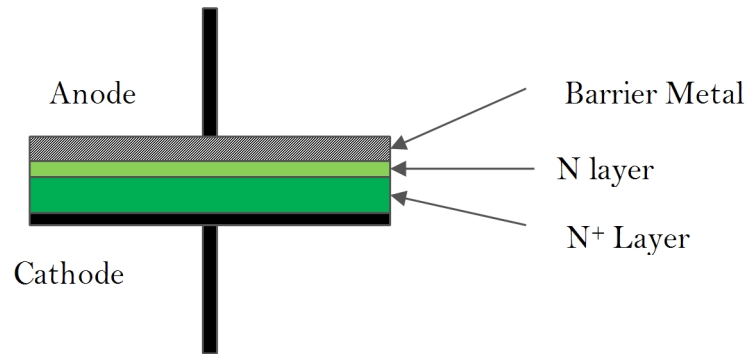


Figure 2.12: Construction of a Schottky diode.

due to their inherently low turn on voltage, low conduction resistance and low junction capacitance [20]. In addition, diodes in the voltage multiplier must have a switching time smaller than the period of the input signal. Schottky diodes are preferred because they are typically faster than normal diodes [21]. Furthermore, higher saturation current can be obtained using Schottky diodes which in turn results in higher conversion efficiency. The Schottky diode is an important device which is widely used in radio-frequency (RF) applications. Unlike conventional semiconductor diodes, which consist of a PN junction, the Schottky diode is made from a metal semiconductor junction as shown in Figure 2.12. This offers a number of advantages in some circumstances as the diode has a very low forward-voltage drop, and secondly it has a very fast switching speed. Both of these properties make it ideal for many RF applications as well as giving it uses in many other areas.

In terms of RF applications, it is particularly useful because of its high switching speed and high-frequency capability. Schottky diodes are similarly very good as RF detectors as their low capacitance and forward-voltage drop enable them to detect signals which an ordinary PN junction would not see. The Schottky diode can be modelled as shown in Figure 2.13. Where  $C_j$  is the junction capacitance and  $R_j$  is the junction resistance.

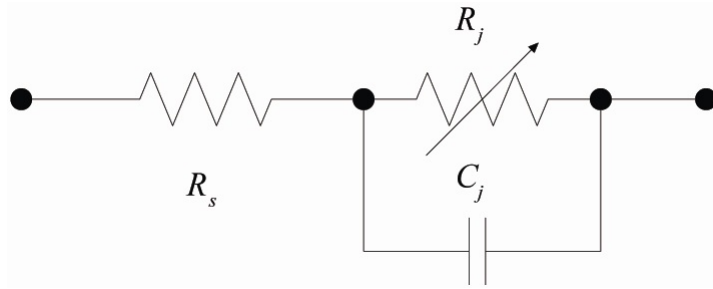


Figure 2.13: Equivalent circuit of a Schottky diode.

#### 2.4.1.2 Input/Output relationship of a multiplier

The relationship between the input and the output of a multiplier can be expressed in terms of the voltage of the received signal at the input and the output D.C voltage at the output of the multiplier. This form of input/output equation was presented by [19] in detail. The output voltage  $V_{out}$  of an N-stage multiplier with an input voltage  $V_{in}$  was proved to be

$$V_{out} = \frac{(N + 1)(V_{in} - V_t)}{1 + \frac{N}{fCR_L}} \quad (2.34)$$

This equation describes how the output behaves when design parameters are changed. Output voltage increases as more stages ( $N$ ) are added, but also loses  $V_t$  increases as each stage is added which will present a limit to the increase in  $V_{out}$  as  $N$  increases. The fractional term in the denominator,  $\frac{N}{fCR_L}$ , also suggests that the frequency, stage capacitance and the load resistance affects the output voltage.

#### 2.4.1.3 Power efficiency of the multiplier

Power efficiency is defined as the ratio of power that makes it to the output without getting dissipated over the power supplied [22]. It can be expressed in terms of its individual components as

$$\eta = \frac{P_{out}}{P_{in}} = \frac{V_{out}I_{out}}{V_{in}I_{in}} \quad (2.35)$$

When the expressions for  $V_{out}$ ,  $I_{out}$  and  $I_{in}$  as derived by [19] are substituted into Equation (2.35), the resultant equation for efficiency becomes

$$\eta = \frac{\left(1 - \frac{V_t}{V_{in}}\right)}{1 + \frac{N}{fCR_L}} \quad (2.36)$$

Equation (2.36) shows how the circuit parameters affect power efficiency. Increasing frequency, stage capacitance, and load resistance all increase efficiency as well as decreasing the number of stages. Efficiency becomes almost frequency independent for  $f > \frac{N}{CR_L}$ . Efficiency also depends on input voltage. For large inputs, the  $\frac{V_t}{V_{in}}$  term is negligible, and efficiency becomes large. For small inputs, the  $\frac{V_t}{V_{in}}$  term dominates, and efficiency becomes small. This circuit is only useful for scenarios where  $V_{in} > V_t$  [19]. In summary, for maximum efficiency

$$\frac{V_t}{V_{in}} \approx 0 \quad (2.37)$$

$$\frac{N}{fCR_L} \approx 0 \quad (2.38)$$

The diodes are the only circuit components that dissipate power besides the load resistor, and their threshold voltage is fairly constant for any diode current. Reducing the current passing through the diodes for any given load resistance will increase power efficiency. Large loads require less current than small loads for the same output voltage. Large stage capacitors absorb less charge than small capacitors for constant frequency. Reducing the number of stages reduces the number of diodes. All of these things reduce the current through the diodes and increase power efficiency. Equation (2.37) points to the fact that the voltage drop across the diodes should be minimum for maximum efficiency which validates the selection of Schottky diodes, which have very low forward bias voltage  $V_F$ .

#### 2.4.1.4 Ripple voltage of the multiplier output

The input/output equation gives a value for the maximum voltage the output can be. Output ripple voltage determines how far the output voltage drops from the final value given in Equation (2.34). The load may require that voltage does not drop below a certain percentage of its specification. If it does, the load device may turn off, break, or do something else that is undesired. So, it is important to determine what the output ripple voltage will be based on circuit parameters.

The output capacitor usually has different capacitance than the stage capacitors because it directly influences the magnitude of the output ripple voltage,  $\Delta V_{out}$ , whereas the stage capacitors directly influence  $V_{out}$ . Stage capacitance does affect ripple voltage indirectly. It is primarily chosen to control the output voltage.  $C_{out}$  is commonly chosen to be large in order to reduce output ripple voltage [22]. The difference in capacitor size affects the voltage gained by  $C_{out}$  during charge transfer. The relationship between  $\Delta V_{out}$  and  $V_L$  is found by equating charge lost by the last stage capacitor with capacitance  $C$  and charge gained by  $C_{out}$ .

$$Q_L = CV_L = C_{out} \Delta V_{out}$$
$$\Rightarrow \Delta V_{out} = \frac{C}{C_{out}} V_L \quad (2.39)$$

The ratio of capacitor size is an important design parameter because it affects the size of the output ripple voltage. We let the ratio of output capacitance to stage capacitance be  $\zeta$  defined as

$$\zeta = \frac{C_{out}}{C} \quad (2.40)$$

Also, percent ripple voltage, or  $\frac{\Delta V_{out}}{V_{out}}$  is a common specification for the output of a DC to DC converter. We let the percent ripple voltage be  $\alpha$  defined as

$$\alpha = \frac{\Delta V_{out}}{V_{out}} \quad (2.41)$$

After substitution, Equation (2.41) can be re-arranged to become

$$\frac{C_{out}}{C} = \frac{V_L}{\Delta V_{out}}$$

Then, a substitution for  $V_L$  as derived by [19] is made, resulting in

$$\frac{C_{out}}{C} = \frac{I_{out}}{fC \Delta V_{out}} \quad (2.42)$$

Then, using Ohm's Law to replace  $I_{out}$ , Equation (2.42) becomes

$$\frac{C_{out}}{C} = \frac{V_{out}}{R_L fC \Delta V_{out}} \quad (2.43)$$

Finally, the substitutions for  $\eta$  and  $\alpha$  are made resulting in

$$\eta = \frac{1}{R_L fC \alpha} \quad (2.44)$$

Then, the expression for output voltage ripple factor is

$$\alpha = \frac{\Delta V_{out}}{V_{out}} = \frac{1}{R_L fC_{out}} \quad (2.45)$$

## 2.4.2 Common approaches used in powering WSNs

Storing and using the harvested energy is one of the most important aspects of an energy harvester. Once the energy has been conditioned using the appropriate circuitry, it can either be used by the WSN directly or stored. Using the harvested

energy directly is usually very challenging due to the fact that the power output from the harvester is not constant and varies proportionally as the input power. Secondly, the harvested power is usually less than the required power and thus the harvester may fail to power the WSN directly.

Storing the harvested energy is the most practical and most commonly used approach to power WSNs. The harvested energy can be directly stored in a battery which will then supply the power to the WSN or it can be stored in a capacitor which then discharges through the battery. The value of the capacitance has an effect on the life of the battery, smaller values will result in quicker but shorter charging pulses while a larger value will result in slower but longer charging pulses [23,24].

### **2.4.3 Supercapacitors**

Supercapacitors also known as ultracapacitors differ from regular capacitors in that they have very high capacitance [25]. Traditional capacitors store energy by means of static charge while a supercapacitor stores energy by means of static charge and chemical reactions. Supercapacitors have high frequent charge and discharge cycles at high current and short duration, and operate at voltage range of 2.5-2.7V. Despite having high capacitance, these capacitors cannot be used to power devices directly due to the non-linear nature of their output. They are therefore commonly used to recharge batteries or supply power to the load during short power blackouts or interruptions. Figure 2.17 shows basic construction of a supercapacitor and Table 2.3 compares the supercapacitor with a typical Li-ion battery.

The time required to charge a typical supercapacitor is about 10 seconds, the charging characteristics is similar to that of a normal battery and is primarily affected by the charging circuit. The supercapacitor has little tendency to go into

Table 2.3: Comparison between Li-Ion battery and Supercapacitor [26]

PARAMETER	SUPERCAPACITOR	LITHIUM-ION
Charge time	1-10 seconds	10-60 minutes
Cycle life	1 million or 30,000h	500 and higher
Cell voltage	2.3 - 2.75V	3.6-3.7V
Specific energy (Wh/Kg)	5	100-200
Specific power (W/Kg)	Upto 10,000	1,000-3,000
Cost per Wh	20.00 dollars	0.5-1.00 dollars
Service life	10-15 years	5-10 years

overcharge and therefore does not require full-charge detection. Unlike the electrochemical battery, the supercapacitor can be charged and discharged an unlimited number of times, giving it an edge over other types of energy storage components. Additionally its efficiency drops by only 20 per cent in a span of 10 years. However, the stored energy of a supercapacitor drops more quickly than that of a conventional electrostatic capacitor or a battery, this is attributed to the fact that a supercapacitor has higher leakage current than a normal capacitor or battery [27].

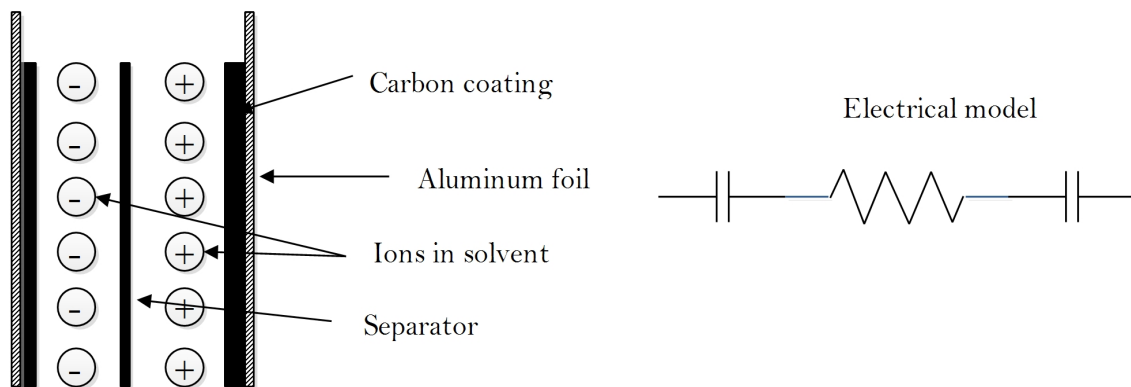


Figure 2.14: Construction of a supercapacitor [23]

## 2.5 Previous work on RF energy harvesting and optimisation

One way of improving the harvester's efficiency is to optimise the parameters of the components used in the harvester's circuit. This can be achieved experimentally or with the help of a software. Mikeka and Arai [9] considered optimising the RF energy harvester circuit by optimising the conversion efficiency of the RF energy harvesting circuit under stringent conditions such as arbitrary polarisation, low power incidences and varying incident power densities. They optimised the harvesters power output by selecting the optimum operating conditions for the harvester using Advanced Design Simulation (ADS) software.

The study involved designing a modified Digital Television (DTV) antenna printed on FR4 substrate. The antenna fed the signal to an RF-DC converter that was made from Schottky diodes. The Schottky diodes were selected to produce very efficient conversion rates between the input and the output. The research also investigated the effect of Schottky diode's junction capacitance and resistance, the harvester was then used to carry out experiments on low power DTV rectenna and medium power rectenna placed at a distance of less than 100m from the transmitter. They were able to power a wide range of low power sensors and produced voltage levels of up to 3.7 V when there is no load on the harvester.

Molnar et al. [28] investigated the possibility of designing an ultra-low power transceiver for WSNs. They optimized the circuit by minimising the power consumption of the circuit from the battery. The study investigated the effect of reusing the bias current of the circuit to run other low power components in the circuit. They included a single high-Q off-chip inductor to drive all other RF circuits. Their research showed that the circuit consumed 1.3 mW while radiating

250  $\mu\text{W}$  of power and consumed 1.2 mW when receiving the signal. The sensitivity of the transceiver was maintained at 94 dBm and was able to send and receive at a distance of 16 m when operated indoors.

Another research was carried out by Kavuri et al. [29]. The research investigated the optimisation of the voltage doubler stages in an energy conversion module for RF energy harvesting system at 900 MHz band. The function of the energy conversion module was to convert the RF signals into direct-current (DC) voltage at the given frequency band to power the low power devices/circuits. The design was based on the Villard voltage doubler circuit. A 7 stage Schottky diode voltage doubler circuit was designed, modelled, simulated, fabricated and tested in their work. Multisim was used for the modelling and simulation work. Simulation and measurements were carried out for various input power levels at the specified frequency band. For an equivalent incident signal of  $\approx 40$  dBm, the circuit could produce 3 mV across a 100 K $\Omega$  load. The results also showed that there was a multiplication factor of 22 at 0 dBm and produces DC output voltage of 5.0 V.

Negin et al. [30] carried out a research on RF harvesting using voltage doublers. In their work the operation of a MOSFET based rectifier, composed of multiple stages of voltage doubler circuits used for RF energy harvesting, was investigated. Analytical modelling of the input stage of the rectifier consisting of short-channel diode-connected transistors was carried out, and the equivalent input resistance obtained was used along with simulation results to improve impedance matching in the harvester. The criteria for voltage boosting and impedance matching, that are essential in the operation of energy harvester under low ambient RF levels, as well as the design considerations for a  $\pi$ -match network to achieve matching to 50  $\Omega$ , were elaborated on. In addition their application was demonstrated through simulations carried out using Advanced Design System (ADS) simulator. Furthermore,

measurement results of an already fabricated dual-band RF harvester were presented, and the approach taken to improve the antenna design from the harvester chip measured input impedance was discussed. The integrated antenna-harvester system tested was capable of harvesting ambient RF power and generating DC output voltage levels above 1 V.

Another optimisation research was carried out by Anchustegui et al. [31]. The work involved optimisation of voltage output at low input RF power. At low power levels, e.g., -10 dBm and below, the corresponding voltage amplitude at the antenna is low compared to the voltage drop of the diodes used in the rectifier. In order to boost the voltage at the rectifier input and thus the rectifier efficiency, an L-network optimized for an input power of -10dBm at 868MHz was proposed in this work. As for the rectifier, a half-wave rectifier with a single zero-bias Schottky diode (HSMS2850) was selected. First, a theoretical analysis was performed followed by simulations with ADS (Harmonic Balance) software. Simulations show efficiencies of 75% for an input power of -10 dBm with ideal components. But by using the actual model of the diode rectifier, the incorporation of the PCB layout effects and the actual components decreases the efficiency to below 50%. Finally, a PCB implementation was performed using a 0.5 pF capacitor and a 27 nH inductor for the L network. The input power was generated by an RF generator. The RF-to-DC efficiency was of 45% at 868 MHz with an optimum load of 2.5 K $\Omega$ . Efficiencies of 34.5% and 22.5% were achieved at -15 dBm and -20 dBm, respectively.

Nintanavongsa et al. [32] also carried out an optimisation research, the study established analytically as well as experimentally, that energy harvesting circuits perform differently under different input power densities. It was established that circuits that have high efficiency under low power density will have poor efficiency

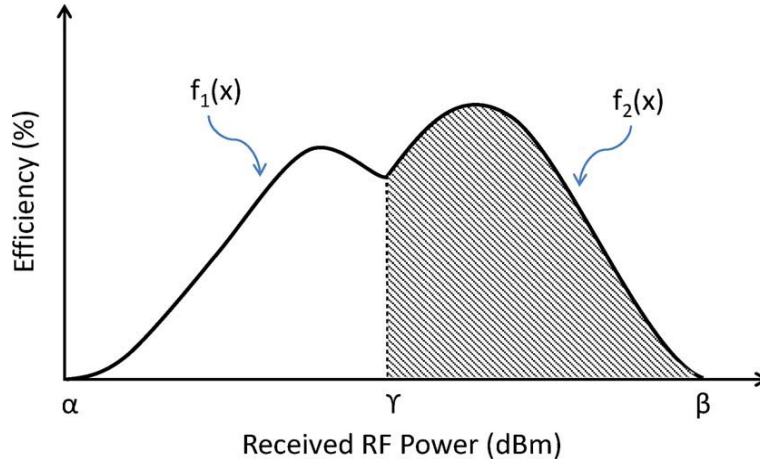


Figure 2.15: Crossover point for LPD and HPD [32]

under high power densities. Therefore, the study proposed a dual-stage energy harvesting circuit composed of a seven-stage and ten-stage design using HSMS 2852 and HSMS 2822 Schottky diodes for each design respectively, the former being more receptive in the low input power regions, while the latter is more suitable for higher power range. Each stage used was a modified Cockroft-Walton voltage multiplier, arranged in series. The study provided guidelines on precise selection of the crossover operational point for these two stages between the high (20 dBm) and low power (-20 dBm) extremities. The study showed that there exists a certain point where the efficiencies of the two systems cross over as shown in Figure 2.15.

Figure 2.15 shows the two efficiency curves of energy harvesting sister-circuits. The efficiency curves  $f_1(x)$  and  $f_2(x)$  belong to low power density (LPD) and high power density (HPD) circuits, respectively. The crossover point,  $\gamma$ , is the point where one of these two circuits become the lead contributor to the total harvested energy. Thus, the LPD is operational if the RF input power is lower than  $\gamma$ , otherwise the HPD circuit is operational. The energy harvesting circuit was simulated using Agilent Advanced Design System (ADS) software using the harmonic balanced analysis. Under extremely low power range of -20 dBm to 0 dBm. The

prototype gives an output voltage of 1 V at -10 dBm and 1.9234 V at -6 dBm, respectively. At these two particular points, the prototype has an efficiency of 10% and 14.73% which are 10  $\mu$ W and 37  $\mu$ W respectively.

Bouchouicha et al. [1] investigated the power densities from broadband and narrow band systems. The research also investigated the effect of the antenna and load on the harvested energy. The results showed that the energy harvested from both the broad and narrow band systems was too low to directly power a low power device, but could be stored in a capacitor or a micro battery. The research also concluded that the choice of load and antenna had an effect on the harvested energy due to impedance matching.

Arrawatia et al. [7] studied the feasibility of harvesting energy from cell tower in the frequency band of 900MHz. The cell towers they investigated were broadcasting a CDMA signal. The research used a broadband electromagnetically coupled Square microstrip antenna (SMSA) and yielded promising results. The harvester developed was able to produce voltages of 0.87 V when a single stage voltage doubler was used and 2.78 V when a six stage voltage doubler was used. The effect of using Schottky diodes on the circuit was also analysed. The results showed that the voltage levels increased considerably when Schottky diodes were used. This could be attributed to the low threshold voltage of 230 mV.

Hagerty et al. [8] carried out a research on efficient broadband RF energy harvesting for wireless sensors. The study involved a theoretical and experimental analysis on broadband signals using a dual circularly polarized wideband rectenna "wallpaper" array and an efficient power processing circuitry. Each spiral antenna element received one of the two circular polarizations and coupled the incident power to a Schottky diode, without any additional matching or harmonic tuning circuitry. The primary challenge for the power processor was to continuously ex-

tract energy from the rectenna source at the peak power point despite variations in the incident power and rectenna efficiency, while efficiently integrating the energy to a storage element and delivering regulated power to a sensor load. They were able to achieve and maintain an efficiency of 70% over a wide range of output voltages at a constant input power of  $10 \mu\text{W}$ .

Harrist [12] carried out a research on an RF energy harvester used to charge a phone. In the study, a charge pump with peak detector circuit was used, the circuit discharged when the stored charge was maximum and started recharging before the charge dropped to zero as shown in Figure 2.16. [12]

The research utilised a commercially available quarter-wave whip antenna with a seven stage voltage doubler with an output capacitor to harvest RF energy from a 915 MHz signal transmitted from a dedicated transmitter. SPICE was used to carry out optimisation of the circuit parameters. The software allowed the user to input a range of values for a given parameter and then specifies the value of increment for each of the parameters in order to detect the range of values that would yield maximum output power. The research showed that as number of stages increased, the output voltage also increased, but the voltage stabilized when the number of stages reached 6. Any additional stage resulted in a decrease in the out-

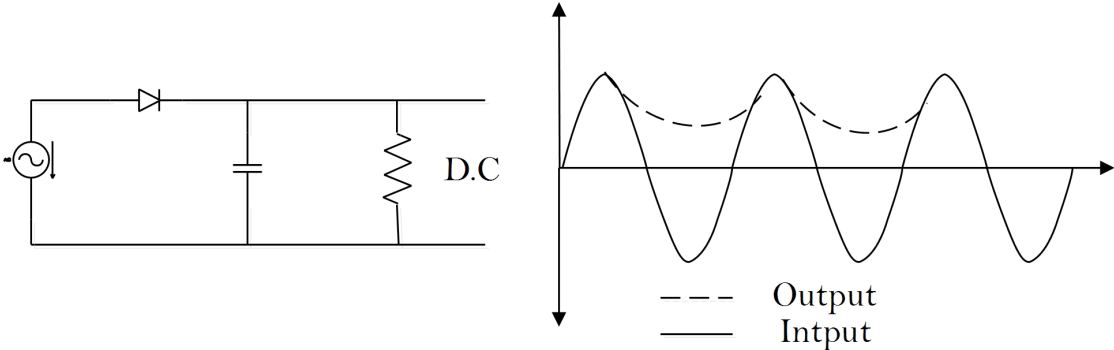


Figure 2.16: Charge pump [12]

put voltage and this could be explained by the fact that the voltage gain becomes negligible as the number of stages reach six, any additional stage will consume power without having any effect on the output voltage.

The harvester was tested on two phones. The first was a Nokia 3570 which required a power of 1.26 Watts to charge the battery, and the second phone was a Motorola V60i which required a power of 2.36 Watts to charge the battery. The harvester was able to only power the phones for a short while and then failed to sustain the power levels required due to low energy output levels. But the harvester was able to recharge the batteries when the phones were off. The study showed that the harvester reduced the charging time of the mobile phone batteries by half [12].

Sim et al. [33] investigated the possibility of enhancing the power harvested by an RF harvester by optimising the antenna design. The research used two antenna designs and evaluated the power output from each design in a soil wireless sensor network. The first design was a low-profile folded shorted patch antenna (FSPA) and the second design was a modified FSPA structure. A dedicated transmitter was used to supply microwave energy at frequencies of 867 MHz and 2.45 GHz to the sensor nodes. The harvester was able to produce power levels of 1.5-2.2 mW, this value is considerably high from an RF harvester, but since the study used a dedicated transmitter, the harvested power is much less than the power transmitted, which caused the efficiency to be very low.

Zungeru et al. [15] researched on optimising the battery life by refining the power management algorithm in WSN nodes. The research used an Improved Energy Efficient Ant Based Routing Algorithm (IEEABR). In this algorithm, it was possible to efficiently manage the power from the battery so that the WSN nodes only get power when they needed it. The study experimented on two commercial WSN nodes using powercast's TX91501 Transmitter and P1110 and P2110 RF receiver.

Two different antennas were used on the receiver circuit. The first was a dipole antenna while the second was a patch antenna, the battery recharge time from these two setups was then measured and compared. The set up in which a patch antenna was used took almost twice as long to recharge the battery as the one that used a dipole antenna.

The research also established that the harvested energy reduced exponentially as the distance between the receiver and the transmitter increased, but the patch antenna has a better reception at longer distances than the dipole antenna. The study also managed to show that the IEEABR was able to increase the battery life by 91.9 hours.

Another research which was carried out by Hong et al. [34] investigated the performance of a Wi-Fi harvester, the study utilised a 7-stage Cockcroft-Walton multiplier with equal stage capacitance of 1  $\mu\text{F}$  and an output capacitance of 1 nF. The study also showed that there is a limit to the number of stages that can be cascaded to achieve maximum voltage output by the multiplier, this was due to the build-up in parasitic capacitances of the components and junction capacitances of the Schottky diodes used. The research identified that seven stage rectification is optimum under low input power. Lower voltage was attained with 8 stage circuit when input signal was unable to overcome parasitics from increased diodes. ADS simulation results showed that 7 stage rectifier with low pass filter (LPF) had the best performance below -5 dBm input signal with extra voltage gain over standalone rectifier. Experimental results concurred that 7 stages was indeed optimum. In the context of boosting higher output voltage, the research utilised a multilayer ceramic Band Pass Filter (BPF). The results were verified on an Integrated BPF and LPF with 7 stage rectifier on 1.57 mm RO5880 laminate it was observed that the minimum input power to achieve 2 V improved from -8 dBm

(0.16 mW) to -9 dBm (0.13 mW) while using this approach.

Noguchi and Arai [35] carried out a research that harvested energy from FM signals. The research presented a small loop antenna and high output voltage rectifier in wide frequency band for RF energy harvesting of FM broadcasting signals. Input power level of -20dBm was used to design a loop antenna for DC output voltage-boosting. The RF energy harvesting on suburb area provided a 924 mV DC output for a single rectenna and 1.72 V DC output for twin rectennas by receiving several FM broadcasting signals simultaneously.

## 2.6 Research gaps

From the researches that have so far been carried out, it can be seen that considerable effort has been put to investigate the possibility of harvesting energy from RF sources such as DTV, GSM and AM. However, the energy that has been harvested by the previous researchers is still low to power commercial devices. In addition, very little research has been carried out to investigate the possibility of harnessing the energy from FM signals despite their abundance [35]. This research therefore, sought to design, optimise and analyse the performance of an FM harvester to be used in WSN.

# 3. METHODOLOGY

## 3.1 Introduction

In order to harvest a significant amount of energy from RF sources, it is important to optimise the harvester to operate at its optimum. This will ensure sufficient power is available for the WSN, the aim of optimisation is to increase the harvesters efficiency given by Equation 2.4.

All design processes are guided by a set of values or conditions called constraints. Constraints represent some functional relationships among the design variables and other design parameters satisfying certain physical phenomenon and certain resource limitations [36]. In the case of this research work, the major constraint is the power input to the XBee WSN used. The harvester must supply at least the threshold voltage to charge the battery in the XBee transmitter in order for the design to be considered viable. The XBee is shown in Figure 3.1 and it's operating parameters are shown in Table 3.1.



Figure 3.1: XBee Wireless Sensor Node [37]

Table 3.1: Operating Parameters of XBee WSN Node [37]

<b>PARAMETER</b>	<b>VALUE</b>
Supply Voltage	2.8-3.4 V
Transmission Current	45 mA (at 3.3 V)
Reception Current	50 mA (at 3.3 V)
Transmission Range	30 m Indoor 90 m Outdoor (with line-of-sight)
Operating Frequency	2.4 GHz
Receiver Sensitivity	-92 dBm
RF Data Rate	250,000 bps

From Table 3.1, it can be seen that the battery will be required to produce a minimum voltage of about 2.8 V while supplying a current of 45 mA to the transmitter in order for the data to be successfully transmitted, this translates into 126 mW of power. Therefore, the harvester has to produce at least 2.8 V to replenish the charge lost by the battery.

## 3.2 Design of the FM harvester

During the design of the harvester, the system is broken into its constituent subsystems. These are:

### 3.2.1 Antenna design

The antenna is the first element in the harvester and is responsible for capturing RF signals and feed them into the harvester. Due to scope, a simple off the shelf FM antenna was selected for the design. A  $50\Omega$  4-segment ground plane copper antenna of length 1 m was selected for this application. This antenna is a commercial radio antenna, it is therefore expected to offer a good reception for signals

within the FM range. Figure 3.2 shows the selected antenna.



Figure 3.2: Selected antenna

The output from this antenna was analysed by connecting it to a Tektronix TDS 2014B digital oscilloscope as shown in Figure 3.2. The signal received by the antenna is shown in Figure 3.3. Figure 3.3 shows that the antenna detected a saw-toothed signal with an amplitude of 548 mV. This voltage is sufficiently higher compared to those obtained by other researchers such as [1, 9, 28, 30]. The signal received is a superposition of several FM signals and their cumulative frequency is about 50 kHz.

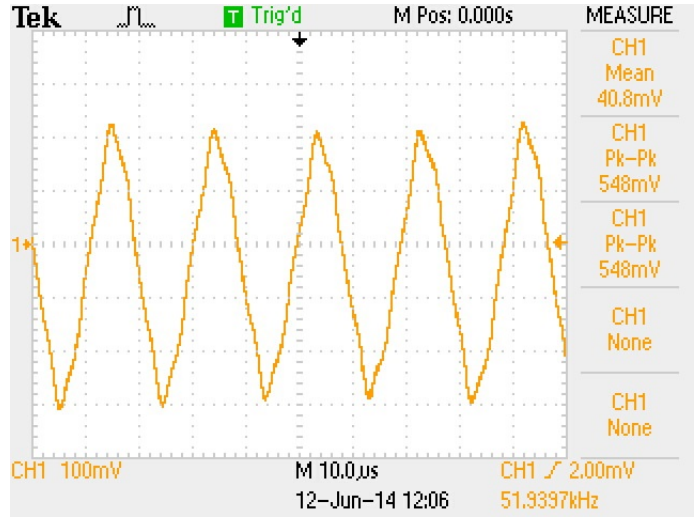


Figure 3.3: FM Antenna output

### 3.2.2 Band pass filter design

A band pass filter enables a particular band, or spread, or frequencies to be filtered from a wider range of mixed signals [39]. Filter circuits can be designed to accomplish this task by combining the properties of low-pass and high-pass into a single filter as shown in Figure 3.4. [38]

In order to minimise loss of power in the filter, a passive RLC band pass filter will be utilised instead of an active one. This type of filter is a two pole second order band pass filter because it utilises two components with reactive impedance as shown in Figure 3.5. The filter is designed to allow frequencies between the upper and the lower limits,  $F_H$  and  $F_L$ , represented by 80 MHz and 108 MHz

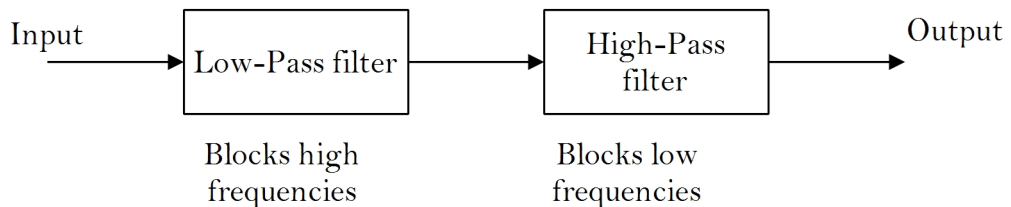


Figure 3.4: Flow diagram of a Band Pass Filter

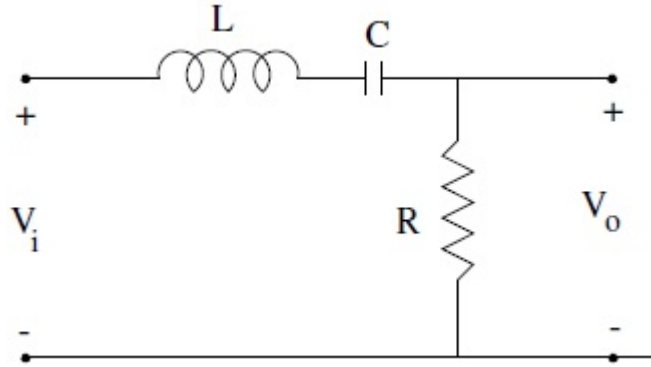


Figure 3.5: Passive RLC Band Pass Filter

respectively. The centre frequency will be:

$$F_C = \sqrt[2]{F_L \times F_H} \quad (3.1)$$

$$= \sqrt[2]{80 \times 108} \times 10^6 = 92.95 \text{ MHz}$$

The centre frequency can be expressed in rad/s as:

$$\omega_0 = 2 \times \pi \times 92.95 \times 10^6 = 5.84 \times 10^8 \text{ rad/s}$$

The band-width (B) and Q-factor(Q) for this filter will be:

$$B = F_H - F_L = (108 - 80) \times 10^6 = 28 \text{ MHz} \quad (3.2)$$

$$Q = \frac{F_C}{B} = \frac{92.95}{28} = 3.32 \quad (3.3)$$

Since  $Q$  and  $\omega_0$  are known, the value of  $R$  is set to  $50\Omega$  so that it matches with the antennas impedance. The value of  $C$  is then obtained using Equation (6.5) from appendix F.

$$C = \frac{1}{RQ\omega_0} = \frac{1}{50 \times 3.32 \times 2\pi \times 92.95 \times 10^6} = 1.03 \times 10^{-11} \text{ F} \approx 10 \text{ pF}$$

A 10 pF capacitor will thus be used. The final step is to calculate the inductance  $L$ , Equation (6.4) gives the inductance as:

$$L = \frac{QR}{F_C} = \frac{3.32 \times 50}{92.95 \times 10^6} = 1.786 \times 10^{-6} H \approx 1.8 \mu H$$

A standard 1.8  $\mu H$  inductor is chosen. The final filter circuit was simulated using LTSPICE IV to verify its operation and the results are presented in Chapter 4.

### 3.2.3 Voltage multiplier design

During the design of the multiplier, for small input voltages of between 0-1V, a ripple factor of 0.03 is considered for this application in order to limit power loss [43]. The load resistance of the WSN is 73  $\Omega$  and the frequency of the incidence signal can be obtained from Figure 3.3 as 50 KHz. The value of  $C_{out}$  can then be calculated using Equation (2.45) as:

$$C_{out} = \frac{1}{R_L f \alpha} = \frac{1}{73 \times 50 \times 10^3 \times 0.03} = 9.13 \times 10^{-6} \approx 10 \mu F$$

A 10  $\mu F$  capacitor is used at the output to limit the ripple factor and consequently limit power loss. Another important component of the voltage multiplier is the diode, the diode to be used has to have a very low forward voltage drop as was depicted in Equations (2.33), (2.36) and (2.37). In addition, they must have fast switching speeds to handle signals in the FM range. The most suitable choices for the diode were found to be HSMS 2820 and HSMS 285X. These diodes are from Agilent Technologies and they are suitable for harvesting energy from weak signals because they have voltage sensitivity of 40 mV/ $\mu W$  and 45 mV/ $\mu W$  and forward voltage of 150 mV and 340 mV for HSMS 285X and HSMS 2820 at 915MHz respectively [40]. Since the HSMS 285X diodes have lower forward voltage, it were chosen for this application

The next thing to be considered in the design of the multiplier are the stage

capacitors and the number of stages. According to Equations (2.36) and (2.38) fewer stages are favourable for efficiency. However, Equation (2.33) shows that if the number of stages ( $n$ ) is low, the output voltage will consequently be low. On the other hand, a high capacitance in the multiplier stages is favourable for efficiency as depicted in Equation (2.38), but if the capacitance is too high it will not be able to fully charge within the short cycles provided by the FM signals. Therefore, the optimum value of the stage capacitance and the number of stages will be determined through computer simulations.

### **3.3 Computer simulation of the FM harvester sub-systems**

The computer simulations were carried out using LTSPICE IV. The simulations were carried out to verify the design of the bandpass filter and the WSN as well as determine the optimum values for the stage capacitance and number of stages for the voltage multiplier circuit.

#### **3.3.1 Simulation of the RLC band pass filter**

The band pass filter was designed in section 3.2.2 and the values obtained were used in the simulation. The filter schematic used in the simulation is shown in Figure 3.6. The input to the filter was set to be a sine wave of amplitude of 1 V, the circuit was analysed using the a.c analysis function and the output voltage was plotted against a frequency range of 1 MHz to 100 GHz. The operation of the filter was verified by observing the magnitude of the output voltage within the mentioned range. The results are presented in Chapter 4.

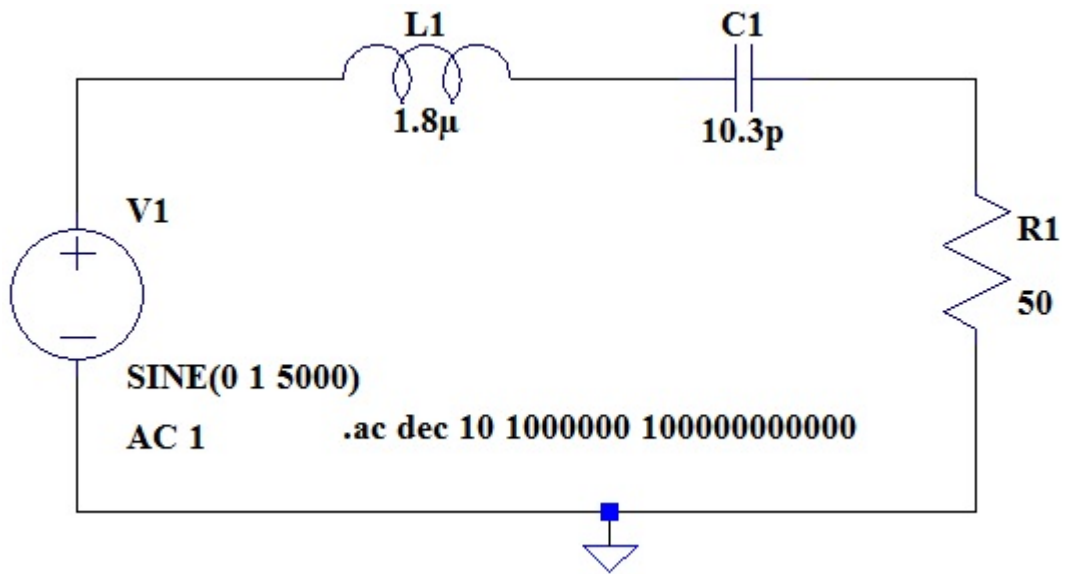


Figure 3.6: LTSPICE IV model of the designed RLC filter

### 3.3.2 Simulation of voltage multiplier

The multiplier was simulated to determine the effect of stage capacitance and number of stages on the performance of the multiplier. Through this, it will be possible to determine the optimum values for these two parameters. A multi-stage Cockroft-Walton multiplier configuration was chosen because it occupies less space than Villard multipliers and produce slightly higher voltage than Dickson multiplier [22]. The schematic of the single stage multiplier is shown in Figure 3.7.

In order to simulate the multiplier schematic, the SPICE DIRECTIVE command was used to incorporate the HSMS 285X Schottky diodes into the simulation software since they are normally not available in the software library. In the directive, SPICE parameter for the diodes are specified so that the software can determine the behaviour of the component when the simulation is run. The SPICE parameters of the HSMS 285X are shown in Table 3.2. After the schematic has been drawn, a transient response analysis was carried out to determine the behaviour of output voltage, current and power over time.

Table 3.2: SPICE parameters of HSMS 285X [37, 40]

Symbol	Parameter	Units	Value
IS	saturation current	A	22e-9
RS	ohmic resistance	$\Omega$	6
CJO	zero-bias junction capacitance	F	0.7e-12
EG	band-gap energy	eV	0.69
M	grading coefficient	-	0.5
N	emission coefficient	-	1.08
Vpk	peak voltage	V	15
mfg	manufacturer	-	Agilent

Table 3.2 shows a few of the parameters that need to be specified to fully describe a diode in the SPICE environment. The DC characteristics of the diode are determined by the parameters IS, N, and the ohmic resistance RS. Charge storage effects are modeled by a transit time, TT, and a nonlinear depletion layer capacitance

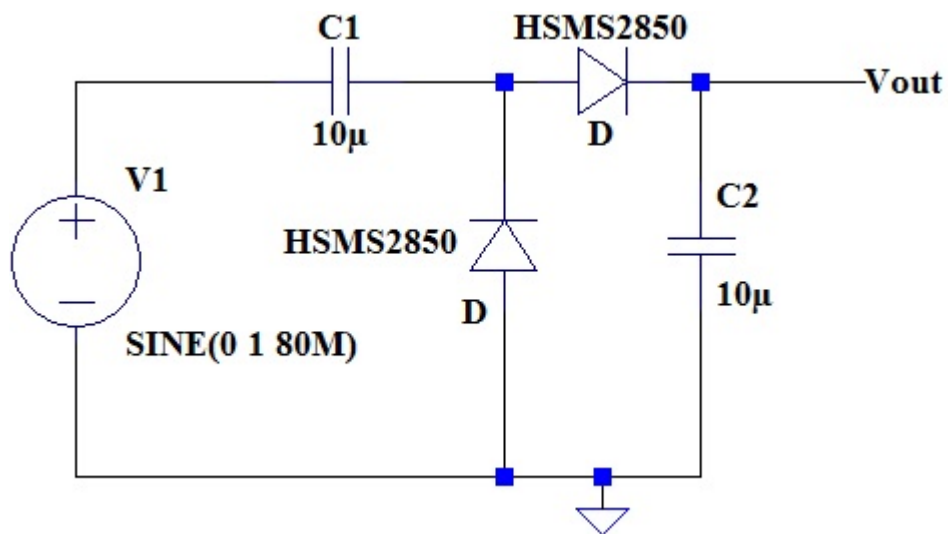


Figure 3.7: Circuit Model of single stage multiplier in LTSPICE IV

which is determined by the parameters CJO, junction potential VJ, and M. The temperature dependence of the saturation current is defined by the parameters EG, the band gap energy and XTI, the saturation current temperature exponent. Reverse breakdown is modeled by an exponential increase in the reverse diode current and is determined by the parameters BV, the reverse breakdown voltage and IBV, current at breakdown voltage, both of which are positive numbers.

The effect of stage capacitance was investigated by giving the multiplier a fixed 80 MHz FM input of 2 V and varying the value of the capacitance from 100 pF to 100 mF in multiples of 10. At each value, the output voltage, power and current was recorded. From the output power, the efficiency of the multiplier was also calculated for different capacitance values. The optimum value of the stage capacitance was then determined based on the efficiency.

After the value of the stage capacitance was determined, the effect of the number of stages was also determined by giving the multiplier a fixed 80 MHz FM input of 1 V and determining the output voltage, power, current and efficiency at the node of each stage in a 13-stage Cockcroft-Walton(CW) multiplier, each node was assigned a netlist label (V1-V13). The schematic of the 13-stage multiplier used is shown in Figure 3.8. The optimum number of stages was also determined based on the efficiency.

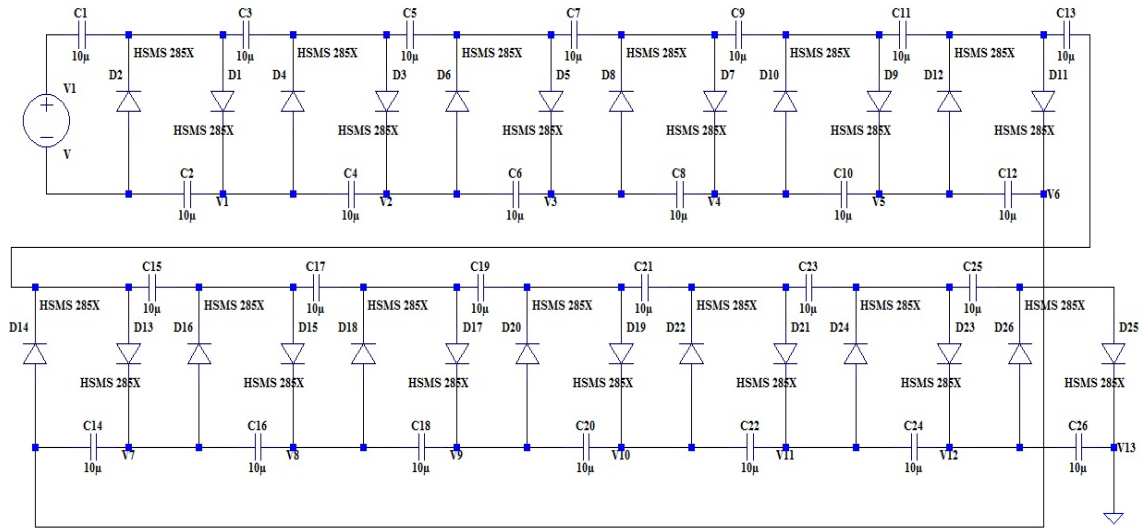
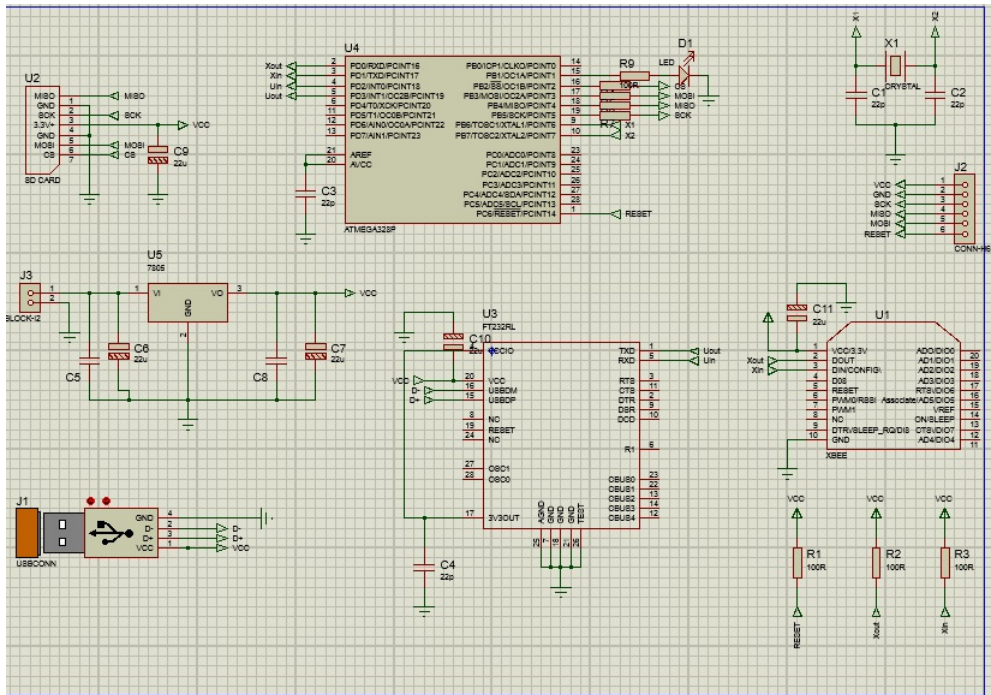


Figure 3.8: Circuit Model of 13-stage CW multiplier in LTSPICE IV

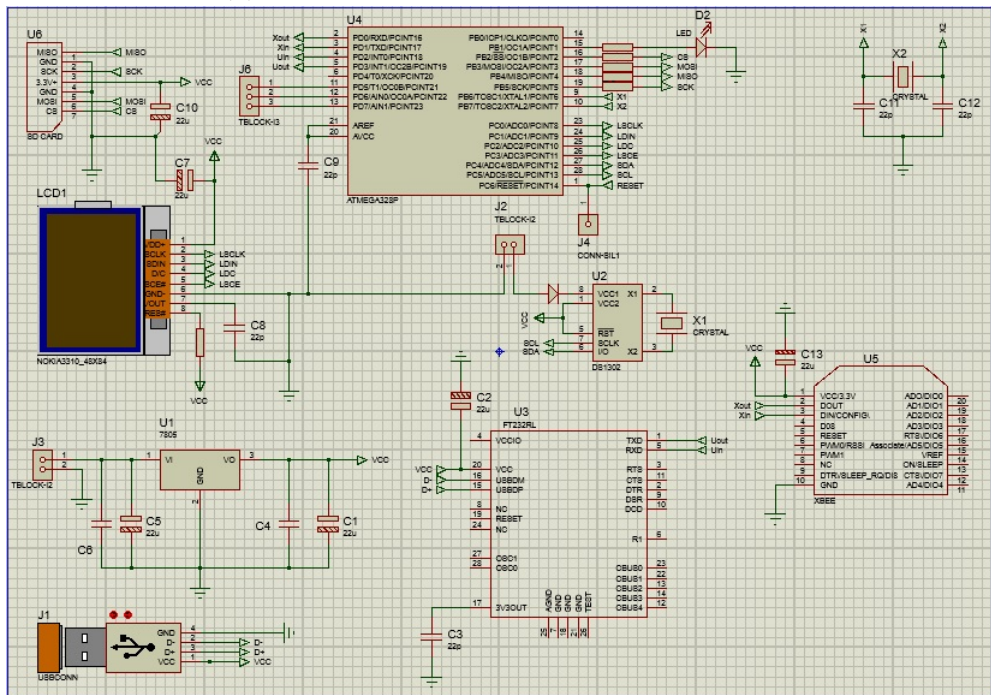
### 3.3.3 Simulation of WSN

The WSN was implemented using an XBee transceiver, a pair was used where one acted as the transmitter and the other as the receiver. The circuit designs of the transmitter and the receiver were developed using Proteus and are shown in Figure 3.9(a)-(b).

After the design was carried out, the operation of the WSN was verified by giving the transmitter known message strings and receiving them at the receiver. The PCB layout was generated using the same software. The layout of the sensors was also designed and is shown in Figure 3.10. However in the actual implementation, the force/pressure sensor was replaced with a potentiometer for simplicity purposes.



(a) Circuit design of the transmitter



(b) Circuit design of the receiver

Figure 3.9: Circuit designs for the XBee transceiver

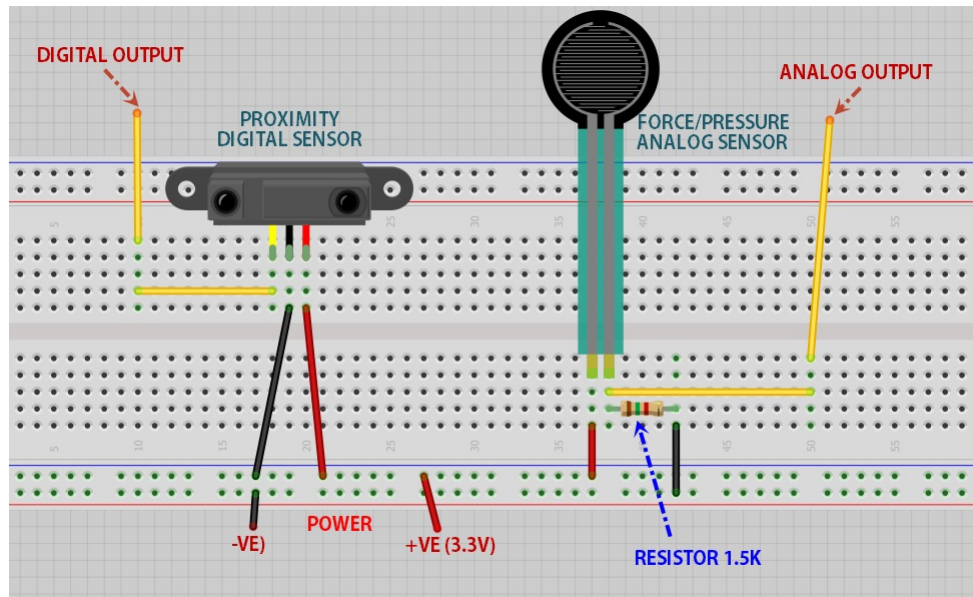


Figure 3.10: Layout of sensors

### 3.4 Development and analysis of the performance of the FM harvester

To experimentally analyse the performance of the FM harvester and integrate it into the WSN, the actual circuits were implemented on a PCB and were assembled with the antenna to form the harvester.

#### 3.4.1 Implementation of the FM harvester

After the computer simulations have been carried out on the multiplier, the actual circuit was fabricated based on the optimum values obtained from the simulations. Figure 3.11 shows the multiplier PCB fabricated for this research. The input to the multiplier was achieved from the antenna through the filter. The output of the multiplier was fed to a 3200 mAh rechargeable battery used by the WSN.

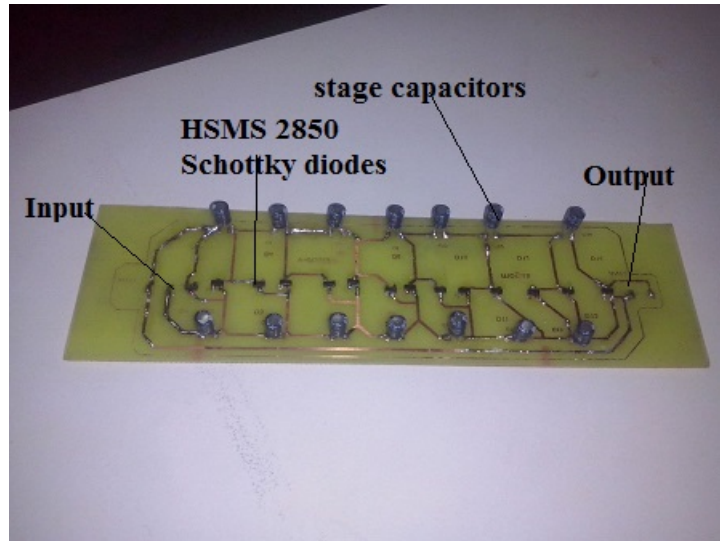


Figure 3.11: Multiplier PCB

### 3.4.2 Analysis of the performance of the harvester

To analyse the performance of the harvester system, all the sub-systems were assembled together and the performance was analysed by monitoring the output while giving known inputs to the system. The input to the multiplier was achieved through GWINSTEK SFG 2120 Synthesized signal generator. This signal generator can produce FM signals in the range of 0 Hz-100 MHz.



Figure 3.12: FM mode of the signal generator

Figure 3.12 shows the FM mode in the generator. The output from the multiplier was then connected to the Tektronix TDS 2014B 3digital oscilloscope and the graphs were saved on a flash drive through the USB port. Figure 3.13 shows the set-up used in this analysis.

The effect of input power, input frequency and load resistance was analysed by varying each of these variables at a time while monitoring the output power, voltage and current of the harvester. The efficiency of the harvester was obtained by comparing the output power to the input power.

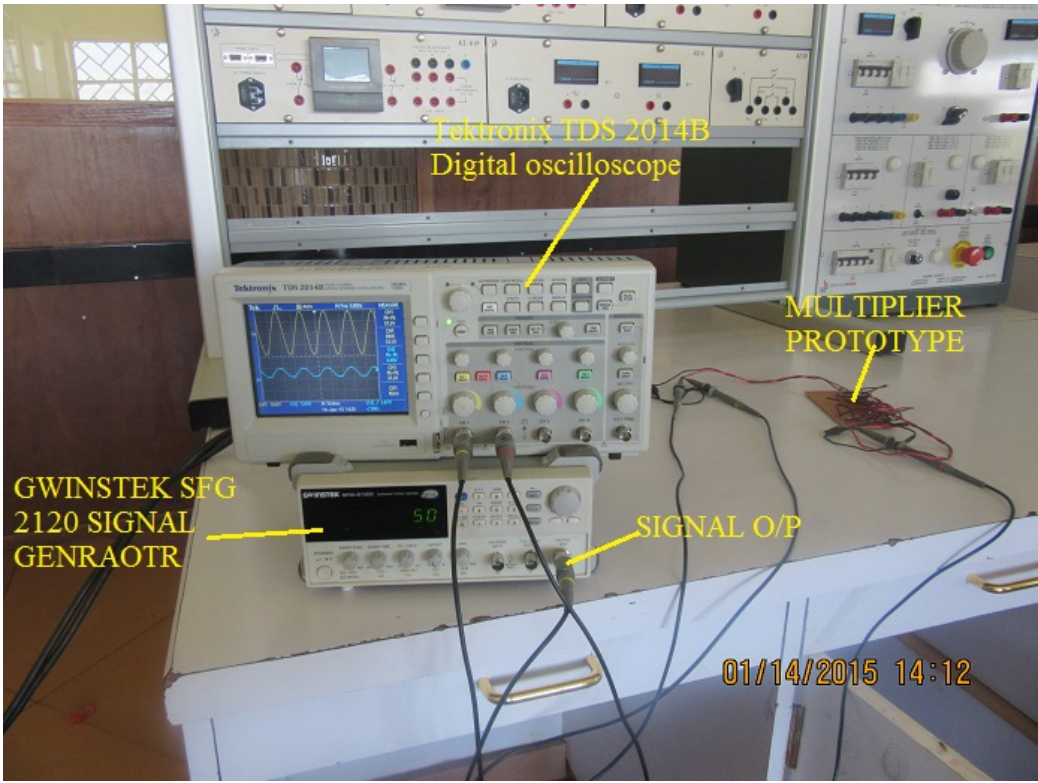


Figure 3.13: Experimental analysis of the FM harvester

### 3.4.3 Measurement of signal strength

The strength of the signals in the area was analysed in order to determine the frequency range that will present the highest power density. High power density results in higher output at the harvester. The power density was measured using

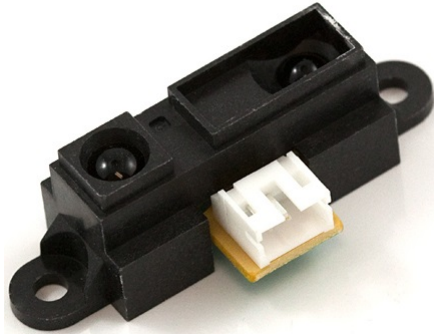
the FSM/LA field strength meter. Figure 3.14 shows the field strength meter that was used. In order to get the actual output voltage from the antenna, a digital multimeter was connected at the EXT. VOLTIMETER terminals to measure the output voltage.



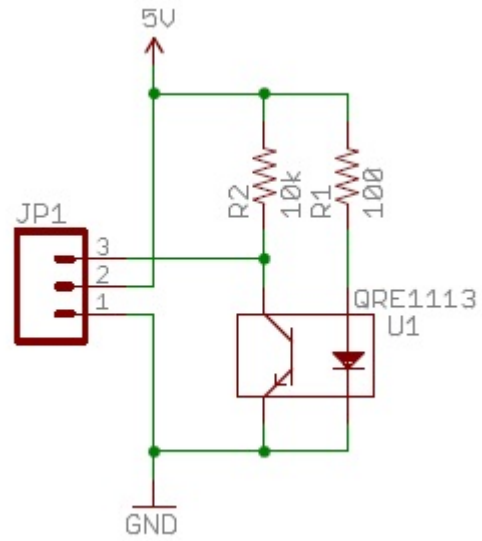
Figure 3.14: Field strength meter

### 3.5 Integration of the harvester into WSN

The WSN was designed in Proteus and the PCB design was also generated using the same software. The transceiver were connected to an ATMEGA328P micro-controller so that it functions as per the specifications of the WSN. The transmitter was connected to a digital Infrared proximity sensor and a potentiometer which simulates an analogue sensor. The infrared sensor and its schematic are shown in Figures 3.15(a) and 3.15(b) respectively.



(a) IR proximity sensor



(b) Circuit schematic of the IR sensor [41]

Figure 3.15: Infrared sensor

The actual WSN was then fabricated on a PCB and the ATMEGA328P was coded using C++ to run the network. Some of the code is presented in appendices A-E. Figure 3.16 shows the receiver and the transmitter.



(a) Receiver

(b) Transmitter

Figure 3.16: WSN implementation

The receiver was connected to the laptop through type A USB cable and the data was received through COM PORT 21. Figure 3.17 shows the receiver connected to the laptop. The transmitter was powered using a rechargeable 3200 mAh battery.



Figure 3.17: Receiver set-up

The harvester was integrated into the transmitter to recharge the battery as data was being transmitted. The effect of integrating the harvester into the WSN was analysed by monitoring the charge of the battery in two set-ups. The first set-up used the developed FM harvester to recharge the battery while the other one did not use any harvester. The effect of integrating the harvester was then analysed by monitoring the charge left in the battery for a period of 48 hours in 2-hour intervals for both set-ups.

### 3.6 Summary

The methodology outlined three key steps. The first is the design of the harvester system where the appropriate components to be used and their values were determined. A suitable antenna was chosen, and optimum values of the components in the filter and multiplier circuit were also calculated. The second stage involved the simulation of the designed circuits. The operation of the filter was verified

and the effect of stage capacitance and number of stages on the performance of the multiplier was also investigated using LTSPICE IV. Finally, the actual circuits were fabricated in a PCB and the performance of the harvester was analysed under different conditions. The effect of the harvester on the operational lifetime of the WSN was also investigated.

# 4. RESULTS AND DISCUSSIONS

## 4.1 Verification and optimisation of harvester subsystems through simulations

To verify the design of the harvester, computer simulations were carried out. The signal strength of different signals was simulated to verify that FM signals present higher input power to the antenna than other common RF sources. The operation of the filter was also verified. Lastly, the voltage multiplier was simulated to verify the effects of the stage capacitance and the number of stages. From these results, the optimum values were selected for the final harvester system.

### 4.1.1 Effect of RF source on the received power

The generalised Friis equation was applied to different types of signals to determine the received power of each signal. The transmitted power was maintained at 10 KW for all sources for consistency of the results. 10 KW is a typical transmitted power for many RF source and as a result, that value was chosen. Figure 4.1 shows the received power for different signals. From Figure 4.1, it can be seen that the power received from FM signal is the highest compared to all the other signals. FM signals provide approximately 40 dBm more than Digital T.V (DTV) signals. This is attributed to the low power losses associated with the FSPL. When the frequency of transmission is lower as in the case of FM, the losses due to FSPL are lower and as a result, the power received at a common distance will be different based on the frequency of transmission.

To verify that the density of FM signal is higher than other types of RF signals, the FSM/LA field strength meter with an operating frequency range of 0-3 GHz was used to experimentally analyse the type of signals available in the vicinity with

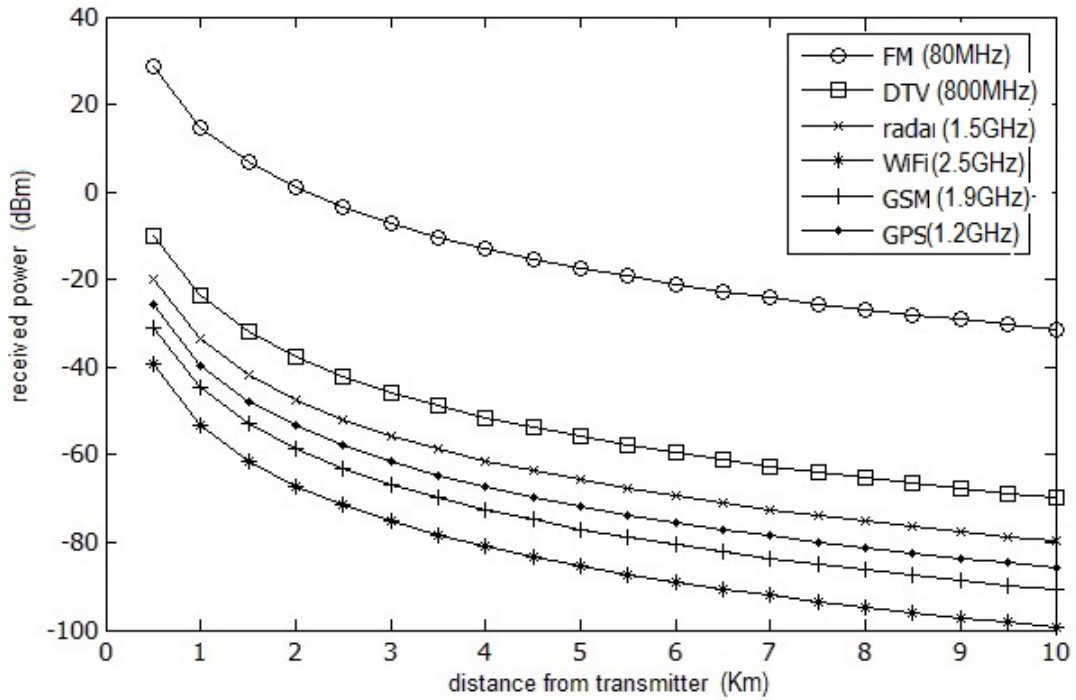


Figure 4.1: Received power for different RF sources

their strength. A wide band dipole antenna with a gain of 1.5 and a bandwidth of 0-5 GHz was used to capture the signals. The antenna was placed approximately 6 km from the nearest transmitting bases. The results are shown in Figure 4.2.

Figure 4.2 shows that the power levels are generally low, about -60 dBm, throughout the range except for a few specific frequency ranges that produce high power levels. These spikes in power levels represent specific signals available in the vicinity and are the ones that present a promising opportunity for energy scavenging. The spikes in received power can be attributed to the signals in their respective frequency range as shown in Figure 4.3.

With respect to Figure 4.3, FM signals register a power of -1 dBm, which is the highest received power than any other type of signal. This can be attributed to the fact that FM base stations are many in any given vicinity, especially within urban centre where FM radio stations are the most abundant. In addition, FM trans-

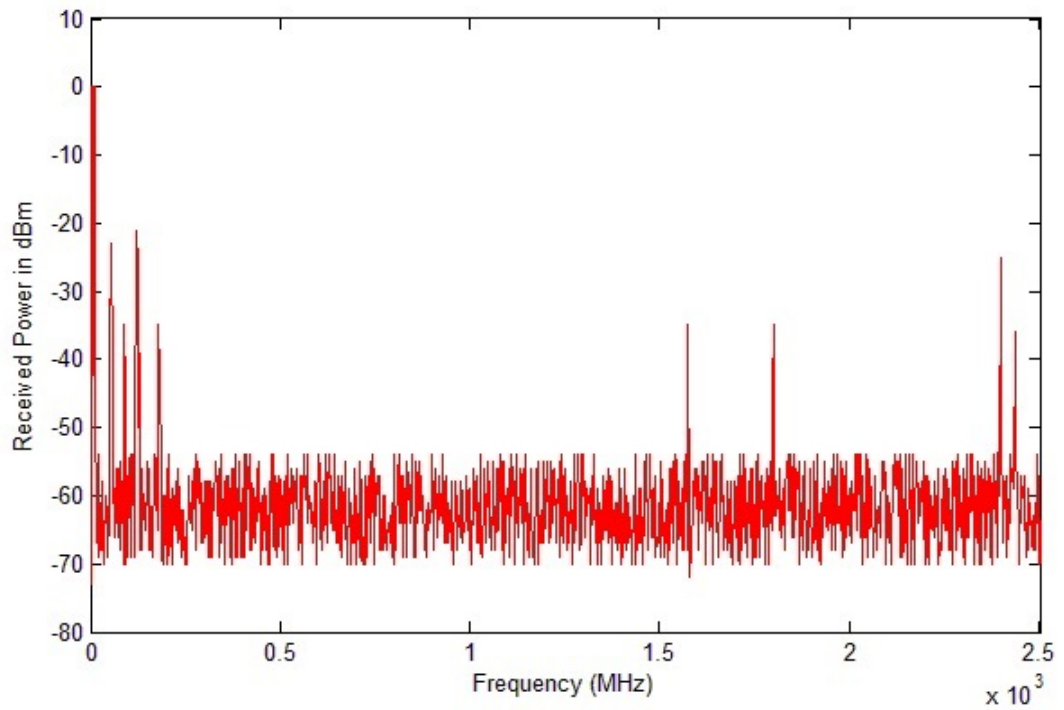


Figure 4.2: Power spectrum for frequency range of 0-2.5GHz

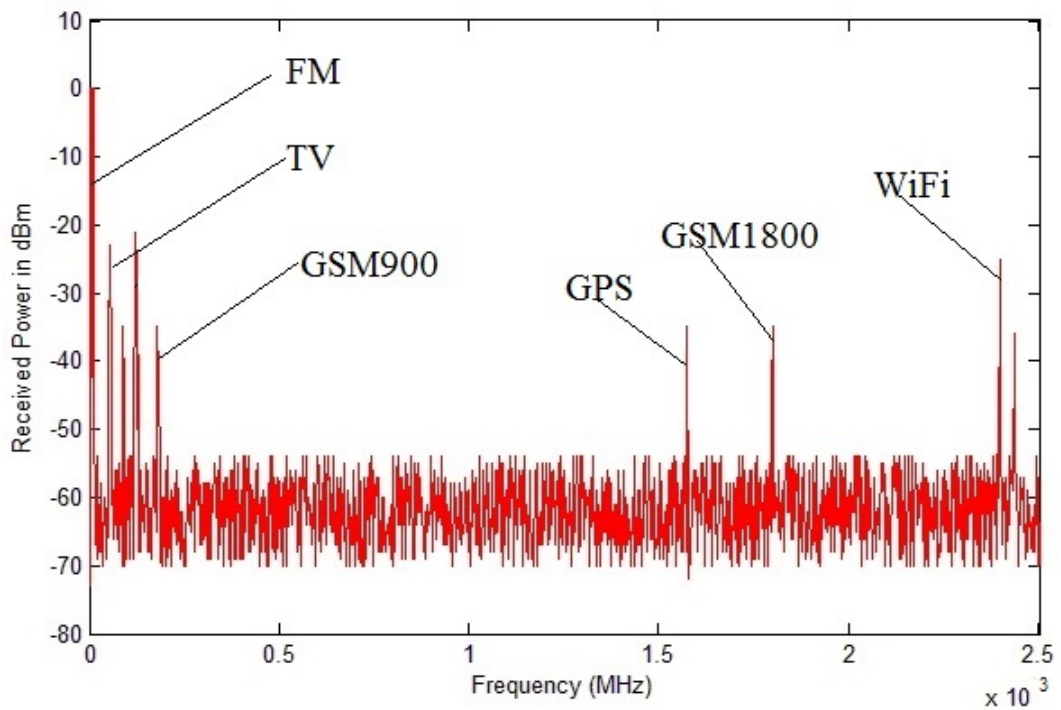


Figure 4.3: Signal identity in power spectrum

mitters use low frequencies to transmit the signal which consequently minimises the losses due to FSPL as was mentioned earlier.

### 4.1.2 Verification of the operation of the RLC filter

After the filter was designed, its operation was verified using LTSPICE IV and the output of the filter is shown in Figure 4.4. It is observed that the input signal is attenuated in all frequencies, but when the frequency approaches the FM range, the output grows gradually to a maximum value and decays as the frequency goes beyond the FM range, demonstrating a typical bandpass response. The physical implementation of the filter produced a similar trend but the magnitude was slightly lower due to voltage drop in the connecting wires and leakages in the RLC components.

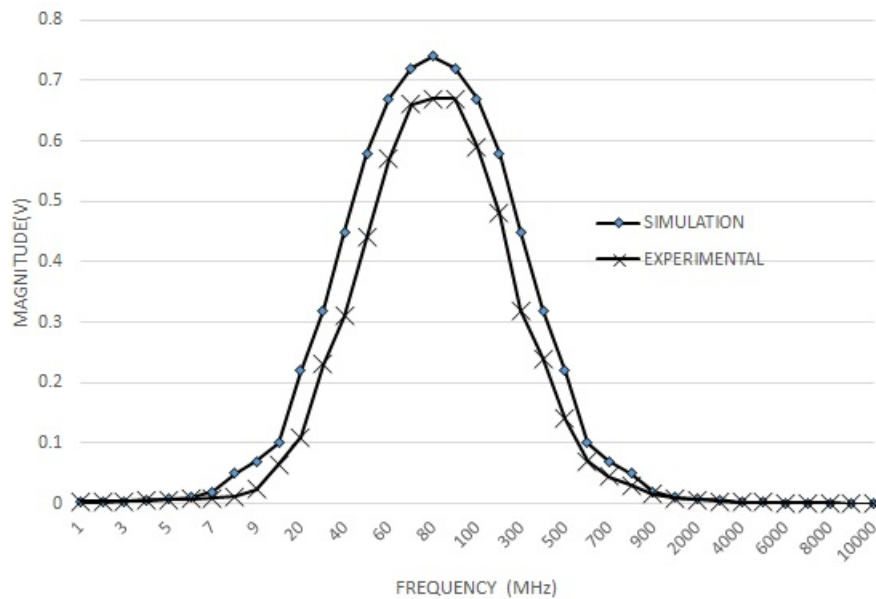


Figure 4.4: Output of RLC filter

### 4.1.3 Effect of stage capacitance on the multiplier output

The effect of stage capacitance on the output voltage was analysed and the results are shown in Figure 4.5. The graphs show that when the stage capacitance is

too low, the output is also too low. In addition, the output is highly sinusoidal for low values of capacitance. As the value of the stage capacitance is increased, the output voltage also increased and became more linear with less ripples until a maximum value is reached, beyond which any further increase in capacitance resulted in a decrease in the output voltage but the ripples decreased. When the output RMS voltage is plotted against the capacitance, the results are as shown in Figure 4.6.

The trend observed is due to the transient nature of capacitors during charging and discharging. When the capacitance is too low, the charge stored is too little and does not build up to a high value in time to boost the voltage. On the other hand, if the capacitance is too high, the time taken to charge the capacitor goes

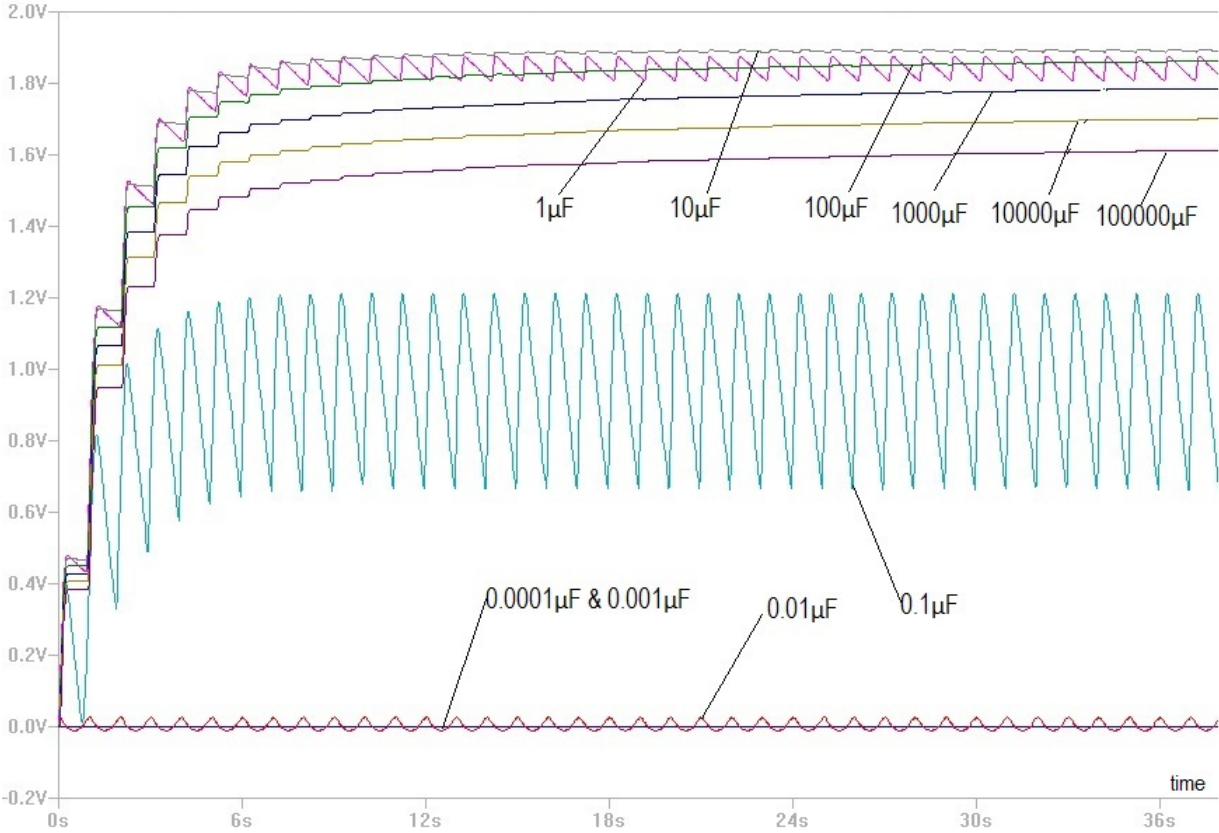


Figure 4.5: Effect of stage capacitance on output voltage

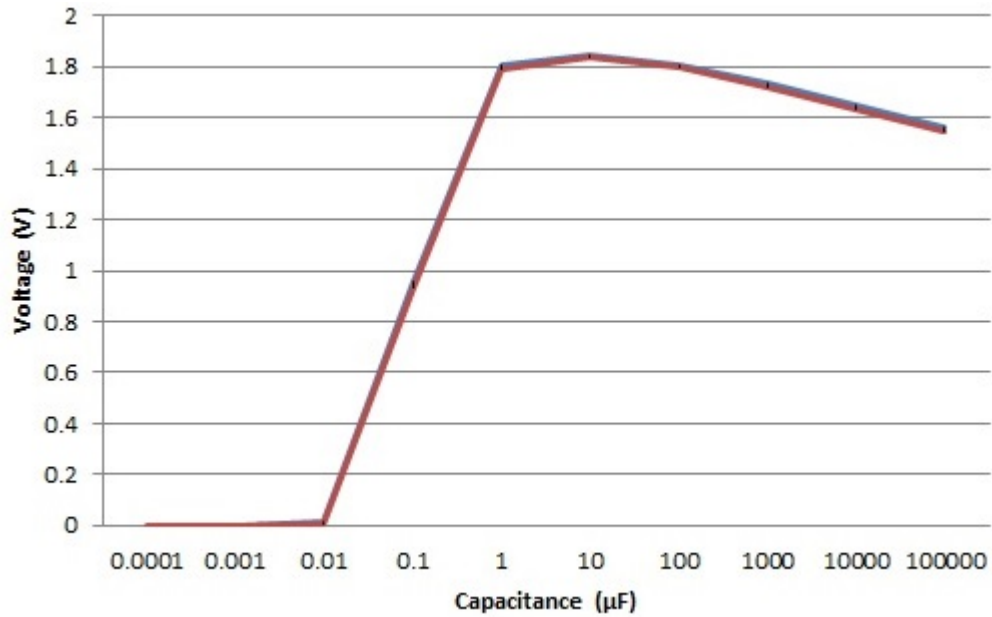
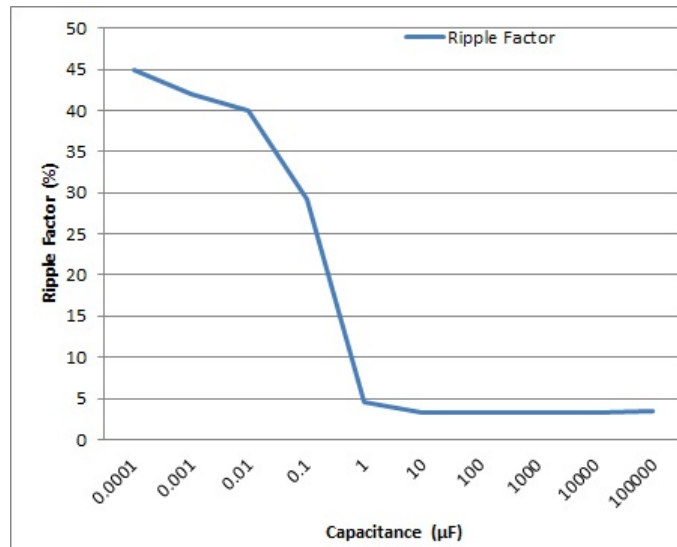


Figure 4.6: Effect of stage capacitance on RMS voltage

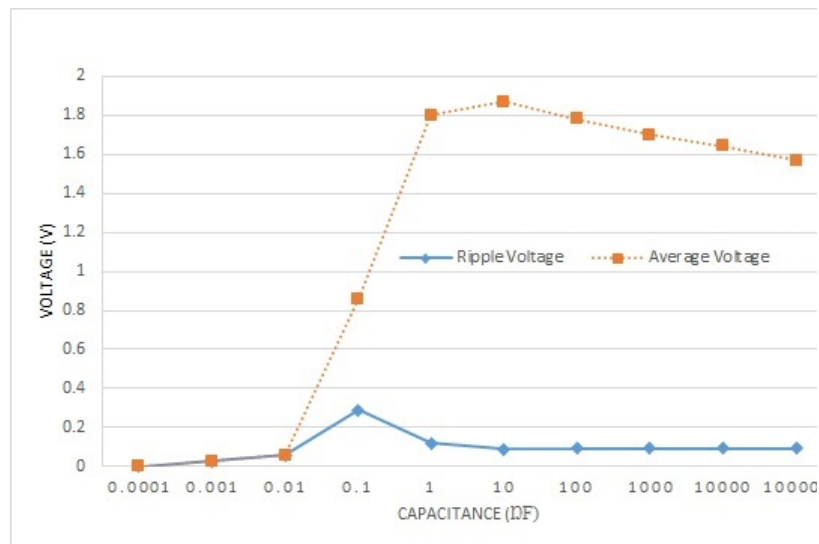
up and as a result, the capacitor does not get sufficient time to charge to its peak and thus the voltage output goes low. When the capacitance is between  $3.3 \mu\text{F}$  and  $10 \mu\text{F}$ , the output voltage is highest at around  $1.8 \text{ V}$ , this value represent the optimum stage capacitance because the charging and discharging times are marched at this value. The time constant for a capacitor is related to the value of the capacitance through Equation (4.1).

$$\tau = RC \tag{4.1}$$

In section 2.3.1, it was mentioned that the capacitance not only affected the level of output, but also affected the nature of the signal produced. Figure 4.7 demonstrates the effect of stage capacitance on the ripple factor and voltage. Figure 4.7 shows that the ripple factor is highest at about 45% when the capacitance is  $0.1 \text{ nF}$ , but the ripple factor reduce to 3.3% when the capacitance is increased to  $0.1 \mu\text{F}$ . This is because the higher capacitance accumulated more charge for the rectifier to effect the smoothing more efficiently than for lower capacitance values [42].



(a) Effect of stage capacitance on ripple factor



(b) Effect of stage capacitance on ripple voltage

Figure 4.7: Effect of stage capacitance on ripple factor and voltage

The stage capacitance also affects the efficiency of the multiplier. Equations 2.36 and 2.38 suggested that an increase in capacitance would result in an increase in efficiency. Figure 4.8 shows the effect of stage capacitance on the efficiency of the multiplier.

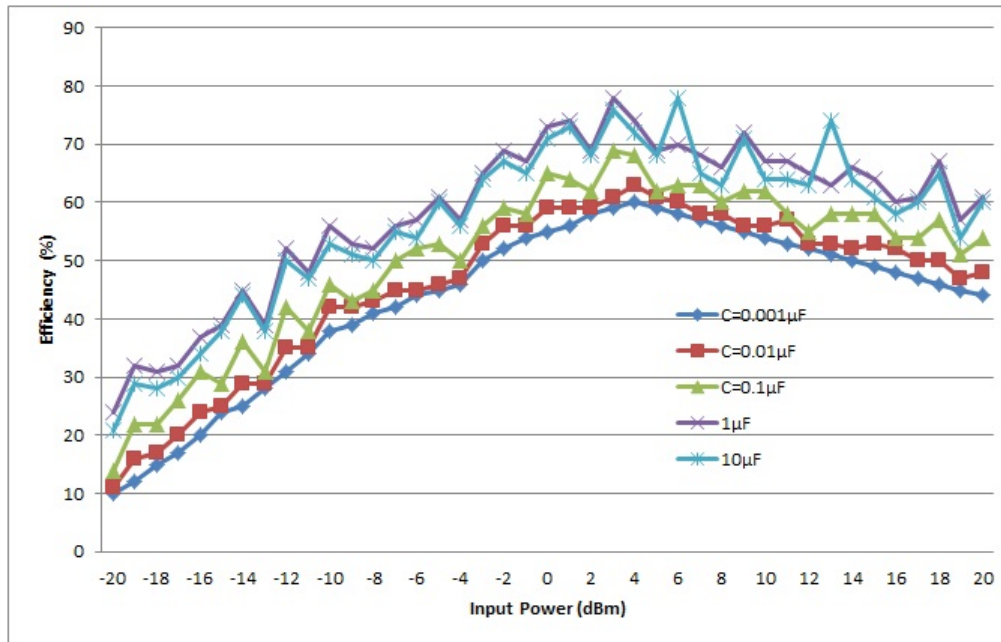


Figure 4.8: Effect of stage capacitance on efficiency

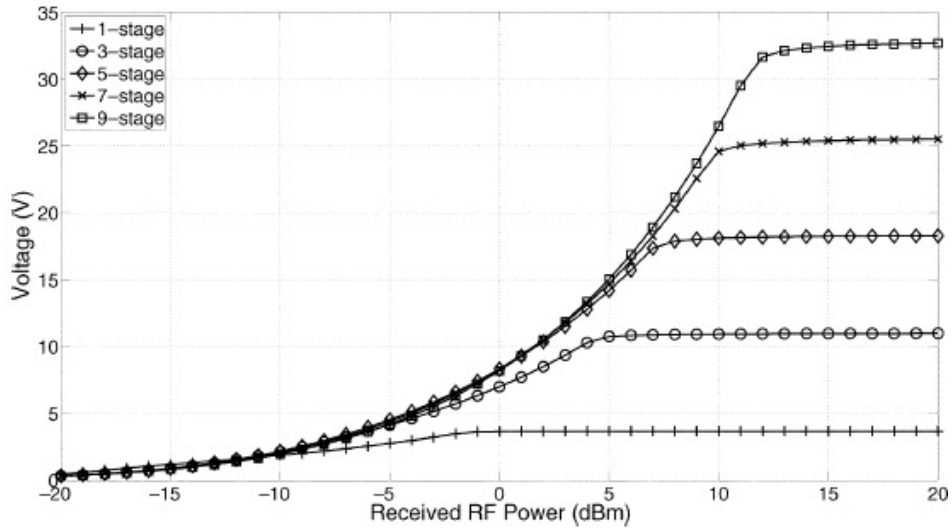
The efficiency increase with increase in capacitance up to around  $1 \mu\text{F}$ , then the efficiency reduces. A maximum efficiency of about 78% was achieved when the capacitance was  $1 \mu\text{F}$ , when the capacitance was increased to  $10 \mu\text{F}$ , the maximum efficiency was reduced to about 75%.

#### 4.1.4 Effect of number of stages on the multiplier output

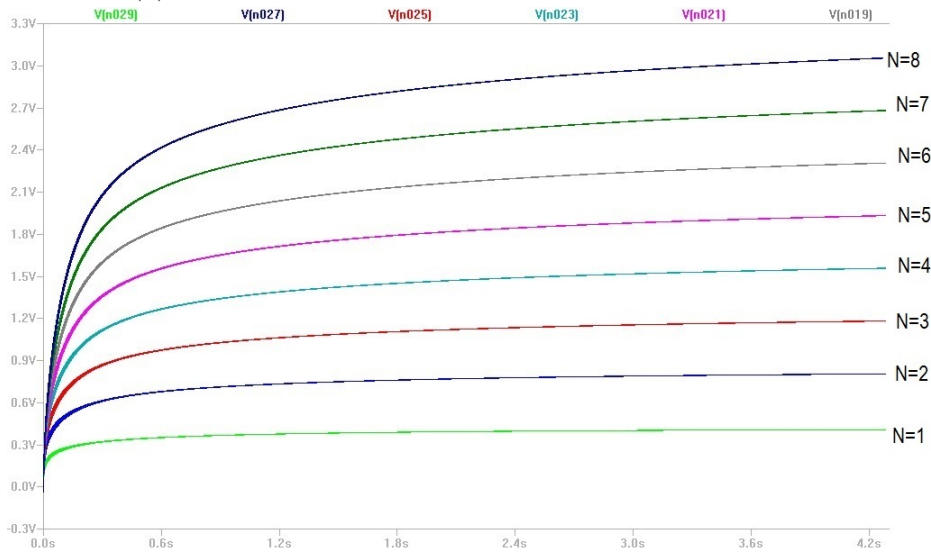
The output of an ideal multiplier is given by Equation 2.33, therefore, it is expected that as the number of stages  $n$  increases, the output should increase. Figures 4.9 (a)-(b) show the output voltage for multistage multiplier.

The graphs show that as the number of stages increase, the output also increases. Further, as the input power is increased, the output voltage also increase. Figure 4.9(b) show that every additional stage results in an increase of about 0.25 V. The variation of output voltage with number of stage is depicted in Figure 4.10

With reference to Figure 4.10, it can be seen that the simulation software produce a



(a) Output voltage against input power for multistage



(b) output voltage for several stages

Figure 4.9: Effect of number of stages on output voltage

linear relationship between the number of stage and the output voltage. However, experimental results show that the output voltage increase with increase in the number of stage up to 10 stages, beyond this the increase in output voltage becomes increasingly smaller. There is a limit to the number of stages that can be cascaded to achieve higher output. Beyond this limit, there will be no any considerable increase in output. This is caused by the presence of parasitic reactive components

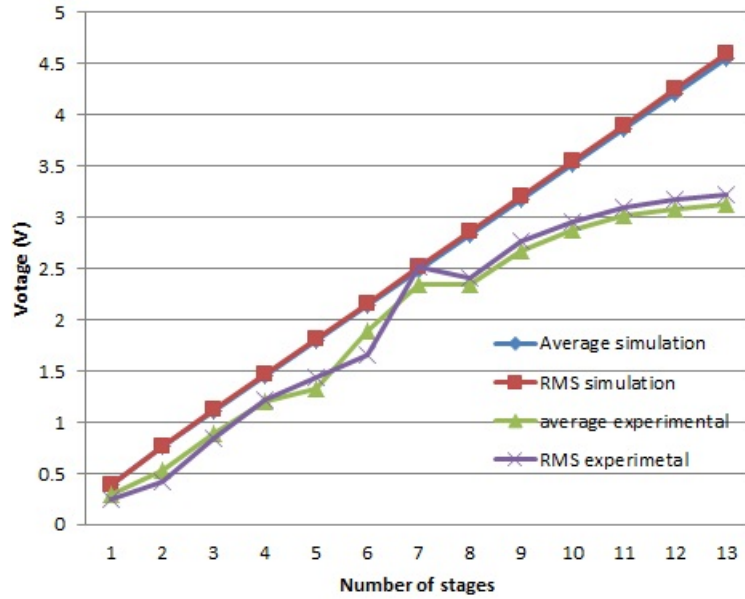


Figure 4.10: Variation of output voltage with number of stages

as well as resistive components within the components and connecting wires. It can also be attributed to build up in parasitic capacitance of the junction capacitance of the Schottky diodes. In addition, it can be noted that the experimental data was lower by almost 0.2 V than the simulation results. This observation is attributed to the voltage lost within the connecting wires.

The number of stages also affect the efficiency of the multiplier as was suggested in Equation (2.38). The variation of efficiency with the number of stages is shown in Figure 4.11. As shown in Figure 4.11, as the number of stages increase, the efficiency reduces for input power below 0dBm. However, above the 0 dBm power, the efficiency increase with increase in the number of stages. This is due to the fact that at higher power levels, the effect of cascading more stages is less pronounced than at low power levels. As mentioned earlier, adding more stages introduces more power consuming components, but each additional stage brings along with it more voltage until a certain limit beyond which any additional stage will result in negligible increase in output. As a result the efficiency will eventually reduce

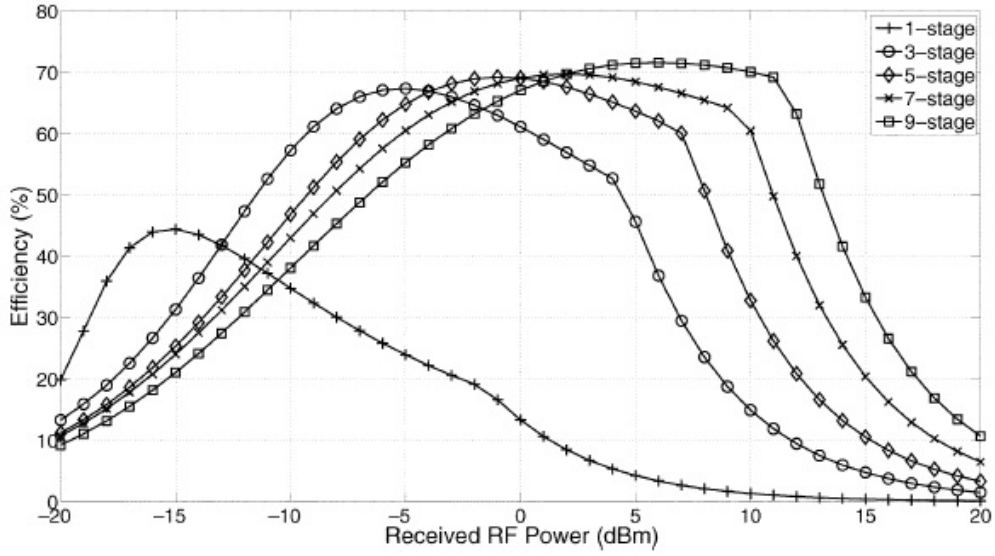


Figure 4.11: Variation of efficiency with number of stages

with increase in the number of stages beyond the optimum value.

It can also be observed from Figure 4.11 that the circuit yields higher efficiency as the number of stages increases. However, as more stages are introduced, the peak of the efficiency curve also shifts towards the higher power region. The voltage plot shows that higher voltage can be achieved by increasing number of circuit stages, but a corresponding increase in power loss is also introduced into the low power region. A similar trend was also observed by [32] in their research.

The effect of number of stages on the output current was investigated and the results are shown in Figure 4.12. It can be seen that as the number of stages is increased from 1 to 7 the output current also increase from  $13 \mu\text{A}$  to  $26 \mu\text{A}$ . Beyond the seventh stage, the output current reduces gradually. This is caused by an increase in the number of power consuming elements within the multiplier.

The output power for different stages are shown in Figures 4.13(a)-(d).

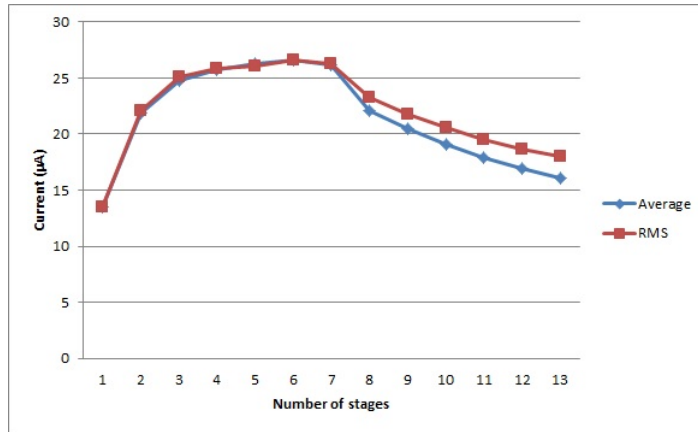


Figure 4.12: Variation of output current with number of stages

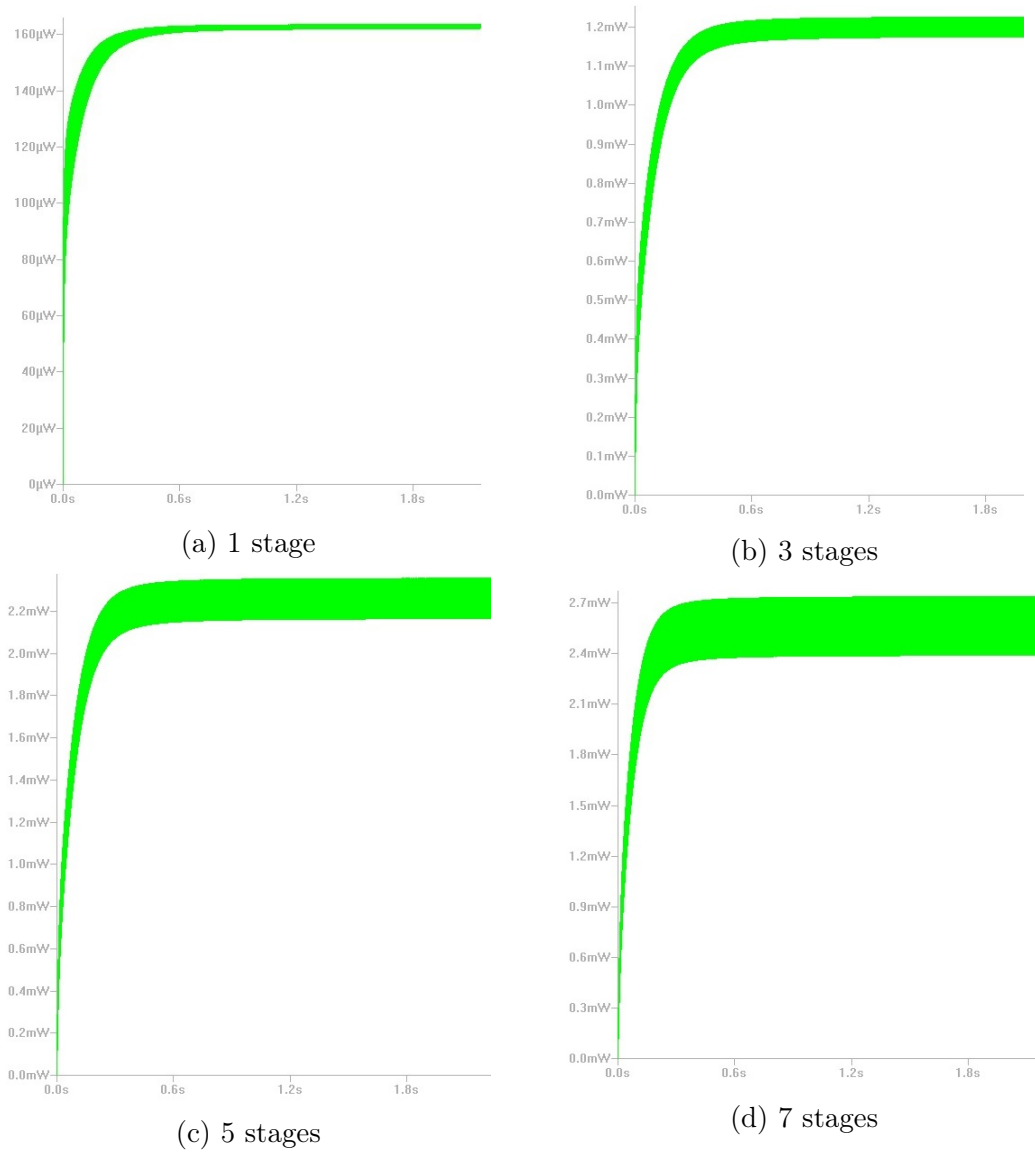


Figure 4.13: Effect of number of stages on output power

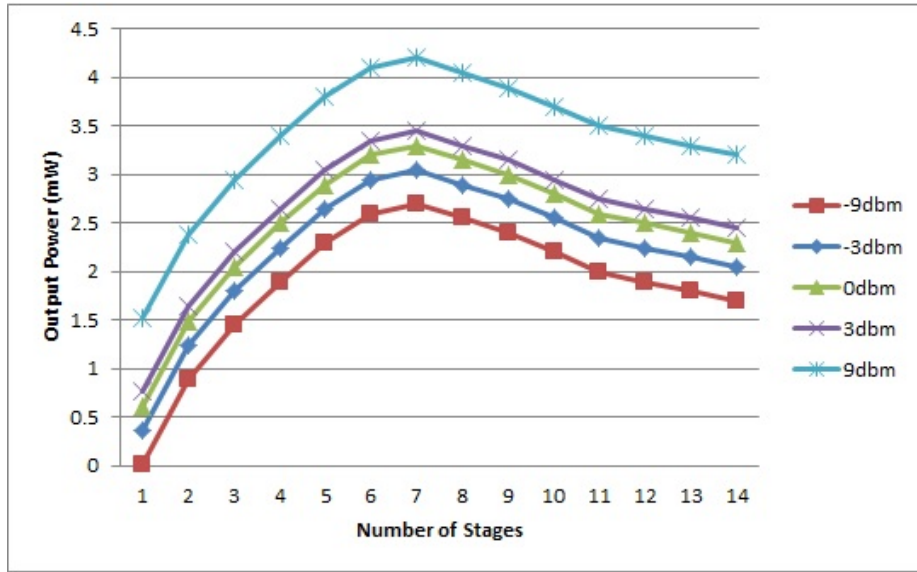


Figure 4.14: Variation of output power with number of stages

Figure 4.13(a) shows that the peak power is about  $160 \mu\text{W}$  when one stage is used. As the number of stages is increased, the peak power also increases up to the seventh stage where the peak power stops increasing. This is because seven stages represent the optimum number of stages, any further increase in number of stages results in a decrease in peak power due to increase in power consuming elements with no any additional boosting of voltage. Figure 4.14 shows the variation of output power with number of stages.

The output power is directly proportional to the number of stages used in the energy harvesting circuit. However, practical constraints force a limit on the number of permissible stages, and in turn, the output power. Here, the output power decreases as number of stages increases beyond the seventh stage due to parasitic effect of the constituent capacitors of each stage, and finally it becomes negligible.

## 4.2 Analysis of the performance of the FM harvester

### 4.2.1 Effect of input frequency on the harvester output

The output for different frequencies is shown in Figure 4.15. The steady voltage is about 1.2 V for a 3-stage multiplier from a 500 mV sinusoidal input for all frequencies. Figure 4.15 demonstrates that the frequency does not affect the magnitude of the output. This is explained from the operating principle of a voltage doubler [45]. The frequency affects the charging cycles only but not the magnitude, this would cause the time taken to rise to a steady output to be affected by the frequency, but the final value would be the same eventually. Figure 4.16 shows the variations of rise time with frequency.

With respect to Figure 4.16, it can be seen that the rise time increase with decrease in frequency. At 50 KHz the rise time is about 0.6 s, but when the frequency is reduced to 50 Hz, the rise time increases to about 3.6 s representing a 600% increase. Hence it can be deduced that the higher the frequency the lower the

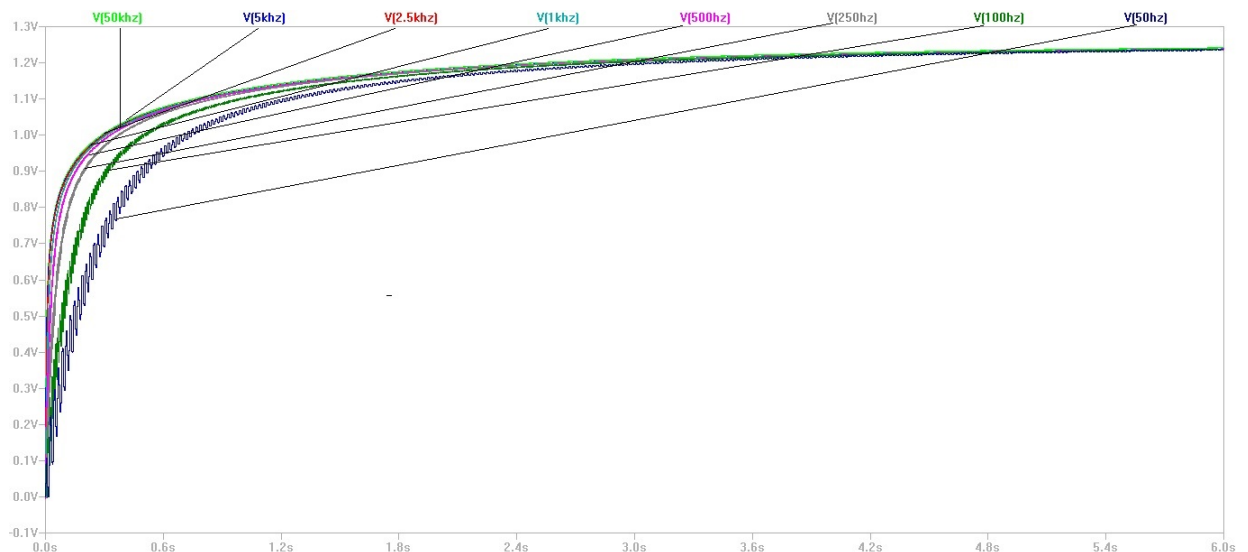


Figure 4.15: Effect of frequency on output voltage

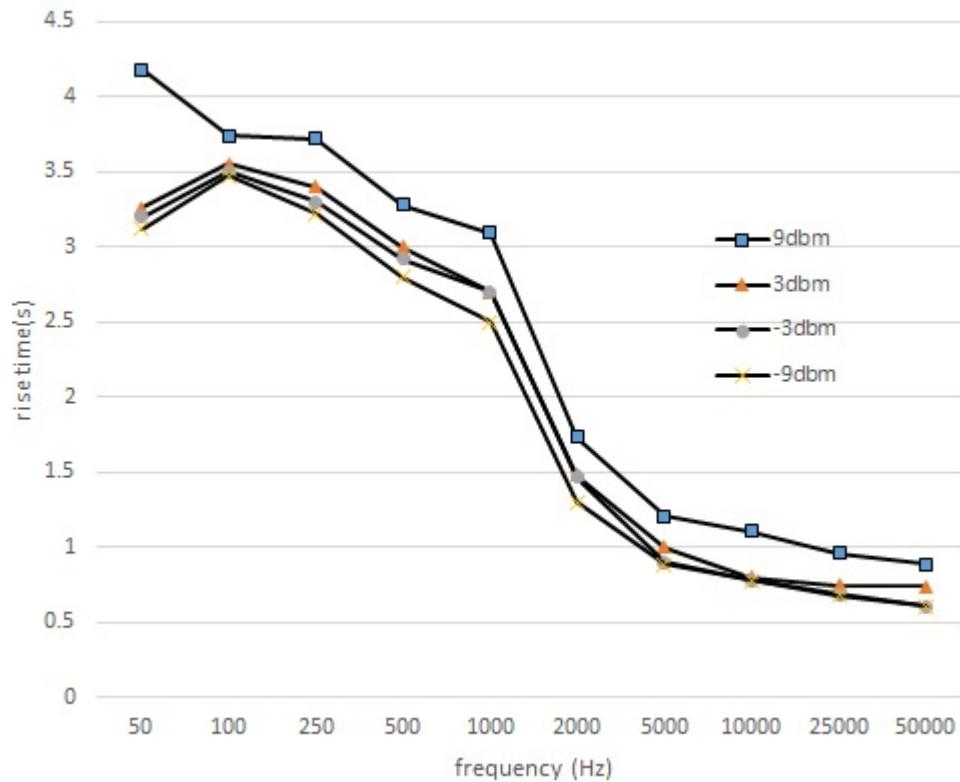


Figure 4.16: Effect of frequency on rise time

rise time, and this could be attributed to the fact that the frequency is cycles per second and the voltage rises to its steady state in steps of the input frequency. As the cycles per second increase, the steps also increase causing the rise time to be lower for higher frequencies.

The effect of frequency on the efficiency of the harvester was investigated and the results are shown in Figure 4.17. Figure 4.17 demonstrates that the harvester's efficiency is highest in the FM frequency range. As the frequency deviates from the FM band, the harvester efficiency also decreases. In addition, the efficiency increases with increase in the input power for any frequency range. This is because the losses are constant for any given input, therefore, for higher input power the efficiency increases.

The effect of input frequency on the output power was also investigated and the

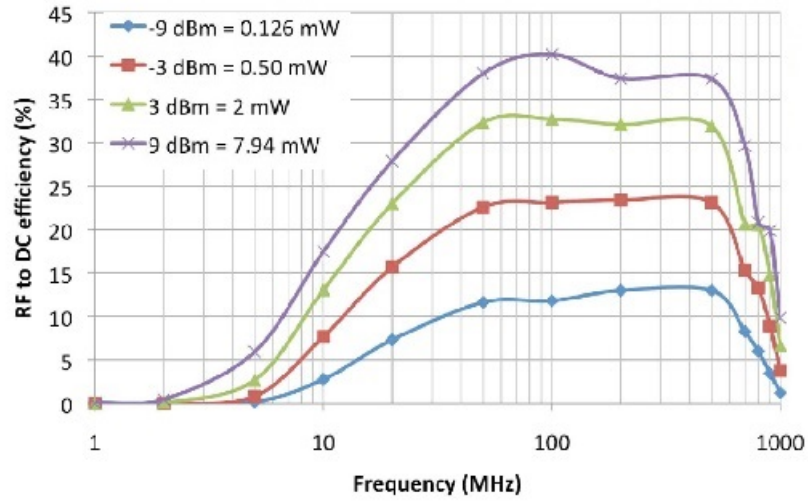
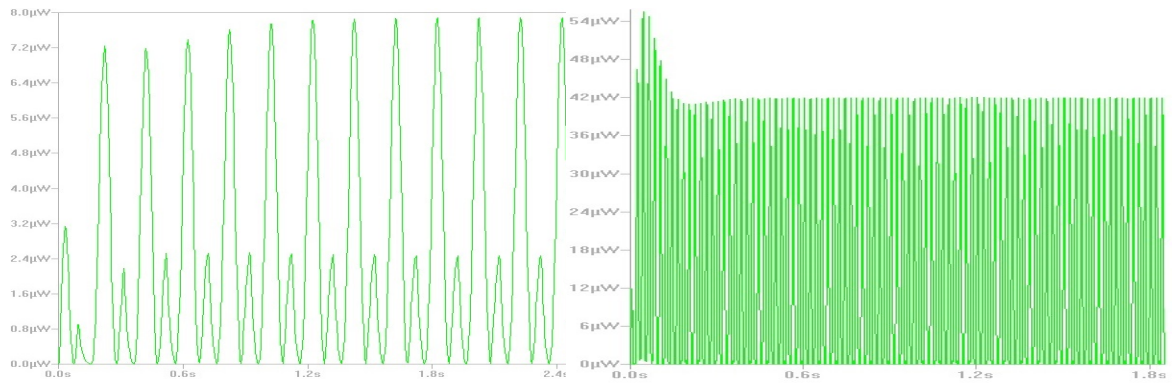


Figure 4.17: Effect of frequency on efficiency

results are shown in figures 4.18(a)-(h). It can be seen that as the frequency is increased from 5 Hz to 500 KHz the output peak power increases from 8  $\mu$ W to 3.6 mW. As the frequency increase the reactance of the capacitors reduce as demonstrated by Equation 4.6. The reduction of the reactance will result in lower power losses which consequently results in increase in the output power. However, as the frequency reaches 50 KHz, the output power does not increase any further due to the limited time offered for the stage capacitors to charge to its optimum value.

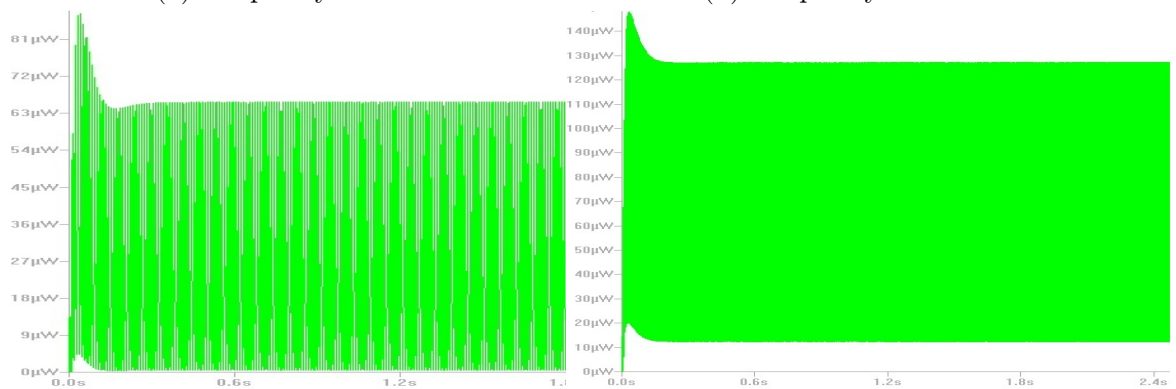
$$X_c = \frac{1}{2\pi fC} \quad (4.2)$$

The results also show that as the frequency increases, the ripples in the output power reduce. Figure 4.19 show the variation of ripple factor with frequency for different input power levels



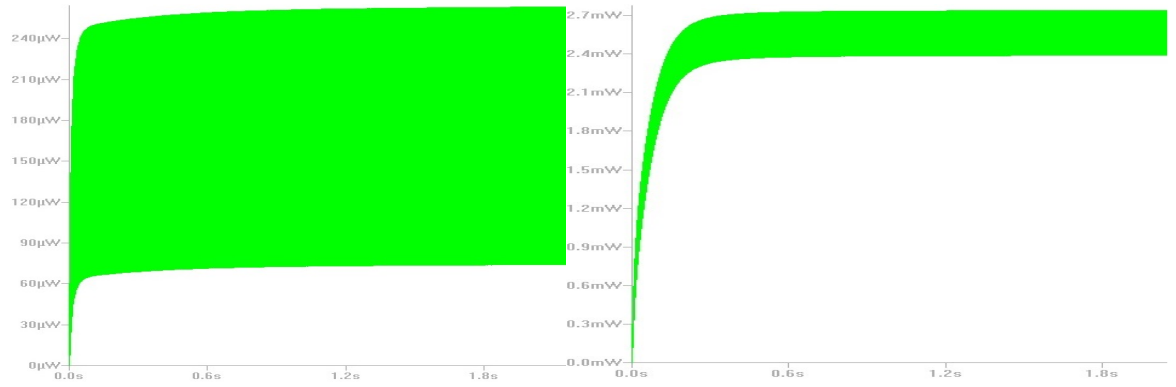
(a) Frequency = 5Hz

(b) Frequency = 50Hz



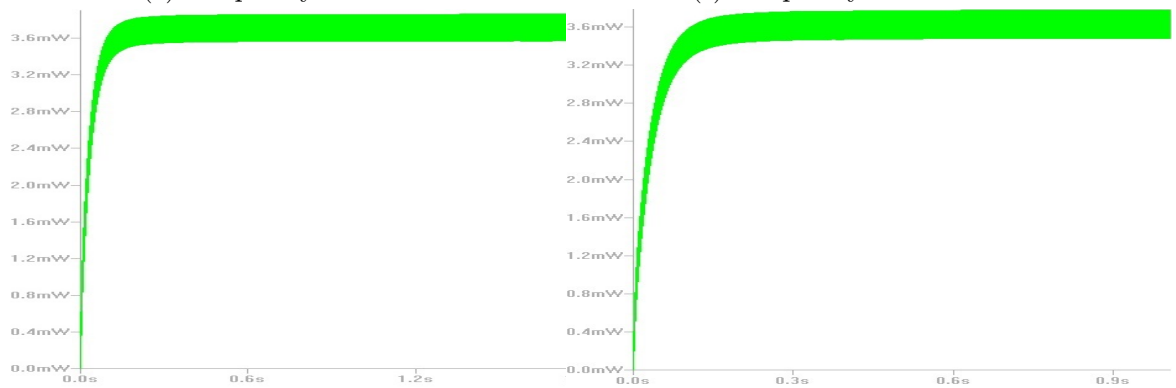
(c) Frequency = 100Hz

(d) Frequency = 250Hz



(e) Frequency = 500Hz

(f) Frequency = 5000Hz



(g) Frequency = 50000Hz

(h) Frequency = 500000Hz

Figure 4.18: Effect of input frequency on output power

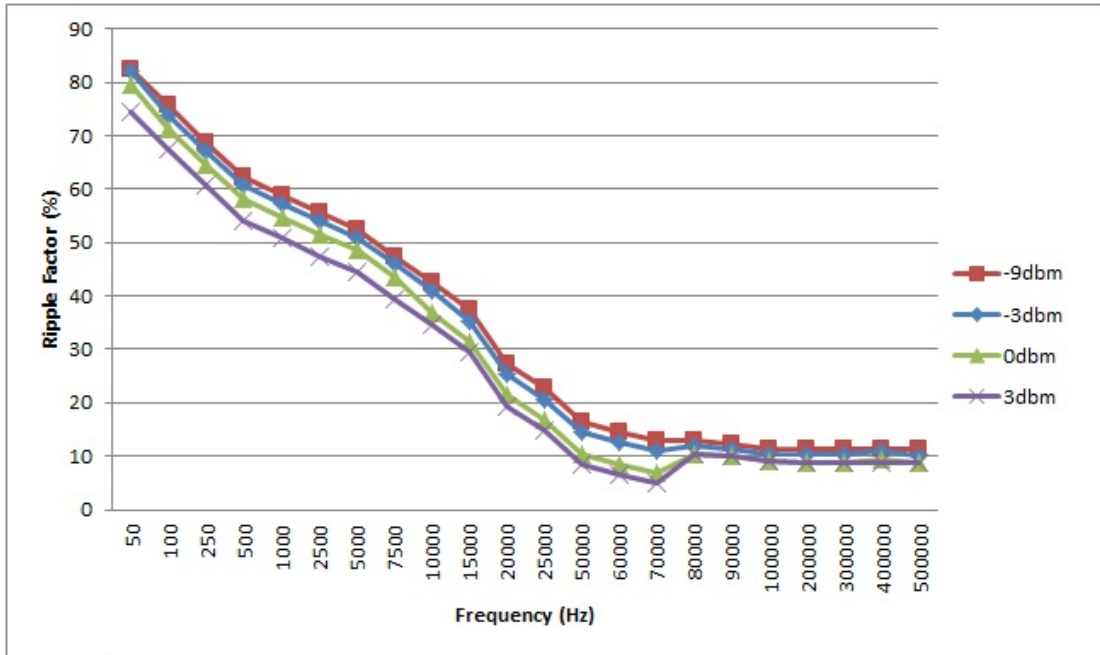


Figure 4.19: Variation of ripple factor with frequency

Figure 4.19 show that as the frequency is increased, the ripple factor reduces until about 10% where the frequency is about 80 KHz, beyond this frequency, there is no any noticeable change in the ripple factor. This is attributed to the fact that the increase in frequency provide optimum condition for the operation of the capacitors which affect the smoothing action.

#### 4.2.2 Effect of input power on harvester output

The input power normally comes from the signals captured by the antenna. The amount of power received is significantly affected by the power density of the signal in that particular area as was mentioned earlier. The input power needs to be sufficient enough to overcome all the losses and provide enough power at the output to charge the battery used in the WSN [44]. The effect of input power was analysed and the results are shown in Figure 4.20. Figure 4.20 shows that the efficiency increases as the input power is increased until it reaches its highest value of about 80% at power levels between 0 dbm and 2 dbm, further increase in input

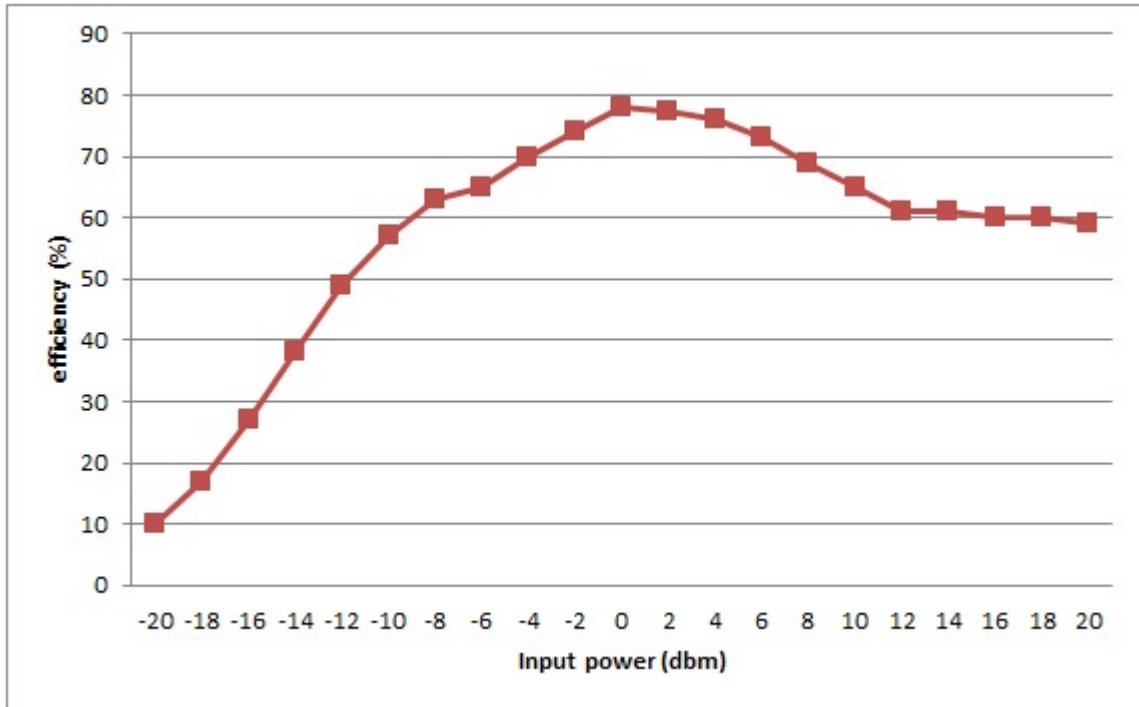


Figure 4.20: Variation of efficiency with input power

power leads to a slight decline in the efficiency because the ratio of output power to input power declines because of the parasitic effects of the stage capacitors as well as the non-linear nature of Schottky diodes.

Since the energy harvesting circuit consists of diodes, which are nonlinear devices, the circuit itself exhibits nonlinearity. This implies that the impedance of the energy harvesting circuit varies with the amount of power received from the antenna.

### 4.2.3 Effect of load resistance on harvester output

Figure 4.21 shows the power output for different load resistances. With respect to Figure 4.21, it is observed that the output power is low when the load resistance is too low or too high, at 10 K $\Omega$  the power is highest with less ripples. This signifies matching conditions for the circuit. Any deviation from this value causes the effect of impedance mismatch to take effect and causes reflection of power to occur at

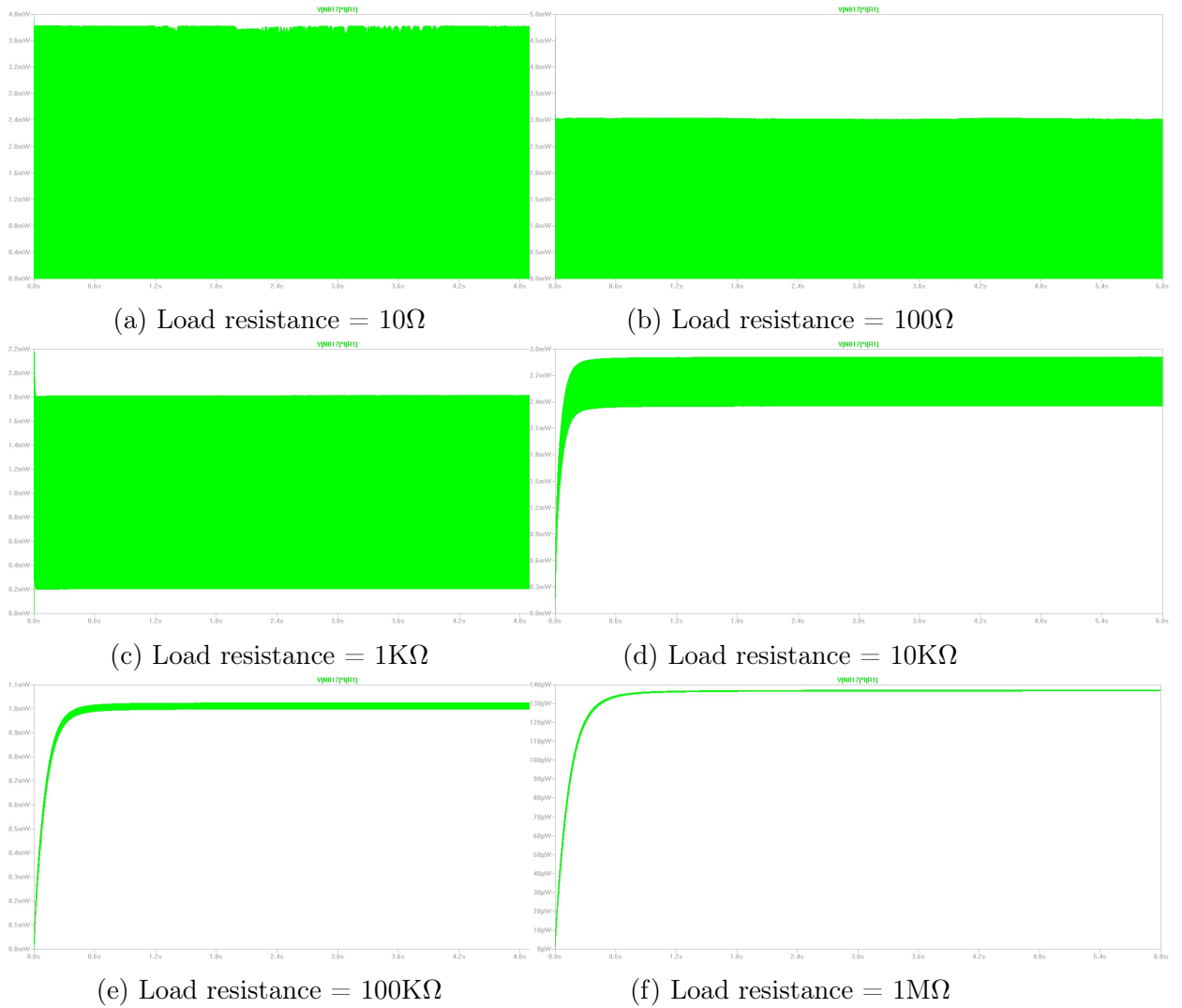


Figure 4.21: Effect of load resistance on output power

the output causing the maximum power transferred to be lower. The variations of average output power with load resistance is shown in Figure 4.22 while the variation of efficiency for different load resistances is shown in Figure 4.23.

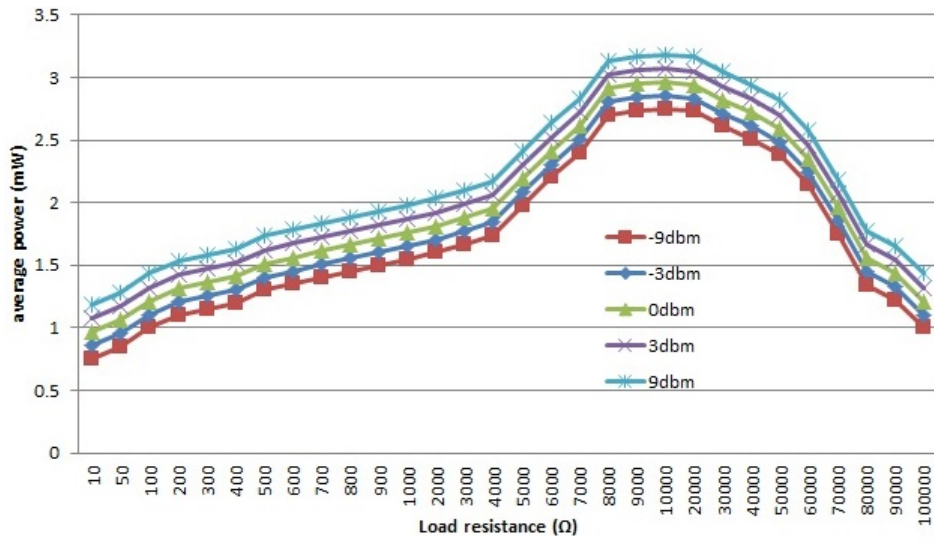


Figure 4.22: Effect of load resistance on average power

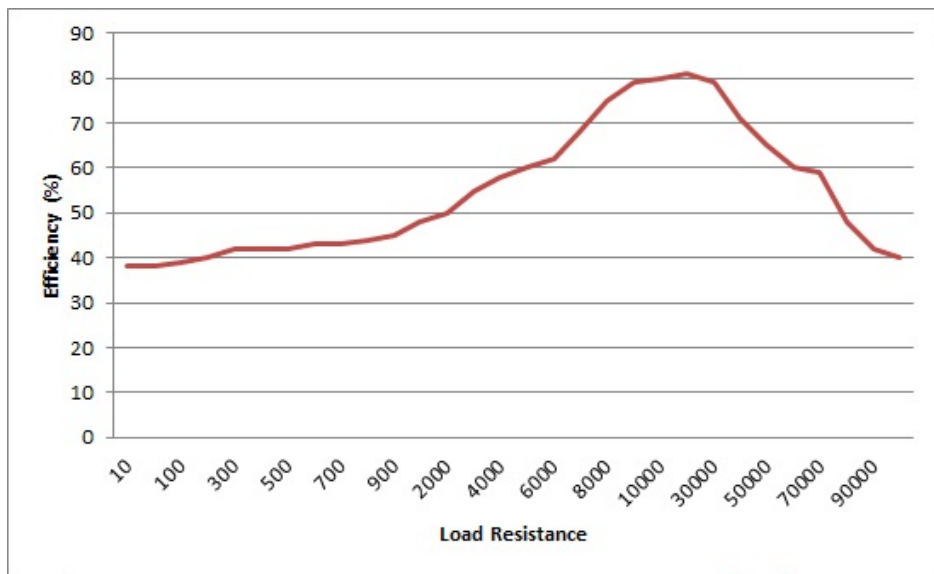


Figure 4.23: Effect of load resistance on efficiency

It is observed from Figure 4.23 that the circuit yields the optimal efficiency at a particular load value, that is, the circuit's efficiency decreases if the load value is too low or too high due to impedance mismatch.



Figure 4.24: Snapshot of data received from WSN

### 4.3 Integration of the harvester into the wireless sensor network

In this research, an XBee wireless transceiver was utilised. The transceiver utilises a voltage of 2.8-3.4 V during operation. This voltage was supplied by a Li-Ion Rechargeable battery of 3200mAh which was obtained from a mobile phone. The data from the sensors was transmitted to the receiver which was connected to the computer. The graphical user interface (GUI) for the WSN was created using C++ and the snapshot is shown in Figure 4.24.

In order to analyse the effect of the energy harvesting circuit on the power drainage of the battery, the battery life with and without the harvester connected to the rechargeable battery was analysed. Figure 4.25 shows the charge of the battery for the two cases over a period of 48 hours taken in two hour intervals.

From Figure 4.25 it can be seen that the setup with the harvester has a higher

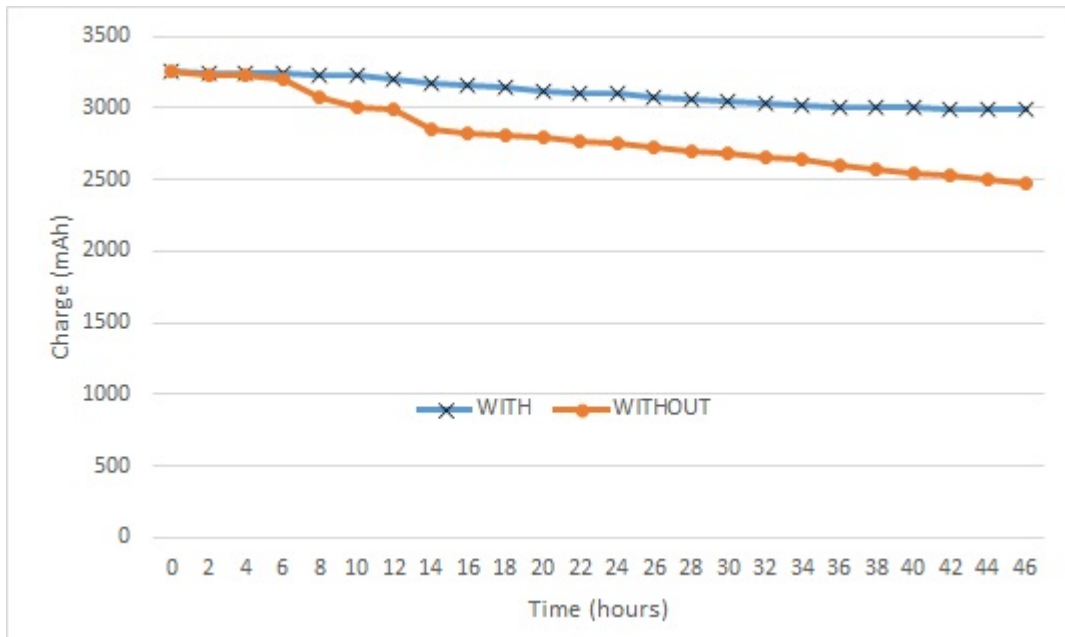


Figure 4.25: Variation of battery charge with time

charge than the one without, this clearly demonstrates the merits of integrating an energy harvesting system into the WSN. The graph also shows that both setups lose charge over time. However, the setup with the harvester is losing charge at a slower rate than the one without. This will in turn affect the time taken to replace the battery. Therefore the setup with the harvester will take longer to replace its battery than the one without and thus improving its operational capabilities and reducing the maintenance cost. In order to quantitatively assess the effect of connecting the harvester, a linear equation was generated using Microsoft's Excel to relate charge and time for the two set-ups and the results are shown in Figure 4.26.

From Figure 4.26, it can be seen that the gradient of the set-up without the harvester is -16.418 mAh per hour, while the one with the harvester is -5.8315 mAh per hour. It can be seen that the harvester slows down the rate of discharge of the battery by almost 64% which indicates a significant improvement. In addition, the total useful life of the battery can be analysed by determining the x-intercept

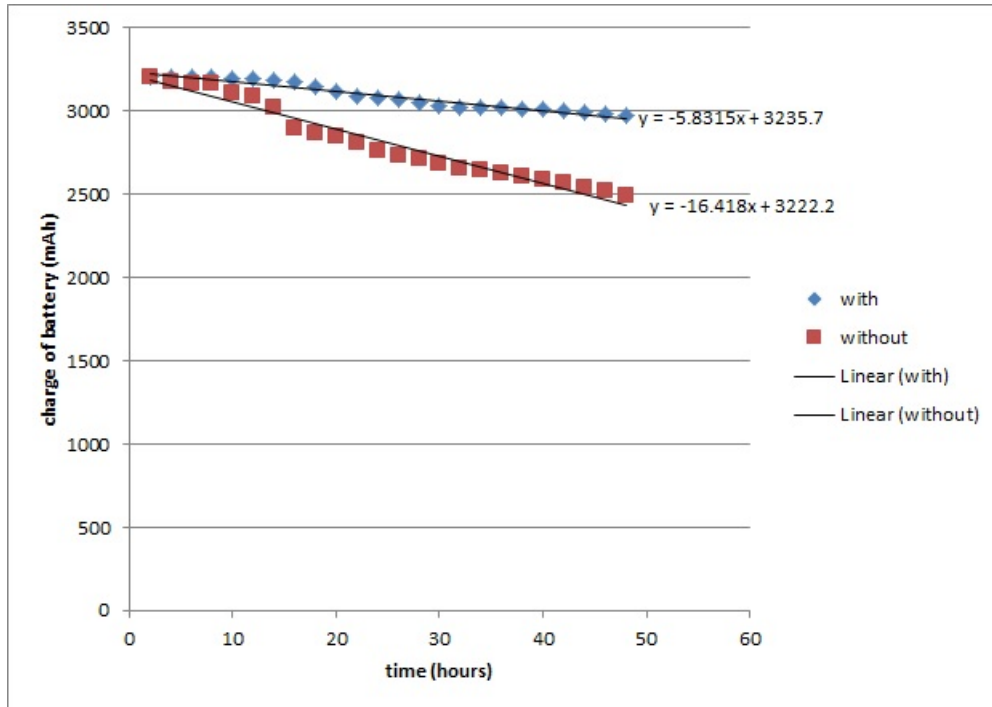


Figure 4.26: Linear relationship between charge and time

of the two setups. If we let the intercepts be  $x_0$  and  $x_w$  for setups without and with the harvester respectively, then the x-intercepts can be obtained by equating  $y$ (the charge of the battery) to 0. The values of  $x_0$  and  $x_w$  are found to be 195.52 hours and 554.866 hours respectively

The battery in the set-up with the harvester will take about 555 hours to fully discharge while the one without the harvester will take 196 hours, this represents about 180% improvement in the battery life of the WSN.

## 4.4 Summary

In this chapter, the signal strength of different signals within the vicinity was investigated and the results showed that FM signals have a higher power density than other RF sources. The operation of the designed filter was verified through simulation. The effect of the stage capacitance and number of stages was also

simulated and the optimum values were determined. The harvesters performance was also analysed under different conditions. It was also demonstrated that the WSN could transmit the data from two sensors to the computer which was running the interface. The results showed that the FM harvester was able to increase the battery life by almost 180% and reduce the battery draining speed by about 64%.

# 5. CONCLUSIONS AND RECOMENDATIONS

## 5.1 Conclusions

In this study the sub-systems that make up an FM energy harvester were designed based on the given constraints of the WSN. Appropriate mathematical formulations were used to come up with the values of the components in a passive RLC filter as well as the voltage multiplier.

Computer simulations using LTSPICE IV were carried out to verify the design of the harvester. The software was also used to asses the effect of stage capacitance and the number of stages on the performance of the multiplier. The results showed that the optimum value of stage capacitance is between  $3.3 \mu\text{F}$  and  $10 \mu\text{F}$ , the optimum number of stages was found to be 7. These optimum values were then used in the final multiplier used for this study.

After the simulations were carried out, the actual harvester was successfully fabricated based on the optimum values. Experimental work was carried out using GWINSTEK SFG 2120 signal generator which was able to produce FM signals and the output was analysed using a Tektronix TDS 2014B digital oscilloscope. The experiments were conducted to analyse the performance of the harvester under different conditions. The harvester's performance under different input frequencies, power levels and load resistance was investigated. The results showed that the efficiency was high within the FM frequency range, the results also showed that higher frequencies produce less ripples than lower ones.

An XBee WSN was also successfully implemented and data transmission was monitored through a user interface that was running on a computer. A network of two sensors was successful developed and implemented using microcontroller algorithm.

The effect of integrating the harvester into the WSN was investigated and the results showed that the FM harvester was able to increase the battery life by 180% and reduce the draining speed of the battery by 64%. The results obtained from this work were significantly better than those achieved by other researchers such as [2, 29, 34]

## 5.2 Recommendations

To improve the FM energy harvester system, the following are areas that could be further addressed.

1. The effect of parasitic reactive components in the PCB and connecting wires which was not considered in the simulations due to time limitations.
2. The harvester system was fabricated using off-the-shelf components due to budgetary constraints. A thorough design that involves miniaturisation should be carried out to commercialise the system.
3. This study utilised a single antenna system harvesting in the FM range only. A multi-antenna system harvesting energy from different frequency ranges should be investigated
4. A power management algorithm should be implemented into the system for maximum power point tracking.

## 6. REFERENCES

# REFERENCES

- [1] Bouchouicha, D., Dupont, F., Latrach, M., Ventura, L. *Ambient RF Energy Harvesting*. International Conference on Renewable Energies and Power Quality, European Association for the Development of Renewable Energies, Granada, 2010. pp. 23-27.
- [2] Mohi El-deen A. *Energy Harvesting Using a Cheap Easy-to-Fabricate FM Rectenna*. The Online Journal on Electronics and Electrical Engineering (OJEEE) Reference Number: W09-0005, Alexandria, Vol. 1 No. 1, 2010. pp. 20-23.
- [3] Mohammed S.S., Ramasamy K., Shanmuganantham T. *Wireless Power Transmission – A Next Generation Power Transmission System*. International Journal of Computer Applications, India, Volume 1 No. 13 2010. pp. 100-103.
- [4] Faruk Y. *Potential Ambient Energy-Harvesting Sources and Techniques*. The Journal of Technology Studies. 2009, pp 40-48
- [5] V. Boonsawat, J. Ekchamanonta, K. Bumrugkhet and S. Kittipiyakul, *XBee wireless sensor networks for temperature monitoring*. The Journal of Technology Studies. 2011, pp 50-58
- [6] Chee, Y. H., *Ultra Low Power Transmitters for Wireless Sensor Networks*. Master's thesis, National University of Singapore, Singapore, 2006.

- [7] Arrawatia, M., Kumar, M., Kumar, G., *RF Energy Harvesting System from Cell Towers in Mumbai*. Indian Institute of Technology, Mumbai, 2006.
- [8] Hagerty, J. A., Zhao, T., Zane, R., Popovic, Z., *Efficient Broadband RF Energy Harvesting for Wireless Sensors*. Proceedings of Government Microcircuit Applications and Critical Technology Conference, University of Colorado, Boulder, 2008. vol 3, pp 1-4.
- [9] Mikeka, C., Arai, H., *Design Issues in Radio Frequency Energy Harvesting System*. Book, INTECH Open Access Publisher, 2011, pp 54-77.
- [10] X. Lu, P. Wang D. Niyato, D. Kim and Z. Han, *Wireless networks with RF energy harvesting: A Contemporary Survey* IEEE communications, surveys and tutorials, 2015, vol 17. pp 757-789.
- [11] H. Nishimoto, Y. Kawahara and T. Asami, *Prototype implementation of ambient RF energy harvesting wireless sensors networks*. IEEE Sensors Conference, 2010, vol 10. pp 1282-1288.
- [12] Harrist, D. W, *Wireless Battery Charging System Using Radio Frequency Energy Harvesting*. Master's thesis, University of Pittsburgh., Pittsburgh, 2004.
- [13] F. Bo, D. Yujie, Z Xiaoxing and L. Yingjie, *Modelling and analysis of power extraction circuits for passive UHF RFID applications*. Journal of semiconductors, 2009, vol 3, no. 1, pp. 1-10.
- [14] D. Patel, R. Mehta, R. Patwa, S. Thapar and S. Chopra, *Radio Frequency Energy Harvesting*. International Journal of Engineering Trends and Technology(IJETT), 2014, vol 16, pp. 382-386.
- [15] Zungeru, A., Ang, L., Prabakaran K., Seng, K., *Radio Frequency Energy Harvesting and Management for Wireless Sensor Networks*. IEEE transactions on

- systems, manufacturing and cybernetics. Part C: Applications and Reviews, Nottingham, 2009. vol 25, no. 2 pp.36-76.
- [16] Y Pantazis, *Decomposition of AM-FM signals with applications in speech processing*. PhD thesis, University of Crete, Department of computer science, 2004.
- [17] Blake P., Lee S., Gruszynski J., Walt P., *Spectrum Analysis: Amplitude and Frequency Modulation*. Test and Measurement Application note 150-1, 2011, pp 1-66.
- [18] G. Babaji, *Design and construction of a 12 KV D.C power supply*. Bayero Journal of Pure and Applied Sciences, 2011, vol. 2, pp. 1-66.
- [19] M. S. Trotter, *Effect of DC to DC converters on organic solar cell arrays for powering DC loads*. Master's thesis, School of electrical and computer engineering, Georgia institute of technology, 2009.
- [20] R. Prince, R Kalaivani, *DC to DC converter based on cascade Cockroft-Wolton voltage multiplier for high voltage gain without using transformer*. International Journal of Engineering Trends and Technology(IJETT), 2013, vol. 2, pp. 464-475.
- [21] S. Davis, *Schottky diodes: the old ones are good, the new ones are better*. Booklet: Power electronics technology, 2011.
- [22] P. Hsu and H. Lin, *Analytical models of output voltage and power efficiencies for multistage charge pumps*. IEEE transactions on power electronics, 2010, vol. 25, pp. 1375-1386.
- [23] Pierre M., Charlie G. *RF Energy Harvesting and Battery-Free Wireless Sensors*. Darnell nano-Power Forum, May 2009.

- [24] Buchmann, I. (2012, December 23). *Supercapacitor*. Retrieved April 4, 2013, from Battery University.com: <http://batteryuniversity.com/learn/article/whats-the-role-of-the-supercapacitor>.
- [25] J. Drew, *Supercapacitors can replace a back-up battery for power ride-through applications*. Design Note: 450. Linear technologies, 2013.
- [26] M. Das, I. Das, et al. *Application of supercapacitor to power small electronic appliances*. IOSR-JEEE, Vol 4, Issue 3, 2013. pp 28-32.
- [27] Pierre M. *Coupling a Supercapacitor With a Small Energy Harvesting Source*. Darnell nano-Power Forum, Dallas, June 7, 2012.
- [28] Molnar, A., Lu, B., Lanzisera, S., Cook, B., Pister, K., *An Ultra-low Power 900 MHz RF Transceiver for Wireless Sensor Networks*. IEEE 2004 Custom Integrated Circuits Conference, Berkeley, California, USA, IEEE, 2004. pp 401-404
- [29] Kavuri K. A. D., Norashidah Md. D., Chandan K. C., *Optimization of the Voltage Doubler Stages in an RF-DC Convertor Module for Energy Harvesting*. Journal of Scientific Research; Circuits and Systems, 2012. pp 216-222.
- [30] Negin S., Neil G., *Resonant Circuit Topology for Radio Frequency Energy Harvesting*. Master's thesis, University of Maryland, College Park., Maryland, 2012.
- [31] Anchustegui-Echearte., Jimenez-Lopez D., *A High Efficiency Matching Technique for Low Power Levels in RF Harvesting*. PIERS Proceedings, Stockholm, Sweden, Aug 2013. pp.12-15.
- [32] Nintanavongsa P., Muncuk U., Lewis D. R., Chowdhury K. R., *Design Optimization and Implementation for RF Energy Harvesting Circuits*. IEEE Jour-

- nal on Emerging and Selected Topics in Circuits And Systems, VOL. 2, NO. 1, MARCH 2012. Boston. pp.24-33.
- [33] Sim, Z. W., Shuttleworth, R., Alexander, M. J., Grieve, B. D, *Compact Patch Antenna Design for Outdoor RF Energy Harvesting in Wireless Sensors*. Progress In Electromagnetics Research conference, IEEE, Manchester, 2010. pp. 273-294.
- [34] Hong S. S. B., Ibrahim R., Khir M. H., Zakariya M. A., Hanita D. *Wi-Fi Energy Harvester for Low Power RFID Applications*. Progress In Electromagnetics Research C, Vol. 40, 2013, Malaysia, 2009. pp. 69-81.
- [35] Noguchi A., Arai H. *Small loop rectenna for RF energy harvesting*. 2013 Asia-Pacific Microwave Conference Proceedings (APMC), Seoul, 2013, pp. 86-88.
- [36] Kalyanmov D. *Optimization for Engineering Design: Algorithms and Examples*. PHI Learning Pvt. Ltd. 2004.
- [37] J. Rahola. *Product Manual v1.xAx - 802.15.4 Protocol: XBee, XBee-PRO OEM RF Modules*. MaxStream, Inc. 2007, Available at [[http : //www.australianrobotics.com.au/sites/default/files/XBee – Manual\\_0.pdf](http://www.australianrobotics.com.au/sites/default/files/XBee_Manual_0.pdf)].
- [38] T. Buch, *Design of RLC band pass filter*. Book, University of Rostock: Institute of communications engineering, 2010.
- [39] H. Hermings, *Infra red, Red robot line sensor*. Book, Creative commons, First Edition, 2013.
- [40] C. Barick, *Agilent HSMS 285X series surface mount zero bias Schottky diodes data sheet*. Data sheet, Jameco part number 1585223, Agilent Technologies, 2012.

- [41] Hempstead, M., Tripathi, N., Mauro, P., Wei, G., Brooks, D., *An Ultra Low Power System Architecture for Sensor Network Applications*. IEEE, Harvard, 2005. pp 238-241.
- [42] R. Shrivastava, *Analysis and design of a 3-stage voltage rectifier multiplier and a 2-stage multi-phase voltage doubler for energy harvesting systems*. Master's thesis, Graduate faculty of Texas technical university, 2012.
- [43] P. Singh, *Output Ripple Voltage for Buck Switching Regulator*. Application Report: SLVA630A, Texas Instruments, 2014.
- [44] Gyuhae P. *Overview of Energy Harvesting Systems (for low-power electronics)*. Engineering Institute: Engineering Sciences and Applications, Los Alamos National Laboratory. The First Engineering Institute Workshop: Energy Harvesting. 2013.
- [45] Patel, A., *Power Harvesting for Low Power Wireless Sensor Networks*. IEEE Conference: Antenna and Propagation Conference, IEEE, Loughborough, 2009. pp. 633-636
- [46] Vikram G., Arvind K., Ragunathan R. *Energy Harvesting from Electromagnetic Energy Radiating from AC Power Lines*. Real-time and Multimedia Systems Laboratory. Carnegie Mellon University, Pittsburgh, PA, 2010 pp 68-72

# A. APPENDICES

## A.1 APPENDIX A: C++ code for Transmitter

```
/*
 * transmitter.cpp
 *
 * Created: 05/30/2014 09:31:18
 * Author: Sultan M. Hamid
 */

#include <util/delay.h>
//put your libraries here

#include <sketch.h>
#include <pin.h>

unsigned int port_one = 0;
unsigned int port_two = 0;

int x= 120;

void initCode(){
    DDRB |= _BV(1);
    pinSet(17, INPUT);
    Serial.begin(9600);
}
```

```

void executeCode(){
    port_one = analogRead(3);
    if (!(port_one > 0)) port_one = 0;

    if (pinRead(17) == HIGH) port_two = 100;
    else port_two = 0;

    Serial.print(port_one); Serial.print(",");
    Serial.print(port_two); Serial.print("\n");
    _delay_ms(500);

    //x>2000 ? x=0:x+=5;

    //toggle transmission led
    PORTB |= _BV(1);
    delay(250);
    PORTB &= ~_BV(1);
    delay(250);
}

```

## A.2 APPENDIX B: C++ code for receiver

```
/*
 * receiver.cpp
 *
 * Created: 11/30/2013 09:31:18
 * Author: Sultan M. Hamid
 */

#include <util/delay.h>
//put your libraries here

#include <sketch.h>
#include <NewSoftSerial.h>

NewSoftSerial mySerial(3, 2);

void initCode(){
    DDRB |= _BV(1);
    mySerial.begin(9600);
    Serial.begin(9600);
}

void executeCode(){
    while(Serial.available() > 0){
        mySerial.print((char)Serial.read());
    }
}
```

```
    }  
    PORTB |= _BV(1);  
    delay(100);  
    PORTB &= ~_BV(1);  
    delay(100);  
}  
}
```

### A.3 APPENDIX C: C++ header file for sketch.h

```
/*  
* sketch.h  
*  
* Created: 11/17/2013 16:43:19  
* Author: Sultan M. Hamid  
*/
```

```
#ifndef SKETCH_H_  
#define SKETCH_H_
```

```
#include "Arduino.h"
```

```
void initCode();
```

```
void executeCode();
```

```
void setup(){  
    initCode();
```

```
}
```

```
void loop(){  
    executeCode();
```

```
}
```

```
#endif /* SKETCH_H_ */
```

## A.4 APPENDIX D: C++ header file for pin.h

```
#ifndef PIN_H_
#define PIN_H_

#include <avr/io.h>
#include <inttypes.h>

#ifdef __cplusplus
    extern "C"{
#endif

/*****
 * structure to hold registers and bit number.
 *****/
struct reg_bit{
    volatile uint8_t* DDRx;
    volatile uint8_t* PORTx;
    volatile uint8_t* PINx;
    uint8_t bit;
};

/*****
 * enumeration to hold bit set/reset values or write mode.
 *****/
/*enum{ LOW, HIGH, INPUT=0, OUTPUT };*/

/*****
```

```

* port registers and bit number.
* DDRx – data direction register.
* PORTx – write register.
* PINx – read register.
*****
static const struct reg_bit pins_def[] = {
    {}, //NONE //0
    { &DDRC, &PORTC, &PINC, PINC6 }, //1
    { &DDRD, &PORTD, &PIND, PIND0 }, //2
    { &DDRD, &PORTD, &PIND, PIND1 }, //3
    { &DDRD, &PORTD, &PIND, PIND2 }, //4
    { &DDRD, &PORTD, &PIND, PIND3 }, //5
    { &DDRD, &PORTD, &PIND, PIND4 }, //6

    {}, //VCC //7
    {}, //GND //8

    { &DDRB, &PORTB, &PINB, PINB6 }, //9
    { &DDRB, &PORTB, &PINB, PINB7 }, //10

    { &DDRD, &PORTD, &PIND, PIND5 }, //11
    { &DDRD, &PORTD, &PIND, PIND6 }, //12
    { &DDRD, &PORTD, &PIND, PIND7 }, //13

    { &DDRB, &PORTB, &PINB, PINB0 }, //14
    { &DDRB, &PORTB, &PINB, PINB1 }, //15
    { &DDRB, &PORTB, &PINB, PINB2 }, //16

```

```

{ &DDRB, &PORTB, &PINB, PINB3 }, //17
{ &DDRB, &PORTB, &PINB, PINB4 }, //18
{ &DDRB, &PORTB, &PINB, PINB5 }, //19

}, //AVCC //20
}, //AREF //21
}, //GND //22

{ &DDRC, &PORTC, &PINC, PINC0 }, //23
{ &DDRC, &PORTC, &PINC, PINC1 }, //24
{ &DDRC, &PORTC, &PINC, PINC2 }, //25
{ &DDRC, &PORTC, &PINC, PINC3 }, //26
{ &DDRC, &PORTC, &PINC, PINC4 }, //27
{ &DDRC, &PORTC, &PINC, PINC5 } //28
};

```

```

/*****
* declare number of physical pins
*****/
static const uint8_t pins = sizeof(pins_def) + 1;

/*****
* check port pin direction.
* pin - physical pin number on the AVR.
* e.g pinStatus(6);
      checks the status of PORTB5 - B5 whether an input or output.

```

```

*****
static inline uint8_t pinStatus(uint8_t pin) {
    if (pin < pins) {
        return (*pins_def[pin].DDRx >> pins_def[pin].bit) & 1;
    } else { return 0; }
}

/*****
* sets i/o direction of a port pin.
* pin - physical pin on the AVR.
* mode - set i/o mode of port bit , 1/0, OUTPUT/INPUT.
* e.g pinSet(6, 1);
      sets PORTB5 - B5 as output.
*****
static inline void pinSet(uint8_t pin , uint8_t mode) {
    if (pin < pins) {
        if (mode) {
            *pins_def[pin].DDRx |= _BV(pins_def[pin].bit);
        } else {
            *pins_def[pin].DDRx &= ~ _BV(pins_def[pin].bit);
        }
    } else {}
}

/*****
* read bit.
* pin - physical pin number on the AVR.

```

```

* e.g pinRead(6);
    reads the bit value of PORTB5 bit.
*****
static inline uint8_t pinRead(uint8_t pin) {
    if (pin < pins) {
        return (*pins_def[pin].PINx >> pins_def[pin].bit) & 1;
    } else { return 0; }
}

/*****
* set/reset bit.
* pin - physical pin number on the AVR.
* Value - set/ reset value , 0/1, HIGH/LOW.
* e.g pinWrite(6, 1);
    sets the bit of PORTB5 - B5 .
*****
static inline void pinWrite(uint8_t pin, uint8_t value) {
    if (pin < pins) {
        if (value) {
            *pins_def[pin].PORTx |= _BV(pins_def[pin].bit);
        } else {
            *pins_def[pin].PORTx &= ~ _BV(pins_def[pin].bit);
        }
    }
}

/*****
* toggle bit.

```

```

* pin - physical pin number on the AVR.
* e.g pinToggle(6, 1);
    toggles bit 5 of PORTB - B5.
*****
static inline uint8_t pinToggle(uint8_t pin) {
    if (pin < pins) {
        return *pins_def[pin].PORTx ^= _BV(pins_def[pin].bit);
    } else { return 0; }
}
/*****
* set i/o mode of many pins at once
* *p - pointer to an array of pins.
* mode - either OUTPUT/INPUT, 1/0.
* uint8_t ar[3] = {4, 5, 6};
* e.g pinMultiSet(ar, 1);
    sets pins 4, 5 and 6 as outputs.
*****
static inline void pinsMultiSet(const uint8_t *p, uint8_t mode){
    while(*p){
        mode ? pinSet(*p++, 1) : pinSet(*p++, 0);
    }
}
/*****
* write many pins at once
* *p - pointer to an array of pins.
* mode - either HIGH/LOW, 1/0.
* uint8_t ar[3] = {4, 5, 6};

```

```

* e.g pinMultiWrite(ar , 1);
    sets pins 4, 5 and 6 High.
*****
static inline void pinsMultiWrite(const uint8_t *p, uint8_t mode){
    while(*p){
        mode ? pinWrite(*p++, 1) : pinWrite(*p++, 0);
    }
}

/*****
* activate pull-up resistor on an input pin
* pin - port pin to activate pull-up.
*e.g activatePullUp(3);
    activates internal pull up resistor on pin 3
*****
static inline void activatePullUp(uint8_t pin){
    pinSet(pin , INPUT);
    pinWrite(pin , HIGH);
}

/*****
variable to set the pin array
e.g
    multiPins outPins[4] = { 2,3,4,5 };
    pinsMultiWrite(outPins , HIGH);
    set pins 2,3,4,5 high.
*****
typedef uint8_t multiPins;

```

```
#ifdef __cplusplus
}
#endif

#endif /* PIN_H_ */
```

## A.5 APPENDIX E: C++ header file for newserial.h

```
/*
NewSoftSerial.h
Multi-instance software serial library for Arduino/Wiring
*/

// #if defined(ARDUINO) && ARDUINO >= 100
// #error NewSoftSerial has been moved into the Arduino core as of vers
Use SoftwareSerial instead.
// #endif

#ifndef NewSoftSerial_h
#define NewSoftSerial_h

#include <inttypes.h>
#include <Stream.h>

/*****
* Definitions
*****/

#define _SS_MAX_RX_BUFF 64 // RX buffer size
#define _SS_VERSION 12 // software version of this library
#ifndef GCC_VERSION
#define GCC_VERSION (__GNUC__ * 10000 + __GNUC_MINOR__ * 100 + __GNUC_
```

```

#endif

class NewSoftSerial : public Stream
{
private:
    // per object data
    uint8_t _receivePin;
    uint8_t _receiveBitMask;
    volatile uint8_t *_receivePortRegister;
    uint8_t _transmitBitMask;
    volatile uint8_t *_transmitPortRegister;

    uint16_t _rx_delay_centering;
    uint16_t _rx_delay_intrabit;
    uint16_t _rx_delay_stopbit;
    uint16_t _tx_delay;

    uint16_t _buffer_overflow:1;
    uint16_t _inverse_logic:1;

    // static data
    static char _receive_buffer[_SS_MAX_RX_BUFF];
    static volatile uint8_t _receive_buffer_tail;
    static volatile uint8_t _receive_buffer_head;
    static NewSoftSerial *active_object;

    // private methods

```

```

void recv();
uint8_t rx_pin_read();
void tx_pin_write(uint8_t pin_state);
void setTX(uint8_t transmitPin);
void setRX(uint8_t receivePin);

// private static method for timing
static inline void tunedDelay(uint16_t delay);

public:
    // public methods
    NewSoftSerial(uint8_t receivePin, uint8_t transmitPin, bool inverse_
~NewSoftSerial();
void begin(long speed);
bool listen();
void end();
bool is_listening() { return this == active_object; }
bool overflow() { bool ret = _buffer_overflow; _buffer_overflow = fal
static int library_version() { return _SS_VERSION; }
static void enable_timer0(bool enable);
int peek();

virtual size_t write(uint8_t byte);
virtual int read();
virtual int available();
virtual void flush();

```

```
// public only for easy access by interrupt handlers
static inline void handle_interrupt();
};

// Arduino 0012 workaround
#undef int
#undef char
#undef long
#undef byte
#undef float
#undef abs
#undef round

#endif
```

## A.6 APPENDIX F: Transfer function of RLC Band pass filter

A band pass filter allows signals with a range of frequencies (pass band) to pass through and attenuates signals with frequencies outside this range. Second-order band pass filters include two storage elements (two capacitors, two inductors, or one of each). Using the voltage divider rule, the gain of the filter in Figure 6.1 can be expressed as [38]:

$$H(j\omega) = \frac{V_0}{V_i} = \frac{R}{R + j\omega L + \frac{1}{j\omega C}} = \frac{R}{R + j(\omega L - \frac{1}{\omega C})} \quad (\text{A.1})$$

Dividing both the numerator and denominator of Equation (3.4) by R will result to:

$$\frac{1}{1 + j(\frac{\omega L}{R} - \frac{1}{\omega RC})} \quad (\text{A.2})$$

Equation (6.2) is now in the general form of a second order transfer function which is:

$$H(j\omega) = \frac{K}{1 + jQ(\frac{\omega}{\omega_0} - \frac{\omega_0}{\omega})} \quad (\text{A.3})$$

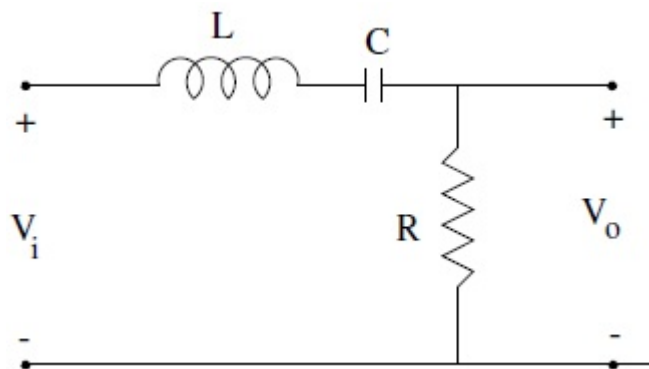


Figure A.1: Passive RLC Band Pass Filter

Where  $\omega_0$  is the center frequency expressed in rad/s. Comparing Equations (6.3) and (6.2) will yield:

$$\frac{Q\omega}{\omega_0} = \frac{\omega L}{R} \longrightarrow \frac{Q}{\omega_0} = \frac{L}{R} \quad (\text{A.4})$$

$$\frac{Q\omega_0}{\omega} = \frac{1}{\omega RC} \longrightarrow Q\omega_0 = \frac{1}{RC} \quad (\text{A.5})$$